To the Graduate Council:

I am submitting herewith a thesis written by Charles Daniel Conway entitled "The Development of Slaty Cleavage and Its Relationship to Mesoscopic and Macroscopic Structure in the Pulaski Thrust Sheet Near Bristol, Tennessee." I have examined the final copy of this thesis for form and content and recommend that it be accepted in partial fulfillment of the requirements for the degree of Master of Science, with a major in Geology.

F. B. Keller
Major Professor

We have read this thesis and recommend its acceptance:

Kula C. Misra

Kenneth L. Wilkes

Accepted for the Council:

L. Evans Roth
Vice Chancellor
Graduate Studies and Research

THE DEVELOPMENT OF SLATY CLEAVAGE AND ITS RELATIONSHIP TO MESOSCOPIC AND MACROSCOPIC STRUCTURE IN THE PULASKI THRUST SHEET NEAR BRISTOL, TENNESSEE

A Thesis

Presented for the

Master of Science

Degree

The University of Tennessee, Knoxville

Charles Daniel Conway

June 1983

118983

ACKNOWLEDGMENTS

I wish to express my gratitude to my major professor, Dr. Fred Keller, for his sincere encouragement and detailed guidance. I also wish to thank Dr. Nick Woodward, who gave me much of his time and helpful advice during the preparation of this manuscript. A special thanks is extended to my committee members, Dr. Misra and Dr. Walker, for their helpful editorial comments and their patience and understanding during the hectic final preparation of this manuscript. I also express thanks to Dr. Robert Hatcher for making available to me the seismic data from upper east Tennessee. I benefited greatly from a personal conversation with Dr. David Gray, who also provided helpful preprints of some of the ongoing research by him and his students.

A note of special gratitude is due the J. R. Delaney, Jr., family of Bristol, who willingly opened their home and facilities to me during much of my fieldwork. I must above all acknowledge my mother, Mrs. Helen L. Conway, whose generous financial support and faithful prayers made possible my whole educational experience.

Funding for this research was partially provided from a National Science Foundation Grant, EAR 78-23402, to Dr. Keller.

ABSTRACT

A mesoscopic analysis of the Tellico-Sevier Formation in the Pulaski thrust sheet of upper east Tennessee constrains the relative timing of the deformations with respect to regional tectonic events and approximately constrains the deformational mechanisms.

There is a general increase in deformation intensity across the 7-km-wide South Holston synclinorium, which lies within the Pulaski thrust sheet. The synclinorium is in contact with a large regional thrust fault, the Holston Mountain fault, on the southeast, and also contains the southwest end of the intraplate regional thrust fault, the Lodi fault. This terminus occurs as a recumbent regional fold, the Little Jacob Creek anticline. Mesoscopic buckle folds, many with axial planar cleavage, vary from a few open, upright forms on the northwest to strongly-inclined-to-recumbent forms in the southeast. Bed-perpendicular extension fractures, mesoscopic fold-discordant faults, and tight kink folds begin to dominate the structure about 1.2 km to the northwest of the axis of the South Holston synclinorium. These structures are best developed (1) on the overturned limb of the Little Jacob Creek anticline, and (2) just beneath the Holston Mountain fault.

These relationships suggest that the dynamic control on the deformation was a continuously applied stress field which was approximately coaxial over time, and whose σ_2 direction remained approximately both parallel to and at zero degrees strike to the bedding, while the σ_1 and σ_3 directions met the bedding obliquely. The principal source for the stress field was the emplacement of the Holston Mountain thrust sheet. An important secondary source of deformation was movement along the smaller Lodi fault, which overprinted the structures produced by earlier movements along the Holston Mountain fault. Movements along the underlying Pulaski fault warped the Holston Mountain thrust sheet, placing the timing of the principal deformations on this part of the Pulaski thrust sheet as earlier than the emplacement of the Pulaski fault.

In all the mesoscopic folds, layering had an active mechanical role in the folding process. Buckles generally formed under low interlayer ductility contrast. The relatively stiff layers exerted subtle control on the shapes of the folds. Relationships between angles of cleavage to bedding, fold interlimb angles, and cleavage fan angles indicate that flexural flow or slip, strongly influenced by heterogeneous pressure solution shape modification, was the likely fold mechanism. In each cleaved fold, the orientations of the cleavage traces are primarily controlled by the

maximum contraction directions of local finite strain ellipsoids. Schmidt net diagrams of folds and faults across regional strike established near coaxiality of principal strain axes for the deformations taken as a whole. Field observations, however, showed that clearly noncoaxial strain histories occurred locally.

TABLE OF CONTENTS

CHAPTER		PAGE
1.	INTRODUCTION	1
	Purpose	1
	Methods and Previous Work	1
	Location and General Geology of Study Area	4
2.	REGIONAL STRUCTURAL FRAMEWORK OF THE TELLICO-SEVIER BELT IN THE STUDY AREA	12
	Introduction	12
	Fabric Elements Used and Structural Features Analyzed	19
	Folds in the Study Area	24
	Summary of Folding	41
	Faults in the Study Area	42
	Macroscopic Interpretation	46
3.	FOLDING AND CLEAVAGE RELATIONSHIPS AND FOLD SHAPE MODIFICATION	65
	Overview	65
	Fold Geometry and Classification	67
	Fold Classification and Fold Flattening Strains in the Study Area	70
	Cleavage-Fold Geometry and Folding Mechanism	86
4.	CONCLUSIONS	112
	Geologic Cross Sections	112
	Regional Trends and Macroscopic Deformation History	114
	Cleavage-Fold Geometry and Fold Mechanisms	116
	Suggestions for Future Work	120
LIST OF REFERENCES		122
VITA		129

LIST OF FIGURES

FIGURE		PAGE
1.	Regional Geologic Map of Northeast Tennessee with Location of Study Area	3
2.	Localized Geologic Map, Including Study Area .	6
3.	Palinspastically Restored Stratigraphic Wedge of East Tennessee	7
4.	Interpretive Kinematic History of Strike Belt .	20
5.	Profile of Outcrop at Locality R-1	25
6.	Profile of Outcrop at Locality 0-1	27
7.	Representative Schmidt Net Plots from Selected Localities in the Field Area	28
8.	Three Profiles of Outcrops in the Field Area .	30
9.	Profile of Outcrop at Locality LS-2	31
10.	Profile of Outcrop at Locality R-11b	32
11.	Distant Profile of Part of Outcrop at Section LJ	35
12.	Closeup Profiles of Selected Portions of the Outcrop from Section LJ	36
13.	Profile of a Section of Outcrop at Locality R-14	39
14.	Profile of an Isolated Fold Hinge at Section LJ	45
15.	Two Schmidt Net Plots of Faults in the Study Area for Arthaud's Analysis	56
16.	Classification of Fold Geometries Adopted from Ramsay	68
17.	Fold Profile from Locality 0-1, Lower Sevier, with Dip Isogons Included	72

FIGURE		PAGE
18.	Fold Flattening Curves for Selected Layers from Profile at Locality 0-1, Lower Sevier . .	74
19.	Fold Profile from Locality 0-2, Lower Sevier, with Dip Isogons Included	76
20.	Interlimb Angle Variation with Distance from Fold Core for Fold Set 1 at Locality 0-2 . . .	78
21.	Fold Flattening Curves for Selected Layers from Profile at Locality 0-2, Lower Sevier . .	80
22.	Enlarged Profiles from Two Outcrops Showing Effects of Stiff Layers on Fold Geometries . .	82
23.	Various Parameters Required for Determination of Folding Mechanism by Cleavage-Fold Geometry	88
24.	Three Models of Rigid Body Deformation by Pressure Solution Shape Modification Adopted from Groshong	89
25.	Plots of Limb Dip against Bedding-Cleavage Angle for Two Theoretical Fold Models	90
26.	Plots of Limb Dip against Bedding-Cleavage Angle for Two Viscous Fold Models of Dietrich .	91
27.	Plots of Cleavage Fan Angle against Interlimb Angle for Two Theoretical Fold Models	93
28.	Plots of Limb Dip against Bedding-Cleavage Angle for Three Folds in the Study Area Superimposed on the Corresponding Graph from Groshong's Pressure Solution Shape Modification Fold Models	99
29.	Plots of Limb Dip against Bedding-Cleavage Angle for Three Folds in the Study Area Superimposed on the Corresponding Graph from Ramsay's Flexural Flow Fold Models	100
30.	Plots of Limb Dip against Bedding-Cleavage Angle for Three Folds in the Study Area Superimposed on the Corresponding Graph from Dietrich's Second Viscous Fold Model . . .	101

FIGURE PAGE

31. Field Photographs of Folds Whose Analyses Are Presented in Manuscript 102

32. Plots of Cleavage Fan Angle against Interlimb Angle for Real Data Superimposed on Corresponding Plots for Two Theoretical Fold Models 106

33. Portion of Outcrop at Locality 0-1 108

LIST OF PLATES

PLATE

1. Detailed Sketch Map of Study Area . . . . . In Pocket

2. Interpretive Cross Section through Study Area . . . . . In Pocket

3. Interpretive Regional Cross Section A-A' . In Pocket

CHAPTER 1

INTRODUCTION

Purpose

Geometric means for evaluating the effects of thrust sheet emplacement in foreland fold-and-thrust belts include (1) detailed areal mapping, (2) relative timing relationships among minor and regional structures (kinematic sequence of deformation), (3) S-pole diagrams of small structural elements, and (4) mesoscopic fold profiles.

An understanding of the mechanism of mesoscopic folding and faulting and the relationship of these processes to the large-scale structure is limited in the thrust-dominated southern Appalachians, particularly in Tennessee. The objective of this study is to examine tectonic fabric data from one portion of the Valley and Ridge province in northeast Tennessee in order to describe and constrain deformational sequences and mechanisms.

Methods and Previous Work

This paper is primarily a mesoscopic structural study. It uses Schmidt net analyses of bedding, cleavage, faults, and lineations to establish the geometry of mean strain across the strike belt (Turner and Weiss, 1963; Ramsay,

1967). Possible mechanisms for the formation of mesoscopic folds were determined from a study of fold profile geometries (Ramsay, 1967; Groshong, 1975; Gray and Durney, 1979; Gray, 1981). The relative timing of cleavage with respect to folding was qualitatively constrained from field observations. Field sketches and profile photographs constrained the deformation chronology in each outcrop.

A macroscopic (large-scale) deformation chronology for the South Holston area was developed from all the individual outcrops. A small-scale, interpretive cross-section through the study area shows involvement of only the clastic section (Plate 2, in pocket). The cross-section was constrained by surface data and from the approximately-established depth to the top of the Knox Group at the deepest part of the trough of the South Holston syncline (USGS, 1980). A larger regional cross-section (Plate 3, in pocket) was constructed from earlier reports and from the author's field mapping. The large cross-section extends along line A-A' from the Tennessee-North Carolina boundary to just northwest of Bristol, Tennessee (Figure 1), and it includes a portion of the recently acquired seismic data from upper east Tennessee (USGS, 1980).

Modern geologic studies in the region provided an adequate foundation for the author's interpretations. King

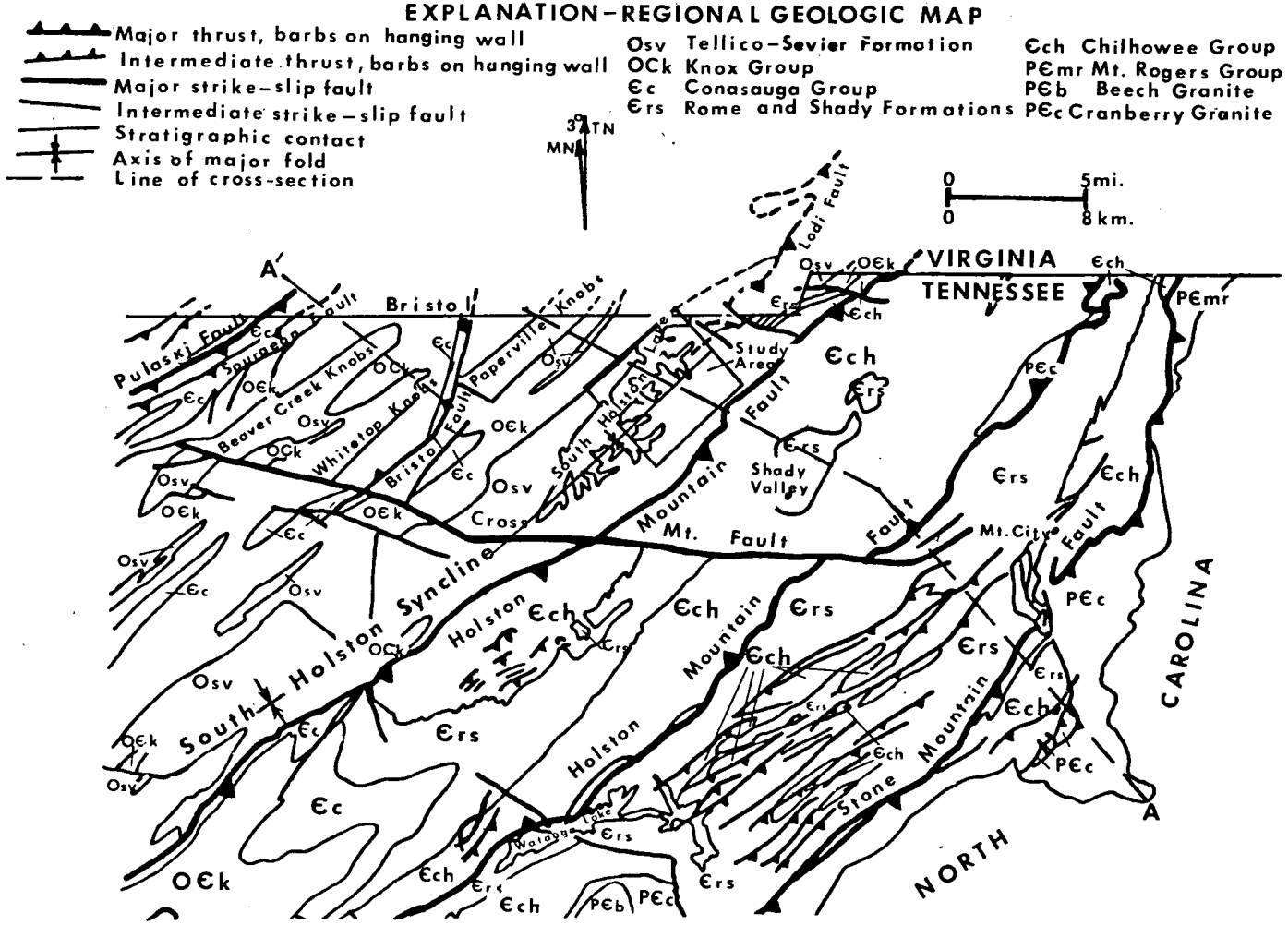

Figure 1. Regional geologic map of northeast Tennessee with location of study area. Location of Lodi fault in southern Virginia after Reks and Gray, 1982.

and Ferguson (1960) did the first and only detailed description of the geology of upper east Tennessee. Recent work in the depositional environments and physical stratigraphy of the Middle Ordovician clastic sequence (Bowlin, 1979; Bowlin and Keller, 1980; Walker and Keller, 1980) clarified the original geometry of the rocks and the expected interlayer variation in physical properties. The published subsurface interpretation of Harris et al. (1981) is the only published interpretation of recently acquired seismic data for this region (USGS, 1980). Detailed cleavage studies in the central to northern Appalachians (Groshong, 1975, 1976; Geiser, 1975; Holeywell and Tullis, 1975) provided important insight into the expected cleavage patterns in the study area. Some recent cleavage studies in southwest Virginia (Simon, 1981; Gray, 1981; Reks and Gray, 1982) suggested means of analyzing the cleavage and its relationship to mesoscopic structure.

Location and General Geology of Study Area

Introduction

The field area lies within the northeasternmost part of the Valley and Ridge province in northeast Tennessee (Figure 1). The region is partly underlain by a thick sequence of Middle Ordovician clastic rocks that are the object of this report. The sequence has been called by

various formation names (Campbell, 1899; Butts, 1940; Rodgers, 1953; King and Ferguson, 1960). In this report, the rocks are referred to as the Tellico-Sevier Formation or the Sevier Formation in abbreviated form. This nomenclature is based on established precedents (Walker and Keller, 1980; Witherspoon, 1981). The area is centered about 12 miles (19 km) east of Bristol, Tennessee, in the vicinity of South Holston Lake (Figure 2). The Tellico-Sevier in this area lies above the Pulaski fault, about one mile (1.6 km) northwest of Bristol, Tennessee, and beneath the Holston Mountain fault on the southeast.

Regional Stratigraphic Framework

Overview. The regional stratigraphy of east Tennessee was worked out in some detail by Harris and Milici (1977). Figure 3 is a palinspastically restored stratigraphic wedge for east Tennessee (Walker, 1980), which incorporates much of the earlier information. Except for the Chota and the Bays formations, which do not occur in the South Holston area, the units of interest are in the acute wedge near the thickened eastern end of the section. Equivalents of this sequence can be found through much of east Tennessee (Walker, 1980), and into parts of southwest Virginia (Read, 1980). The stratigraphy is less complex in the South Holston region than in the equivalent shelf rocks to the northwest. Keller and Walker

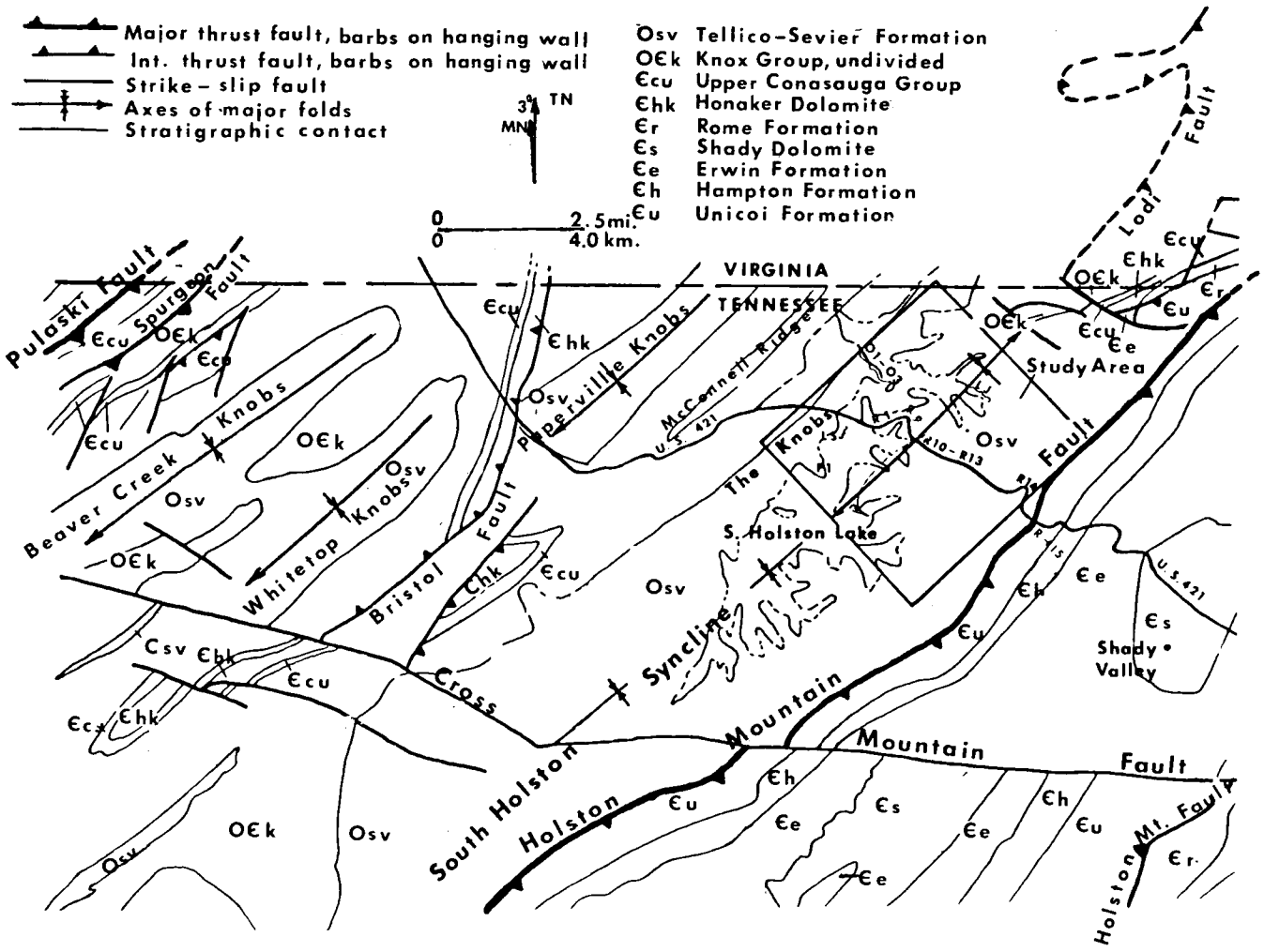

Figure 2. Localized geologic map, including study area.

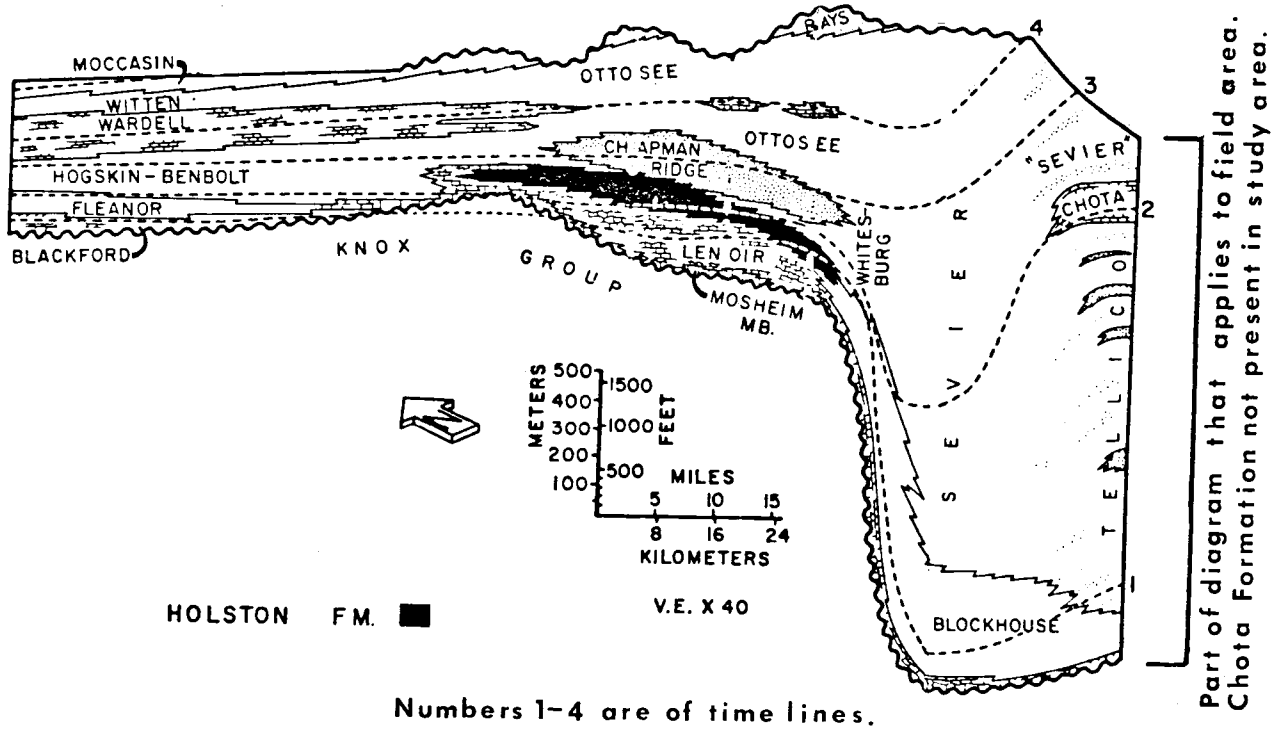

Figure 3. Palinspastically restored stratigraphic wedge of east Tennessee (adapted from Walker, 1980).

(1980, p. 88) recognize only the presence of the Lenoir, Blockhouse and Tellico-Sevier formations within the deformed belt, because the top of the sequence to the southeast has been cut out by thrust sheets of the Blue Ridge province.

Physical stratigraphy in the study area. The oldest formation exposed in the South Holston region is the upper Knox Group of carbonates of early Middle Ordovician age (Bridge, 1956; Walker, 1980). A poorly exposed 10- to 20-meter section of the Lenoir Formation (Bartlett and Biggs, 1980) unconformably overlies the Knox. The Lenoir Formation is conformably overlain by an approximately 60-meter thickness of black, highly fissile Blockhouse Shale (Howze, 1982, personal communication). The Knox-Lenoir contact and the section of Blockhouse shale are both exposed on the north side of Observation Knob Park (Plate 1, in pocket) only at low-water stages of South Holston Lake. The Blockhouse Shale grades upward into the lowermost Tellico-Sevier Formation, made up of consistently fine-grained, calcareous mudrock. It is called the lower Sevier in this report, and it extends from the base of the Knobs southeast to about locality 0-1 (Plate 1). Its total estimated thickness is on the order of several tens of meters. The lower Sevier grades upward into a coarser-grained section of interbedded sandstone and siltstone called the upper Sevier in this report (Walker,

1980, p. 11). This section extends from about locality 0-2 southeast to the end of the strike belt. The actual thickness of this coarser-grained section cannot be determined because of its complex structure, and because a portion of it in the field area has been cut out by the Holston Mountain fault. The coarse conglomerates that are found locally dispersed through this section occur at locality LS-2, just south of locality R-13 at the Lucy Creek embayment, and at the southeast end of section LJ (Plate 1). The uppermost part of Newman's (1955) Sevier Formation and the Bays Formation, characterized by sand beach and tidal-flat lithologies deposited in the waning stages of the infilling of the original basin, do not appear in the field area.

Environmental interpretation. Bowlin and Keller (1980) interpret the portion of the Tellico-Sevier Formation near South Holston Dam, just south of the study area, as part of a prograding submarine fan complex. The total area of such features in the region is estimated at about 600 square miles, including occurrences in southwest Virginia (Bowlin and Keller, 1980, p. 81). The fan complex at South Holston Dam was deposited directly onto starved basinal shales of the Blockhouse Formation (Bowlin and Keller, 1980). The complex contains both proximal and ultradistal environmental packages. The ultradistal packages are made up of consistently fine-

grained siltstone and shale. Intermediate grain sizes occurring in nearly equal proportions of interbedded siltstone and sandstone correspond to the "midfan" (Bowlin, 1979). The proximal packages consist of very coarse-grained conglomerates that occur in lenticular masses, representing submarine channel fill deposits (Bowlin, 1979). Similar appearing strata throughout the study area suggest formation within the same overall environmental system. The original depocenter probably consisted of a number of coalescing submarine fans producing a large, originally horizontal, sheetlike body of sediments.

Structural overview and geologic map. Earlier workers (Rodgers, 1963; King and Ferguson, 1960) established that the South Holston rocks were folded into a regional syncline (South Holston syncline, Bartlett and Biggs, 1979). Its maximum half-wavelength is 4.5 miles (7.2 km), and its total strike extent is about 30 miles (47.5 km) (Hardeman et al., 1966). The South Holston syncline is apparently the largest of several regional folds on the Pulaski thrust sheet (Figure 2). Typically, the regional synclines are floored by the Tellico-Sevier Formation, while the intervening anticlines expose upper Knox Group in their cores. Part of the South Holston syncline is expressed topographically as The Knobs (Plate 1), a row of steep, knobby hills. Northwest of the

field area, McConnell Ridge, Paperville, Whitetop, and Beaver Creek Knobs are surface expressions of the other, smaller synclines on the thrust sheet. The intervening anticlines have a subdued, hummocky topographic expression, typical of terrains underlain by upper Knox carbonates (Newman, 1955).

Metamorphism. Rocks in the study area have apparently not been subjected to a grade of metamorphism sufficiently high to have produced good, diagnostic index minerals, other than for possible metamorphic chlorite (Reks and Gray, 1982). This indicates metamorphism to about lower greenschist facies, although this is only a rough estimate without good quantifying data.

CHAPTER 2

REGIONAL STRUCTURAL FRAMEWORK OF THE TELLICO-SEVIER BELT IN THE STUDY AREA

Introduction

The southern part of the Valley and Ridge and Blue Ridge provinces is characterized by arcuate, discrete, thrust fault traces that may truncate regional anticlinoria and synclinoria (Rodgers, 1953; Simon, 1981, p. 10; Witherspoon, 1981). The architecture of the thrust belt is that of a major zone of bedding-plane detachment or decollement in the Cambrian Rome Formation from which the major faults rise northwestward stratigraphically through the Paleozoic section in the Valley and Ridge province. Roeder et al. (1978) show a series of cross-sections through the Virginia and Tennessee portions of the Valley and Ridge illustrating this decollement principle and their interpretations of the structure associated with particular localities in this belt. This and all previous interpretations of the structure in the Tellico-Sevier belt in the Bristol area (Rodgers, 1953; Bartlett and Biggs, 1979) show a relatively simply synclinorium, the South Holston syncline, that folds the Knox Group and the Tellico-Sevier at the surface. Some investigators have interpreted the South Holston syncline as overturned on its southeast limb (Roeder

et al., 1978; Bartlett and Biggs, 1979), so the belt has been shown on their maps and cross-sections as containing predominantly vertical or steeply dipping sections that show reversals in the direction of stratigraphic facing as the main fold is crossed. Investigation of outcrops in the study area, however, indicate that the megascopic structure of the belt is more complex than previous investigators have recognized. In Tennessee, the structure is complicated by a series of outcrop-to-map scale parasitic folds with the same general northwest vergence as the major synclinorium. This chapter discusses the megascopic structure of the belt through synthesis of megascopic and mesoscopic analysis of critical localities, and also addresses the overall relationship of the cleavage with the tectonic framework.

Overview of Interpretive Cross-Sections

The author was aided in the analysis by seismic data (USGS, 1980) and by one interpretation of it (Harris et al., 1981). This includes part of the field area and most of the Blue Ridge and Piedmont provinces across strike to the southeast. The small-scale cross-section, A-A' (Plate 3), extends along the seismic line from the Tennessee-North Carolina border to the line's northwest end about one-third of the distance through the study area. From there it extends to a point about 2 kms northwest of Bristol,

Tennessee, near the surface expression of the Pulaski fault. Construction of the small-scale cross-section was aided by the seismic data. Earlier reports helped in the interpretation where no seismic data were available (Rodgers, 1953; Roeder et al., 1978; Bartlett and Biggs, 1979).

Balancing cross-sections. Balancing of the regional cross-section (Plate 3) was attempted by conserving cross-sectional areas and thicknesses of stratigraphic units following the techniques outlined by Roeder et al. (1978). However, the seismic data from upper east Tennessee (USGS, 1980), on which much of the interpretation in this paper was based, does not provide an interval velocity for each stratigraphic unit, and the overall resolution of the data was only fair. Therefore, the actual thicknesses for most units were impossible to determine from the data. The cross-section was not exactly restorable to its original length, either, because true points of slip along the faults could not be determined accurately. The interpretation here is therefore an approximation and not a rigorously balanced section. The smaller cross-section (Plate 2) across the field area could not be balanced, because its complex structure was not amenable to balancing by the techniques outlined above. The lack of rigorous constraints on the structure at depth, and other difficulties, such as shale

flowage, prevent balancing of it. The cross-section was instead constructed to exemplify the major interpretations of the author, and it is constrained in its general appearance by mesoscopic and surface information and by data discussed in other publications on the area, mentioned previously.

Regional structural interpretation. The author's regional cross-section assumes a "thin skinned" (Rich, 1934) tectonic style for the region. The Paleozoic strata have all been transported to the northwest above gently southeast sloping Precambrian basement. Later imbricates which join a master basal decollement at depth have folded all the first order faults, and they have also thickened the entire Paleozoic section in several places. In my cross section, these effects are most pronounced just southeast of the Mountain City window (Plate 3). This folding of structurally higher faults and the tectonic thickening by ramping and uplift at lower structural levels establishes a general east to west progression of deformation.

Local structural interpretation. The interpretation of the main study area (Plate 2) required intraformational structures, such as imbricate thrusts at depth and recumbent, parasitic folds to accommodate the across-strike extent and approximately known amplitude of the synclinorium. Other workers in deformed equivalents of the Tellico-Sevier (Weitz,

1982, and Gray, 1982, personal communications) have noted that the Knox Group is not involved in the complex structure of the overlying strata. This constraint allowed the author to interpret the displacement on the large folds as dying out in bedding-parallel slip near the Knox-Sevier contact. The overturning of the large folds shown in Plate 2 was observed in the field and is consistent with observations in other synclinoria adjacent the Blue Ridge front in the southern Appalachians (Kellberg and Grant, 1956).

Application of seismic data. The seismic data (USGS, 1980) provided little resolution within the study area itself. The contact between the Knox Group and the Middle Ordovician clastics is a relatively poor reflector. Harris et al. (1981, Fig. 3) interpret it as a subtle loss of resolution just beneath the Tellico-Sevier, seen at the northwest end of the seismic line. From these data, the depth to the top of the upper Knox Group at a deep part of the trough was approximately determined as 3700 feet. This same depth was maintained throughout most of the across-strike extent of the section, although this is an interpretive feature and not a unique solution. Better seismic data would be necessary to establish the actual configuration.

Basic Definitions

The following set of definitions of terms used in this chapter are standard in geologic literature (Ramsay, 1967, pp. 518-553; Hobbs et al., 1976, pp. 1-27). They have been condensed in the present discussion, because exhaustive definitions would be beyond the scope of this study.

External stress. Externally applied stresses on rock can always be referenced as components of three "principal stresses" whose directions are parallel to three orthogonal "principal stress axes" σ_1, σ_2, and σ_3. The direction of maximum stress is given by σ_1; the intermediate stress direction is parallel to σ_2; and the minimum principal stress direction is parallel to σ_3. In orogenic belts such as the present study area, the sense of the maximum principal stress is typically compressive. The magnitude of the intermediate principal stress is often small compared with σ_1 and σ_3.

Induced strain. The strains resulting from the application of the external stresses can be referenced with respect to three orthogonal "principal strain axes," λ_1, λ_2, and λ_3. λ_1 is the maximum principal strain axis, corresponding to the maximum extension direction; λ_2 is the intermediate principal strain axis, and λ_3 the minimum strain axis, corresponding to the maximum shortening direction. Earlier structural geologists (Sander, 1948) utilized another

set of terms for folding deformation that are still used in the literature. They have been utilized to an extent in this paper. The earlier terminology involved three coordinate axes that described the folding in terms of a progressive simple shear, the mechanism believed at that time to be responsible for folding (Hobbs et al., 1976, p. 194). These coordinates are termed "kinematic axes." They consist of the A-axis, parallel to the shear planes; the B-axis, normal to A in the shear plane, also called the rotation axis; and the C-axis, normal to both A and B. The shear plane is the AB plane, and the AC plane is called the movement plane. Where these terms are utilized in this paper, they coincide loosely with the principal strain axes of the previous discussion. That is, the "A" direction coincides with λ_3, the "B" direction with λ_2, and the "C" direction with λ_1.

Superposed folds. Complexly deformed fold and thrust belts can be affected by more than one episode of folding. In all the following discussions, the designations F-1, F-2, etc., refer to clearly visible, separable fold generations at a single outcrop. F-1 represents the earliest folding event, F-2 the second, F-3 the third, and so on. The separation into relative chronology is done on the basis of cross-cutting relationships. Folds formed during the F-1 event will have clearly been refolded by F-2, while F-2 will have been

refolded by F-3, and so on until the end of the recognizable fold generations.

Organization of Discussion

Figure 4 presents the author's interpreted kinematic history of the Tellico-Sevier belt on the basis of the structural analysis presented below. The table is presented here as a synopsis from which the reader may view the following discussion. The presentation below is organized around (1) description of the fabric elements and structural features analyzed, discussion of the folds (2) and faults (3) found in the area, and (4) interpretive summary of the macroscopic history of the belt.

Fabric Elements Used and Structural Features Analyzed

Overview

A number of measurements of strike and dip of planar and linear fabric elements were made at each of the localities shown on Plate 1. Bedding (S_0) is the only preexisting or inherited fabric element measured in the investigation. It is assumed to have been oriented more or less horizontal prior to deformation. Because much of the rock is thin-bedded and fine-grained siltstone and shale, stratigraphic facing criteria are not obvious. Careful observation at the outcrop, however, usually yielded information on facing

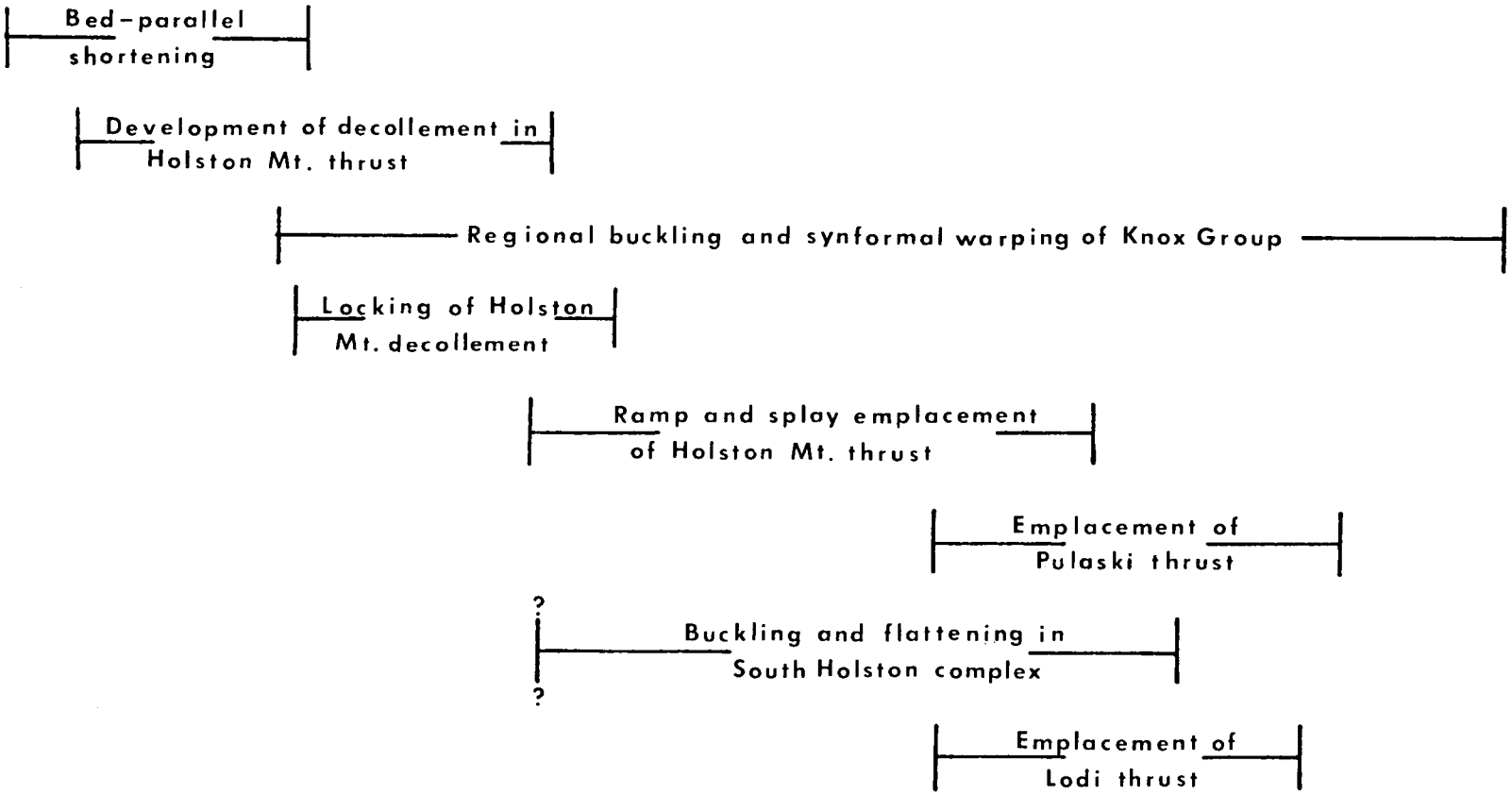

Figure 4. Interpretive kinematic history of strike belt.

directions in the form of fine-scale scour or flute casts at the base of siltstone beds, starved ripples, or locally abundant fossil casts preferentially found at the bases of individual layers. Where facing directions are ambiguous in the field, thin section study usually allowed for recognition of facing criteria. Under high magnification, principal facing indicators were starved ripples, clearly erosional bedding surfaces, and in some cases, normally graded bedding. Cleavage (S_1) is one of the secondary fabric elements of importance. Only one generation of cleavage could be documented, and it was easy to recognize in most cases. A number of cleavage-bedding intersections were also measured at each location in order to establish the statistical orientations of the cleavage with respect to the hinge lines of the folds.

Schmidt Net Analyses

Folds. Schmidt net analyses of the mesoscopic folds provided an important indication of regional structural trends. These in turn are related to the deformation history of the field area. The two main types of folds of interest are kink folds and buckle folds. In this report, buckle folds, or buckles, are those whose axial surfaces develop initially perpendicular to the direction of maximum shortening, while kink folds, or kinks, have axial surfaces that

develop initially oblique to the shortening direction (Hobbs et al., 1976, p. 200). It has been established that the axial surfaces and axes of kinks and buckles in general do not retain their original orientations with respect to the maximum shortening direction throughout folding (Ghosh, 1966; Price, 1967b; Treagus, 1973, 1981). This is due partially to asymmetry of the applied external stresses with respect to the strata (see "Macroscopic Interpretation," this chapter), to the anisotropy of real rock materials, and to the real interlayer variation in physical properties. Therefore, in general one cannot precisely relate the geometry of mean strain of folded strata as shown on Schmidt nets to the actual finite strain axes with respect to any absolute reference frame. But Schmidt net analysis does clearly show the variation in attitudes of cleavage and of folded bedding through a strike belt. This in turn may provide some understanding of the orientations of the applied principal stresses that produced those attitudes with respect to the original undisturbed layered rocks, as well as an understanding of the degree of coaxiality of the induced strains.

Extension fractures. Extension fractures were an important component of strain in the coarse conglomerates referenced previously at several locations (Chapter 1). In all cases, the fractures were calcite-filled. Some of the

calcite crystal fillings exhibited curved fibrous lamellae extending across their walls. They apparently record part of a locally noncoaxial strain history as the fractures opened. Measurements of the attitudes of the fractures were of little value in determining mean strains, because their orientations were quite variable. This was a result of the heterogeneity of the relatively coarse materials in which they formed. They are not treated to any extent in the discussion following.

Faults. Faults constitute a nonpenetrative feature in many outcrops in the study area. Slickensides are often associated with the faults, and where they are present it is sometimes possible to graphically estimate the orthogonal principal "deformation axes" (Arthaud, 1969). A regional comparison of these axial orientations could then be made. For purposes of the Arthaud (1969) strain analysis, the term "fault" is applied to apparent breaks in the continuity across bedding (i.e., brittle deformation), along which there has been displacement. In general, however, I use "fault" to refer to bed-parallel displacement as well. Some authors refer to such displacement as "bedding plane slippage" (Yust, 1976).

Folds in the Study Area

Introduction

The field observations have been treated with a view toward regional synthesis and toward establishing structural trends in the area rather than in an outcrop-by-outcrop basis, per se. From outcrop evidence, the area is naturally divisible into four general subareas that are located with respect to U.S. Route 421 (Plate 1). These subareas extend along regional strike as indicated. Subarea I extends from just northwest of the Knobs southeastward to locality R-3 on U.S. 421. Subarea II extends from locality R-3 southeast to the vicinity of localities R-11a, b on Route 421. Subarea III extends southeast from localities R-11a, and b to the southeast end of the Little Jacob Creek embayment (Section LJ), northwest of Route 421 (Plate 1). Subarea IV extends southeast of the southeast end of Section LJ to locality R-15, along the Holston Mountain fault (Figure 2, p. 5).

Subarea I

This area is dominated by buckle folds that are generally upright or have steeply dipping axial surfaces either to the northwest or southeast, and that exhibit strong axial planar cleavage. The cleavage is most intense in the hinge regions of folds. The profile of locality R-1 (Figure 5) typifies the deformation in most of subarea I: mostly upright, tight

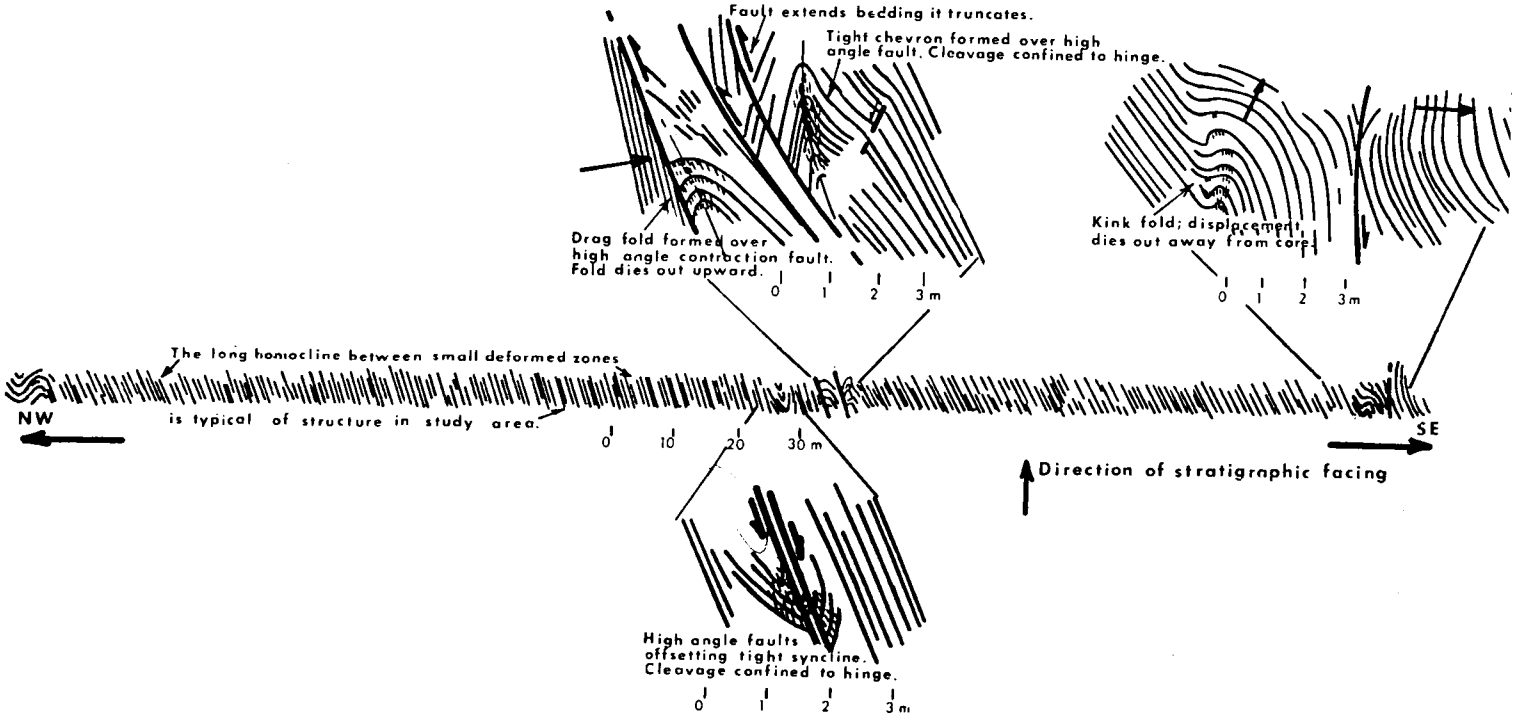

Figure 5. Profile of outcrop at locality R-1.

buckles, often sheared by forelimb thrusts, and separated by thick, planar, homoclinal sections of variable outcrop width. Relatively long sections of nearly structureless homocline interspersed with the zones of deformation form one of the ubiquitous features in the study area and its immediate surroundings (King and Ferguson, 1960). This is also seen in other areas of the Tellico-Sevier basin (Yust, 1976; Weitz, 1981, personal communication). Figure 6 is an outcrop profile from locality 0-1 (Plate 1), also in subarea I. It is typical of the structure of the lower Sevier at the northwest extent of the study area, characterized by folds with well-developed, generally axial planar cleavage, and by the only open buckle folds in the complex.

Fabric diagrams. Figures 7a-i are Schmidt net plots of poles to bedding and to cleavage and of cleavage-bedding intersections at localities R-1, 0-3, and LS-3 within subarea I. Most of the folds' axial surfaces can be well-approximated as bisectors of the folds, even where they are asymmetric, because the limbs are of equal thickness. The trends shown in the plots for each lithology are statistically cozonal to each other, in that their corresponding planar elements are nearly parallel. The cleavage fans symmetrically in each fold set, and it is statistically axial planar to the folds, as the distribution of poles to cleavage is virtually

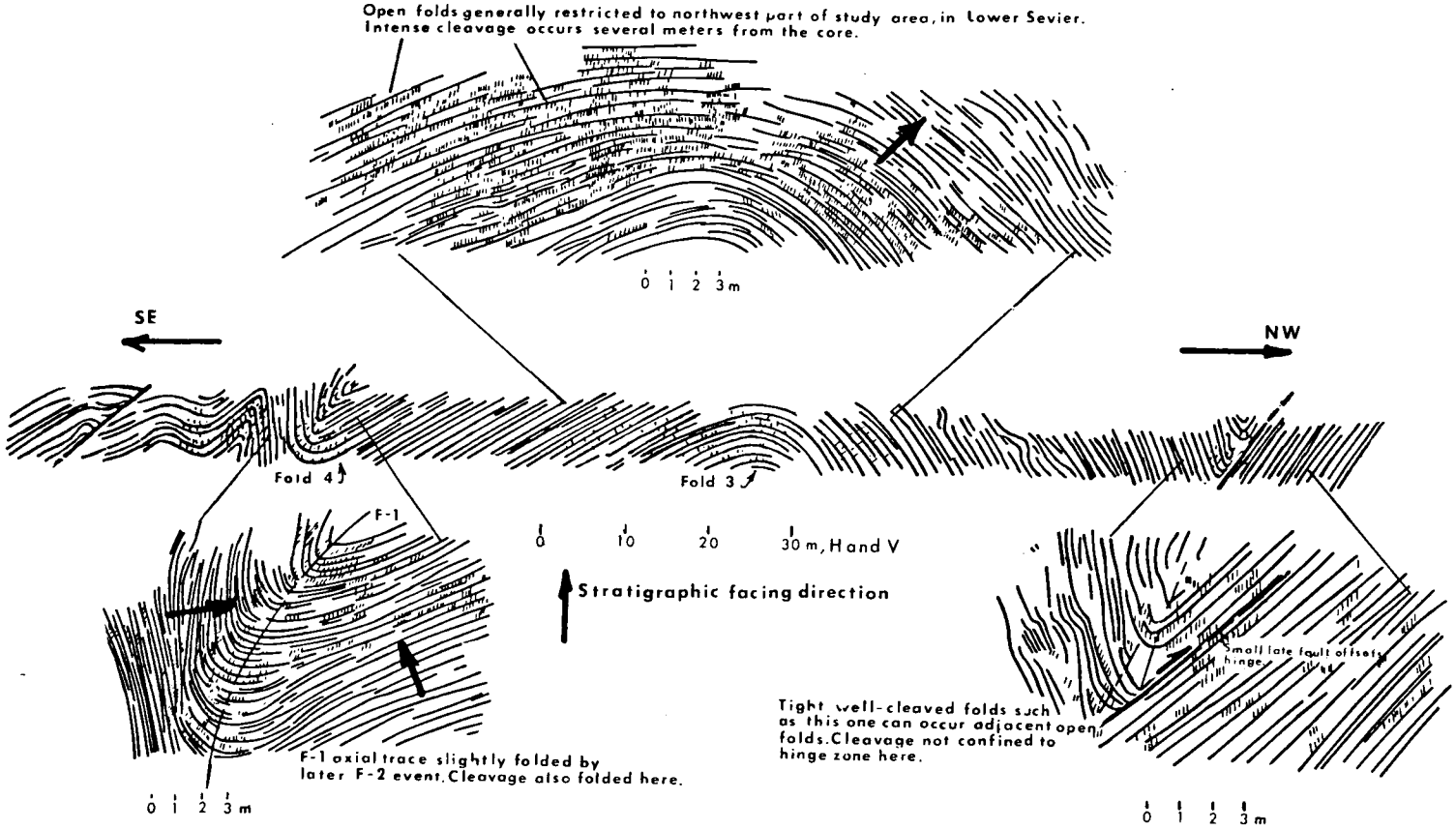

Figure 6. Profile of outcrop at locality 0-1.

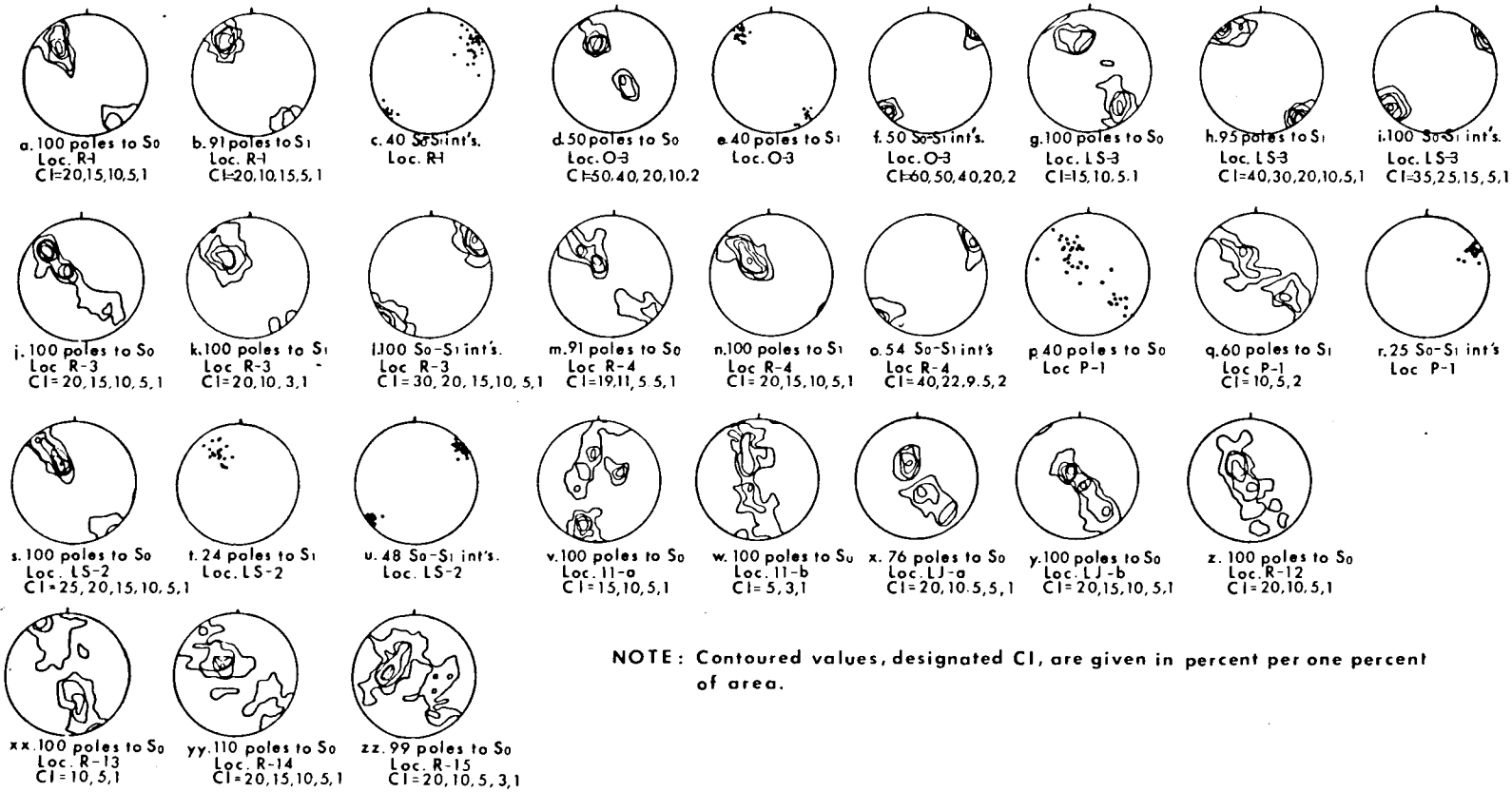

Figure 7. Representative Schmidt net plots from selected localities in the field area.

superposed over the corresponding bedding poles. The plots show variable, shallow fold plunges, with nearly equal numbers of northeast and southwest-plunging cleavage-bedding intersections that statistically parallel the fold axes defined by the A-C planes of the bedding pole plots.

Subarea II

Overview. This area is characterized by strongly inclined, overturned buckle folds, with axial surfaces moderately to gently southeast-dipping. The area is also characterized by the first appearance of intense faulting, particularly at locality R-4 (Plate 1), and by significant development of kink folds, some of which have been refolded. They are best-developed at the southeast end of the subarea at localities R-11a and b. Many of the buckle folds exhibit a strong axial planar cleavage, although the most strongly inclined folds in this area may show relatively little or no cleavage in outcrop. Representative profiles with explanations from localities R-3, R-4, P-1, LS-2, and R-11b are shown in Figures 8a-c, 9, and 10.

Fabric diagrams. Figures 7j-u are Schmidt net plots of poles to bedding, cleavage, and cleavage-bedding intersections where they could be determined for selected localities within subarea II. For the cleaved folds, the diagrams show that

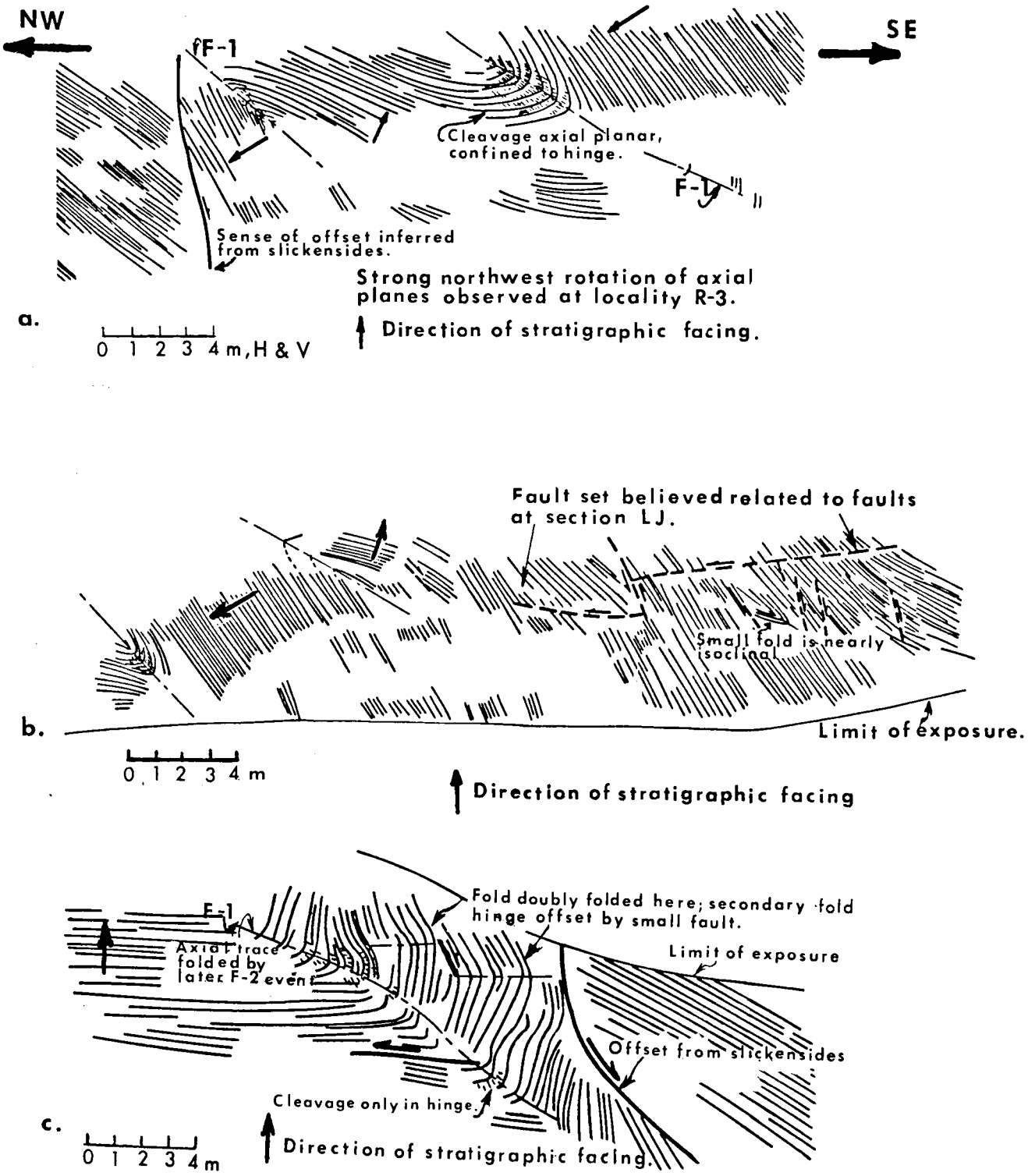

Figure 8. Three profiles of outcrops in the field area. (a) Locality R-3. (b) Locality R-4. (c) Locality P-1.

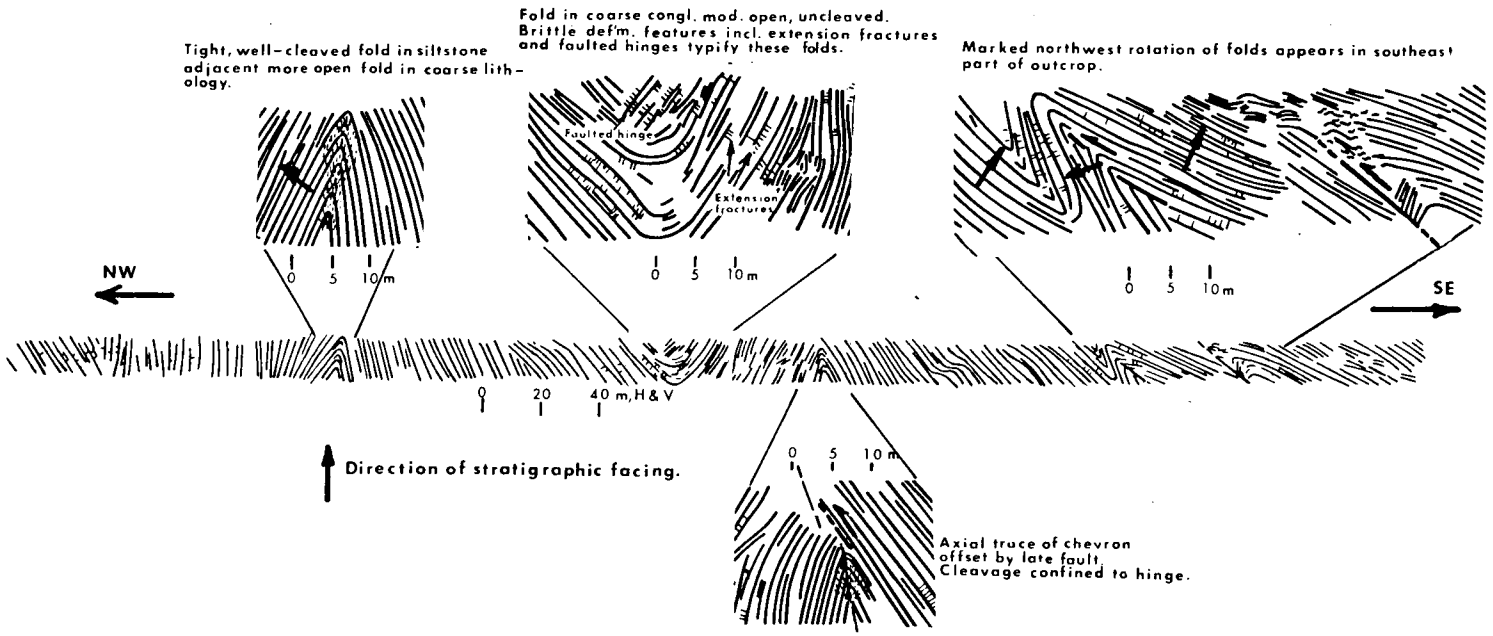

Figure 9. Profile of outcrop at locality LS-2.

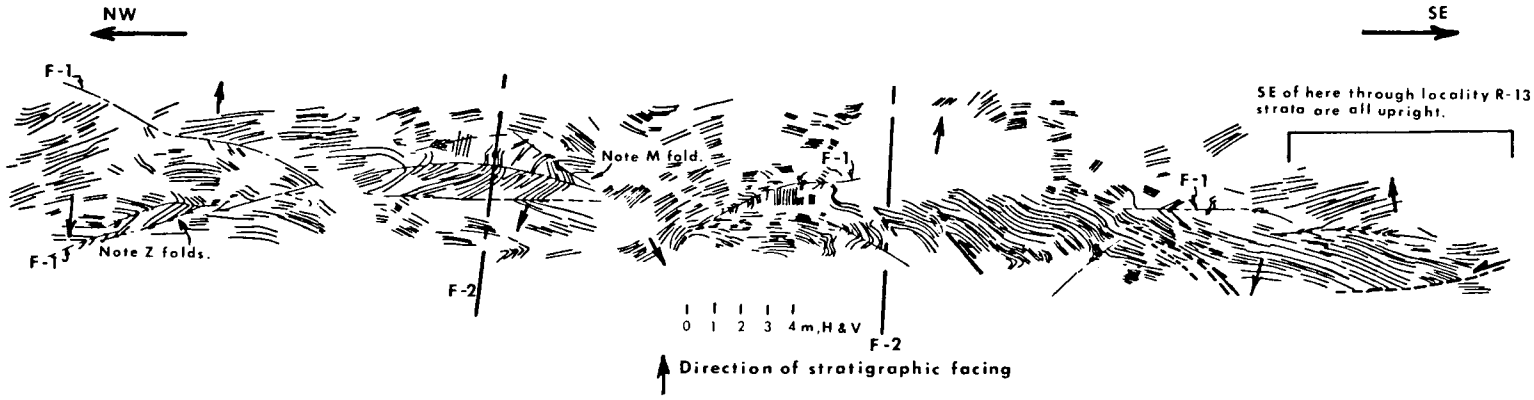

Figure 10. Profile of outcrop at locality R-11b.

each set of cleavage is closely axial planar to its associated fold set and that the fold plunges are shallow and nondirected.

Refolded kinks. Localities R-11a and b, which demarcate the beginning of subarea III, also show significant kink folding. The kinks (F-1) have been refolded by a second fold generation (F-2) about nearly vertical axial planes, as seen at R-11b (Figure 10). The fabric diagram from R-11a indicates the folds are noncylindrical by the clear bimodal distribution of bedding poles in the southern sector of the stereo net (Figure 7v). This distribution, produced by a strong, preferred variation in the strike of the aberrant bedding planes, has generated two partial girdles in the fabric diagram. This contrasts with the fabric diagrams from more northwesterly localities (Figures 7a-u) that have but one girdle each. The fabric diagram from locality R-11b also resembles that of R-11a (Figure 7v) in the nearly north-south orientation of its A-C plane (Figure 7w). This suggests that the outcrop at R-11b is also folded noncylindrically, although its fabric diagram does not exhibit the same bimodal bedding pole distribution. In both exposures, the A-C plane attitudes departed markedly from their regional trends at cylindrically folded northwesterly outcrops (Figures 7a-u). The association of the noncylindrical fold style and the multiple folding events here indicates that the two features are related. At

R-11b, the axial surfaces of the kinks define a fold train resembling the type 3 fold interference pattern of Ramsay (1967, pp. 530-534). By definition, the symmetry of this fold train is heterotactic to the folds to the northwest (Turner and Weiss, 1963, pp. 42-44). At locality R-11b, the whole refolded complex would be "triclinic," since it has no one symmetry plane. The other folds to the northwest would, by the same set of definitions, be "orthorhombic" or "monoclinic."

Subarea III

The structure of this area is best developed in a lake shore exposure along the embayment at Little Jacob Creek (Section LJ, see Figure 11), about halfway from the southeasternmost end of the inlet, and extending to its end. The section is dominated by a large, recumbent anticline (F-1) that has been refolded about nearly vertical axial planes (F-2). The F-2 event is interpreted here as the same event that produced the refolded kinks of localities R-11a, b.

Figures 12a and b are closeup fold profiles of two portions of the longer fold profile, designated in Figure 11. Corresponding Schmidt net plots of bedding poles from the areas shown in the closeup profiles are shown in Figures 7x and y, p. 28. The crumpled bedding in the upper limb of the fold in Figure 12a is responsible for the slight bimodal distribution of bedding poles that has produced two partial

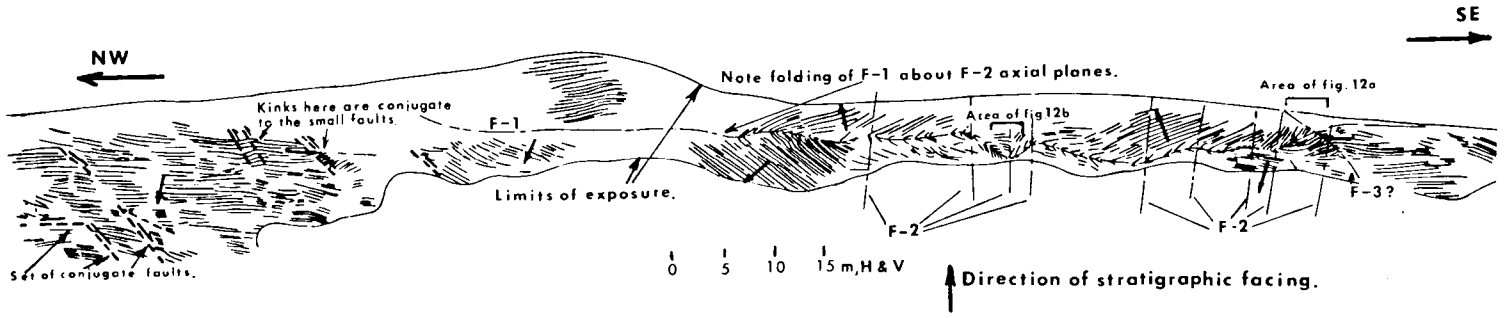

Figure 11. Distant profile of part of outcrop at section LJ.

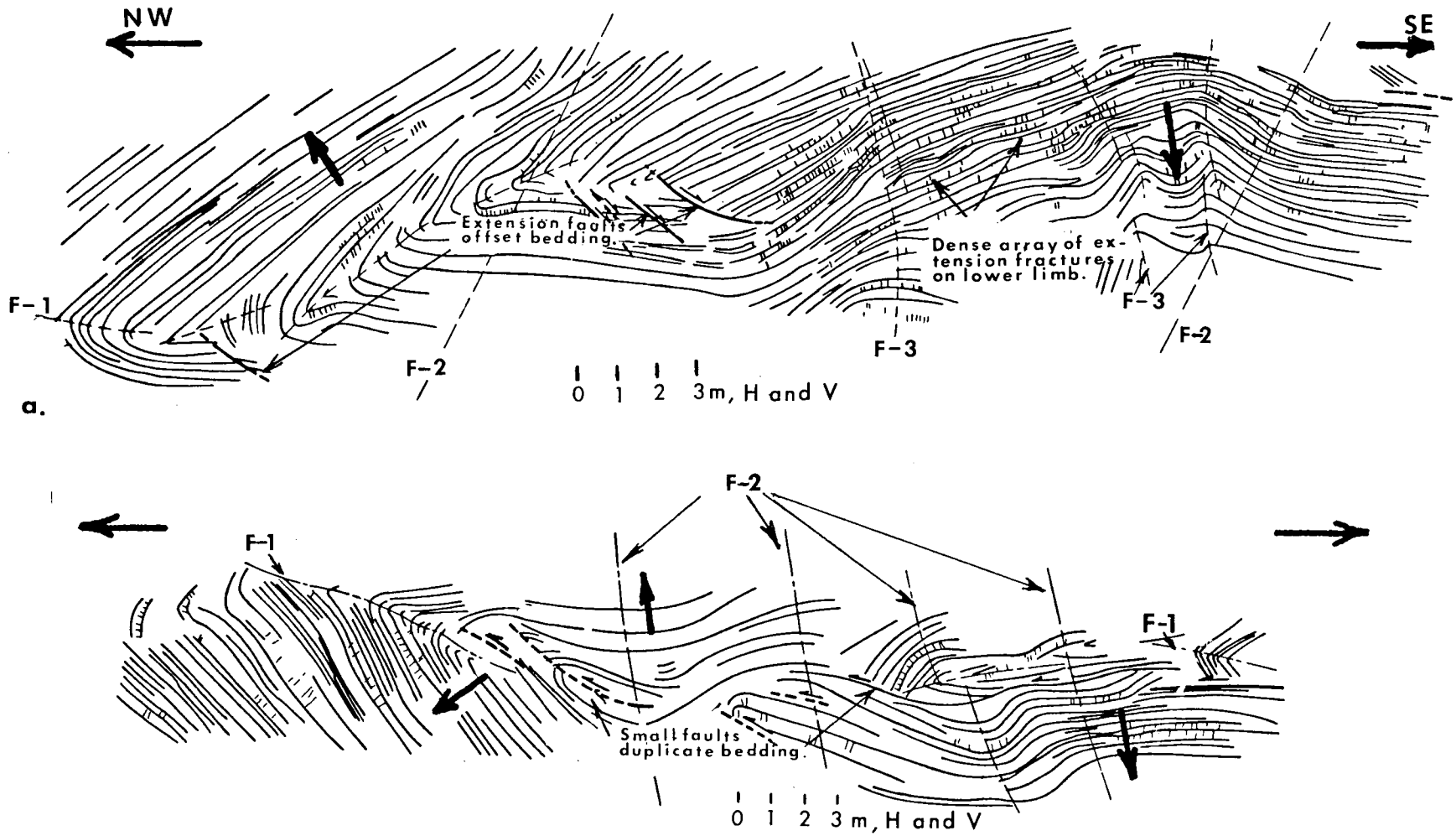

Figure 12. Closeup profiles of selected portions of the outcrop from section LJ (Figure 11). (a) Southeast portion shown on Figure 11. (b) Northwest portion shown on Figure 11.

girdles in Figure 7x. This stereo net configuration is the result of in this case slightly noncylindrical folding in outcrop related to a difference in mean attitudes of the crumpled limbs to either side of their hinges. The noncylindrical distribution here, however, is much less pronounced than in the folds at localities R-11a and R-11b where the AC-plane attitudes are significantly different from that of the folds in the region as a whole. Figure 12a shows that the orientation of the axial planes of the crumpled beds at Section LJ is clearly not the same as that which refolded the anticline (Figure 11). This suggests that a third fold generation (F-3) is recorded here, although evidence for it in the other exposures along strike from locality LJ is not clear.

Also of interest in Figures 22a and b is the presence of extension fractures that are more closely spaced in the lower limb than in the upper limb of the fold. On the upper limb, they nearly disappear at less than a meter from the axial surface trace. This same fracture pattern is seen at all other exposures of the anticline at section LJ, and it is one indication of the origin of the fold (see "Faults in the Study Area," and "Macroscopic Interpretation," this chapter).

The exposures at localities R-12 and R-13 (Plate 1) are also included with subarea III. The outcrop profiles are not included but the measured folds have morphologies resembling those associated with the Little Jacob Creek anticline at

section LJ. The total amount of exposure at R-12 and R-13 is considerably less, however, than at section LJ. Schmidt net plots of bedding poles from these exposures (Figures 7z, xx, p. 28) closely resemble the bedding pole density plots from R-11b in the trend of the AC-plane at each locality. This strong divergence from the trends of AC-planes for folds to the northwest shows a mode of folding for localities R-12 and R-13 that is quite similar to that of R-11a and b, although the clearly bimodal distribution indicating noncylindrical folding is seen only at locality R-11a (Figure 7v).

Subarea IV

This area consists of a relatively undeformed and upright section of coarse-grained conglomerate near the Lucy Creek embayment (Plate 1). This is in contact toward the southeast with a tectonically thickened, overturned section of thinly interbedded siltstone and sandstone (the "lower unit of shale") of King and Ferguson (1960, p. 57). The transition in facing direction toward the southeast reflects the presence of a large subthrust syncline just beneath the Holston Mountain fault (Plate 2). The finer-grained, overturned section exhibits a tight fold style similar to that of the kinks of subarea III. One of the few exposures with this folding style in the subarea is at locality R-14 (Plate 1). Figure 13 is an outcrop profile of a typically deformed section at R-14, derived from field sketches. A

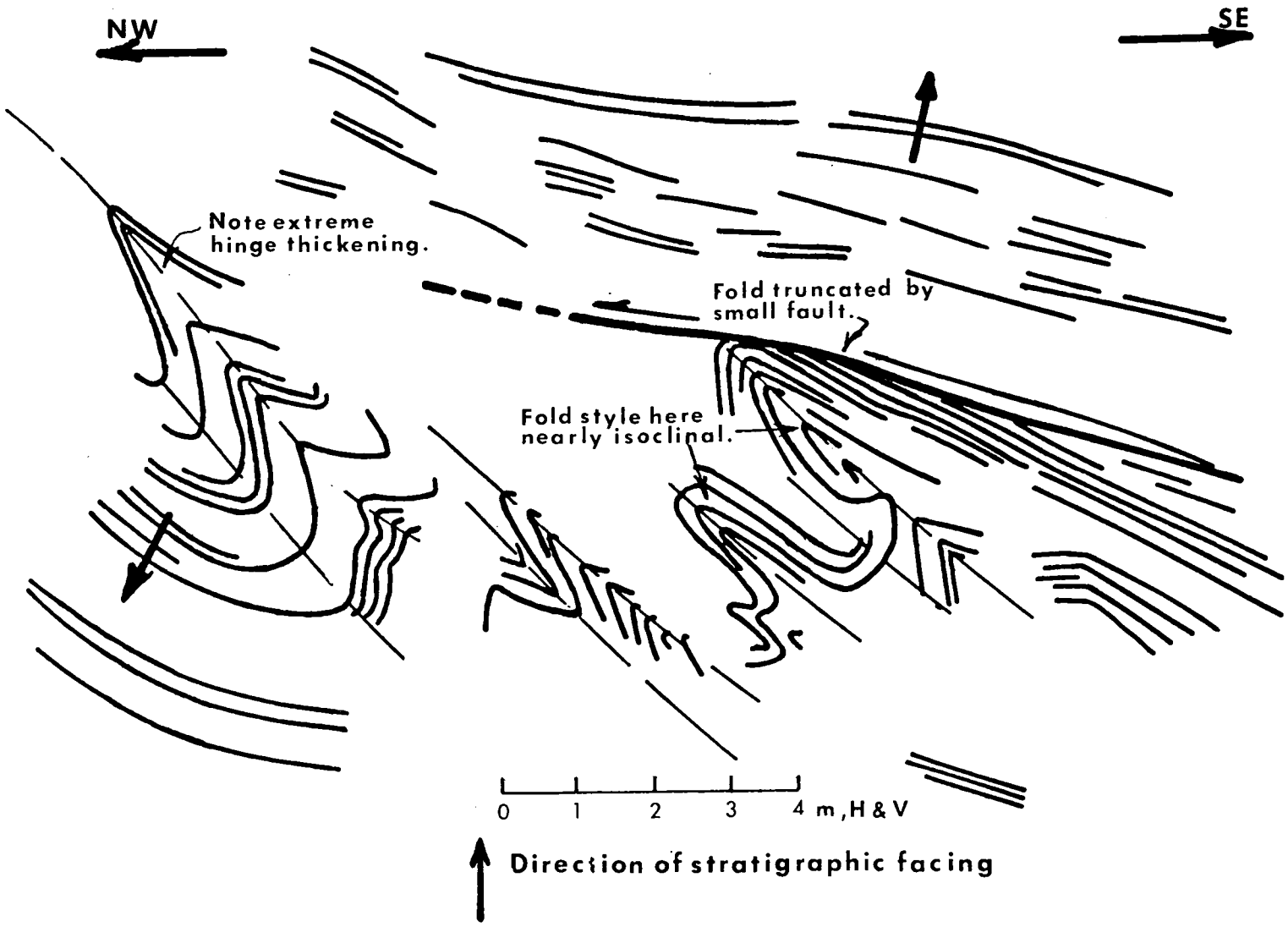

Figure 13. Profile of a section of outcrop at locality R-14.

bedding pole density plot from the vicinity of the profile (Figure 7yy) shows much scatter. This is apparently the result of the loss of coherence of bedding in the vicinity of the large overthrust.

Holston Mountain fault exposure. A portion of the Holston Mountain thrust is exposed at R-15 on U.S. 421, south of locality R-14 (Figure 2, p. 6). Here, early Cambrian-age quartzites of the Chilhowee Group are in contact with overturned bedding of the Tellico-Sevier Formation. Bedding attitudes above and within the fault zone show much scatter (Figure 7zz), as would be expected in the footwall and hanging wall of a major thrust fault (Rodgers, 1953; Harris et al., 1981). The bedding just below the fault has been sheared and stretched, so that in places it is hard to recognize, but it is not tightly folded, nor has it been faulted, in agreement with King and Ferguson (1960, p. 64).

Discussion of lack of obvious cleavage in subareas III and IV. Axial planar cleavage in folds of these subareas is not usually obvious in outcrop. However, the presence of a weak cleavage in subarea III is confirmed by the appearance of minor pencil structures in several folds at section LJ (Plate 1). Pencil structure is formed by the intersection of a weak cleavage with folded bedding (Reks and Gray, 1982). Its presence in some of the folds of subarea III probably

indicates that cleavage was a relatively minor component of the overall strain of these folds. In the folds of subarea IV, no pencil structure exists to confirm the presence of even a fairly weak cleavage. This probably indicates that the folds of this subarea are uncleaved.

Summary of Folding

From the base of The Knobs (Plate 1) toward the southeast, axial planes of F-1 folds, which are initially upright, demonstrate a progressive rotation toward the northwest. Axial planar cleavage, which is most intense in hinge zones, is mainly limited in outcrop to those exposures toward the northwest. Near locality R-4 and toward the southeast (Plate 1) the folds are recumbent and very tight, in some cases nearly isoclinal. Tight kink folds are also an important component of the folding southeast of locality R-4, and in subarea III near the Lucy Creek embayment, markedly noncylindrical folding characterizes the deformation. It is apparently related to a folding event F-2 that has refolded the kinks about nearly vertical axial planes. A separate, less marked F-2 event has also slightly folded axial planes at localities 0-1 and P-1 in subareas I and II, respectively.

In subarea III, the structure is dominated by a recumbent anticline, more than one km in across-strike extent, that has also been refolded about nearly vertical F-2

axial planes. This event was apparently the same one that refolded the kinks at R-11a, b. A suggestion of a later, slightly noncylindrical F-3 fold generation is also recorded in the crumpling of a portion of the bedding seen in Figure 12a.

Faults in the Study Area

Overview

Faults in the study area can be subdivided on three size scales. First-order faults have strike extents of hundreds of kilometers. In the study area, the Holston Mountain and the Pulaski faults are examples of this order of displacement. Second-order faults generally exhibit strike lengths and displacements on an order of magnitude less than first-order faults. The Bristol fault may be an example of this type. However, approximately how much displacement there was on the Bristol fault may not be determinable solely from the author's field evidence. A possible example of a second-order fault in the immediate study area is interpreted as a thrust associated with the Little Jacob Creek anticline (Plate 2). Other investigators recognize the Lodi fault at the same structural position just across the Virginia border (Reks and Gray, 1982, Fig. 1). Minimum displacement along the Lodi is estimated to have been at several tens of meters, and its measured strike length in Tennessee and Virginia is 50 kms,

under the assumption that the inferred subhorizontal fault in the present study area is the southwest extension of it. Except for the Lodi, these named faults are not discussed in great detail here, because they have been adequately mapped and described in other works.

Minor third-order contraction and extension faults (Price, 1967a, p. 44) are ubiquitous in the field area. Their displacement is not more than a few meters, and each fault is not traceable beyond a single outcrop.

Field Observations

Any single movement picture in an orogenic belt can develop four distinct categories of faults that include contraction and extension faults with dips either in the direction of or opposite to the transport direction (Price, 1967a, p. 44). All four of these types are observed in the field area, but they do not occur in the same numbers everywhere. One clear observation is that the intensity of faulting over the area as a whole is in direct proportion to the degree of northwest rotation of F-1 axial surfaces and to the number of kinks observed in outcrop. The most intense faulting and the tightest and most numerous kinks are associated with the overturned limb of the recumbent anticline at section LJ, just as this overturned limb is also characterized by the greatest number of extension fractures of any

outcrop in the study area. Similarly intense faulting and kinking occur in the small exposures of the folded sandstone-siltstone interbeds at locality R-14 just beneath, and at locality R-15 partly within, the Holston Mountain fault (Plate 1; Figure 2, p. 6).

Mesoscopic fold-discordant faults. Mesoscopic faults often cut the bedding down-section where it is overturned. An apparently related set of such mesoscopic faults can be observed in an approximately 2 km wide zone from locality R-4 southeast to R-13. They can all have a discordant relationship to bedding, depending on its local orientation, and they are subparallel across strike (see Figures 8b, 12a, pp. 30, 36). Because they cross-cut folds, while they themselves are not cross-cut, they made up the last phase of the deformation. In a number of cases, faults have apparently isolated mesoscopic fold hinges. Figure 14 is a sketch of one such fold hinge about 50 meters northwest of the recumbent fold profile (Figure 12b) at section LJ. The fold-discordant fault set responsible for the hinge isolation is outlined on the sketch. Other faults, which may make up a conjugate set with the main discordant fault set, are also highlighted. Another characteristic of all the studied discordant faults, as shown in Figure 14, is that they can be either extensional or contractional in sense, depending on their local orientations with respect to bedding.

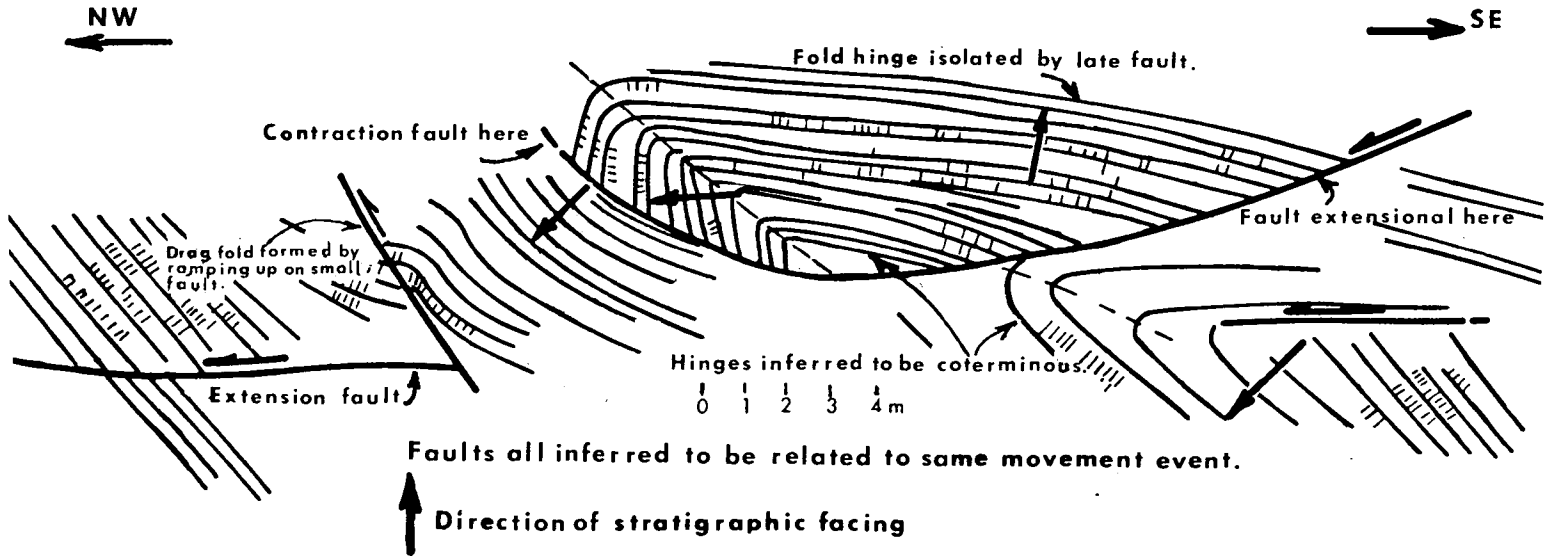

Figure 14. Profile of an isolated fold hinge at section LJ.

Fold-discordant faulting in other areas. The existence of fold-truncating faults in the study area is in accord with the findings of other investigators (Roeder et al., 1978; Witherspoon, 1981; House and Gray, 1982). Their documentation of "fold-discordant thrusting" shows that these features are not only confined to mesoscopic structures in northeast Tennessee. Farther southwest along regional strike, Witherspoon (1981) has interpreted a larger discordant relationship of the Great Smoky thrust sheet to the folds in its footwall. House and Gray (1982) have also observed the truncation of regional folds farther west, across strike in the Saltville thrust sheet in southwest Virginia.

Macroscopic Interpretation

Overview

Any interpretation of the complexly deformed portions of the South Holston area must consider the possible influence of the regional thrust faults. These include the Holston Mountain fault, with its estimated 100 kms of displacement (Harris et al., 1981), and the second-order Lodi fault, which has been documented very near the field area in southwest Virginia (Reks and Gray, 1982). Earlier workers (Bryant and Reed, 1970) have tentatively placed the folding of the Middle Ordovician section in the area as either prethrusting or synkinematic with the emplacement of the Holston Mountain

thrust sheet. The present author suggests that most of the structure from The Knobs (Plate 1) southeastward is synkinematic with the emplacement of the first-order regional thrust sheet, which would have extended its influence well into its footwall. The evidences for this are (1) increasing northwest rotation and tightening of folds in the direction of the Holston Mountain fault, and (2) the strongly kinked and faulted strata, also overturned, just beneath the Holston Mountain fault at locality R-14 (Figure 13, p. 39). The complexly refolded structure within section LJ and at the several localities along strike of it to the southwest (Plate 1) is tentatively interpreted as synkinematic with movements along the Lodi fault.

Discussion of the Lodi Fault

The Lodi fault has been interpreted as one of two intermediate-sized thrust faults within the Pulaski thrust sheet (Reks and Gray, 1982). One other, the Spurgeon, is shown in the regional cross-section (Plate 3). By the most recent mapping (Reks and Gray, 1982, Fig. 1), the Lodi climbs up section from the Conasauga Group in Virginia and cuts intraformationally through the Sevier just north of the State boundary, where it loses all its visible stratigraphic separation. The author observed an approximately 2 km wide zone in the study area, approximately along the strike of the

Lodi, involving several small, apparently related thrusts, as previously indicated. The zone extends from about locality R-4 to just southeast of section LJ, past the last exposure of the Little Jacob Creek anticline (Plate 1). The author's interpretation of the subhorizontal thrust fault (Plate 2) as being coterminous with the Lodi and as related to the Little Jacob Creek structure is generally upheld by a structural analysis of a portion of the Saltville fault in southwest Virginia (House and Gray, 1982) and by theoretical and field studies of other workers (Heim, 1921; Dahlstrom, 1970; Elliott, 1976). House and Gray established that the north termination of the first-order Saltville fault was a regional, northwest-facing, overturned fold, the Sinking Creek anticline. This fold formed by a displacement transfer phenomenon in which faulting movements along the Saltville thrust were taken up by folding in the anticline as the fault died out. Two similarities exist between the small, regional fold in the present field area and the larger structure documented in southwest Virginia. First, as confirmed by their field observations (House and Gray, 1982, p. 833), theory (Elliott, 1976) requires strongly noncylindrical folding near the closure of such a fold. Second, they observed significantly higher strains in the overturned limb than in the upright limb of the structure. In the present study, the significant development of extension fractures,

kinks, and mesoscopic faults in the overturned limb of a portion of the fold exposed at section LJ has already been documented (Figure 12a, 36). Additionally, from fabric diagrams, I observed markedly noncylindrical folding at localities R-11a,b. Similar Schmidt net patterns were observed at localities R-12 and R-13 (Figures 7z, xx, p. 28). These localities are very near the place where the fold closes, apparently just southwest of the Lucy Creek embayment. Noncylindricity can also be noted in the map view in the vicinity of the southwest fold closure at localities R-12 and R-13, where there occurs a marked divergence of the fold's hinge line by comparison with its other exposures at section LJ, about two kms northeast (Plate 1), where the mapped axes are essentially parallel to those of the other folds in the region. Evidence for relatively more cylindrical folding at section LJ is also provided by fabric diagrams from the area (Figures 7x, y) that mimic those of the cylindrical folds to the northwest in their trend, although Figure 7x is slightly noncylindrical. These evidences implicate the Lodi fault in the formation of the Little Jacob Creek structure by displacement transfer. However, displacement transfer may have been partially accommodated by the previously documented two-to-three-km-wide zone of fairly intense mesoscopic faulting observed roughly along the strike of the Lodi fault from locality R-4 to R-13. The total displacement from this cause

could have been considerable, although this is a conclusion that the field evidence can only tentatively support.

Field data from just southeast of section LJ suggest that much of the strain in the section was relieved by the movements that formed the recumbent fold. The intensity and amount of strain increases again, however, in the vicinity of the Holston Mountain fault exposure, as shown by locality R-14 (Figures 7yy, 13, pp. 28, 39).

Macroscopic deformation mechanisms. Movements along subsurface decollements can cause folding in the overlying strata by either (1) passive formation above ramps due to upright shearing of detachment thrusts, or (2) buckle folding of the overlying strata due to movements along subsurface decollements (Simon, 1981; House and Gray, 1982). The presence of large, upward-shearing thrusts has been established as a general tectonic style from seismic data, and it is required to balance regional cross-sections. Other investigators studying large regional folds in the southwest Virginia Valley and Ridge (House and Gray, 1982) have suggested that at least one formed passively by the upward-shearing of the regional fault with which it was associated. My geometric analyses of the mesoscopic folds in the present study area have established active buckling in a regional compressive stress field as the predominant mechanism (see

Chapter 3). One possible source for the buckling in the Tellico-Sevier is provided by the synformal folding of the Knox Group. The total magnitude of movements along the Holston Mountain fault was considerable during emplacement of the Holston Mountain thrust sheet. Much of the folding of the South Holston synclinorium would have been directly related to this emplacement. Imbricate ramps in the Tellico-Sevier infilled the regions that were constricted as a result of the faulting movements (Plate 2).

Relative deformation chronology. Faulting movements due to emplacement of the Holston Mountain thrust sheet occurred earlier than the movements along the Pulaski fault. This is shown by the folding of the Holston Mountain sheet by the Pulaski (Plate 3). Therefore, many of the structures in the South Holston complex formed prior to final emplacement of the Pulaski thrust sheet, on which they were transported. The second-order Lodi fault, interpreted as a splay off the Pulaski, surfaces about 14 kms east of Bristol (Reks and Gray, 1982, Fig. 1). This implies that whatever deformation in Tennessee is associated with the Lodi would likely have occurred later than the emplacement of the Holston Mountain thrust sheet, but before final emplacement of the Pulaski. The Lodi deformations would have overprinted earlier structures formed when the Holston Mountain thrust occurred. The actual

quantitative extent of the overprinting may not be determinable, but it does seem responsible for the well-defined gradient of increasing structural complexity that is approximately contained within the zone occupied by the Little Jacob Creek anticline (Plate 1). The two or possibly three fold events recorded in subarea III (Figures 10, 11, pp. 32, 35) are also a reflection of these later generations of fold-fault movements.

Effects of later fault imbricates. Warping of the underlying Pulaski fault by later movements from beneath may have affected the final orientation of the folds in the study area. The author's regional cross-section, among others (Roeder et al., 1978; Harris et al., 1981), indicates that these later disturbances were not significant in the vicinity of the study area. The cross-sections also indicate that later movements beneath the Pulaski have affected the folds within the area of investigation to the same extent. Thus, conclusions drawn on the basis of mean strain analyses from Schmidt nets are valid within their limits of accuracy with respect to these deep movements. Any warping by later movements along decollements within the Tellico-Sevier, as in the case of the Little Jacob Creek structure, would be closely associated with the primary structures in the strike belt. These effects should not lead to erroneous conclusions, as long as they can be recognized.

Analysis of Brittle Deformations

Overview. A graphical study of a number of faults at locality P-1 and at section LJ (Plate 1) was undertaken to estimate the orientation of the associated "deformation axes" (Arthaud, 1969) in order to compare these orientations at two separate localities across strike. In Arthaud's (1969) technique, the attitude of a fault surface and the trend and plunge of its associated slickenside are measured. The method is applicable only to brittle deformation, and it is based on two general principles: (1) that the geometry of the rock after deformation depends only on the orientation and direction of movement of faults during the tectonic phase considered and (2) that one can always characterize three orthogonal directions in the deformed rock after a given phase of deformation such that the projection of one of those axes on a fault surface is the direction of relative movement of the block separated by those faults (Arthaud, 1969, p. 6). The three principal directions are defined as X, the maximum extension direction; Y, the intermediate principal direction; and Z, the maximum contraction direction. With each fault, one can associate a plane that is perpendicular to the fault and contains the striation direction. This plane is called the "m" plane, or movement plane, and by the second principle it contains at least one of the principal directions of the

deformation. All the "m" planes which contain a given principal direction will have a common intersection that corresponds to that principal direction. Theoretically, since the deformed rock contains three principal directions, the "m" planes should be grouped into three families that together follow the three orthogonal directions that correspond to the principal deformation axes. Once X, Y, and Z are fixed, one can determine the sense of movement shown by the striations in each plane and then fix the relative positions of the X, Y, and Z axes that give the correct movement for each displacement observed. In practice, one graphically finds the deformation axes on a stereonet by a four-step process (Arthaud, 1969, p. 8):

1. Plot the pole of the fault plane (F) and the trace of striations (S) on that fault plane on a stereonet.
2. F and S are rotated to a great circle that is the trace of the "m" plane, from which the pole (m) is fixed.
3. Repeat Nos. 1 and 2 for each fault.
4. All the "m" planes containing a given principal direction that is their common intersection have their pole in the plane perpendicular to this direction. The "m" poles will plot along great

circles, and the pole of one of these great circles corresponds to a principal axis of deformation.

Results of fracture analysis. Figures 15a and b are stereonet plots of measured faults at locality P-1 and at section LJ, with the traces of slickenside orientations, the great circles defined by the "m" poles through which they passed, and the "m" poles themselves plotted. Also shown are the piercing points defining the X, Y, and Z deformation axes. The piercing points determined the trends of the three principal deformation axes for each plot. Although the two localities exhibit quite different structural styles (Figures 8c, 11, pp. 30, 35) and are separated across strike by more than two kms, their deformation axes are oriented quite similarly (Figures 15a, b). The result indicates that the faulting movements which produced these structures are nearly coaxial across strike. Because the faults always crosscut the folds, the faults constituted the last phase of deformation. However, the principal strain axes defining folding movements may not have been oriented much differently with respect to an absolute frame of reference during the earlier phases of movement. If so, this would indicate that the overall, or bulk strains for the folding deformation were closely coaxial, also.

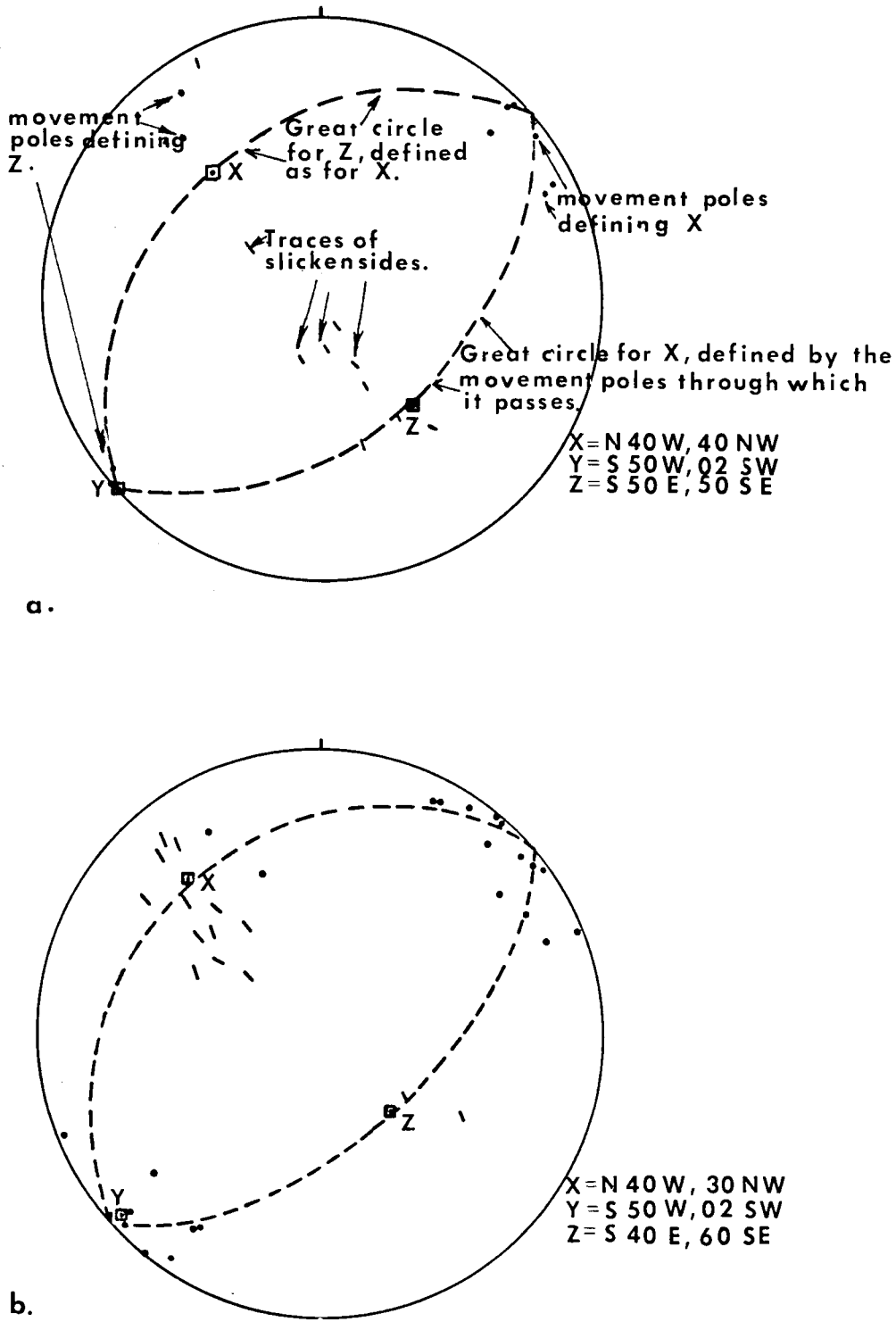

Figure 15. Two Schmidt net plots of faults in the study area for Arthaud's (1969) analysis. (a) Fault population at locality P-1. (b) Fault population at section LJ.

Regional Trends in Schmidt Net Analysis

Table 1 is a summary of the estimated orientations of AC-planes and B-axes at a number of studied localities southeastward of The Knobs in the vicinity of the study area. Except for locality R-0, that seems anomalous, the data show a fairly consistent westward variation in strike for each AC-plane up through locality R-4. Past R-4, the AC-attitudes fluctuate until locality R-11a, at the northwest end of subarea III, through locality R-13, where the noncylindrical folding believed associated with the Little Jacob Creek anticline has dominated the structure. Throughout subarea IV, the AC-planes again mimic those of the region affected by predominantly cylindrical folding.

Relationship of structure to applied stress. Recumbent and asymmetric folds, such as are common in the field area, are usually believed to have formed in an external stress field, one or more of whose principal directions were not precisely parallel to the layered rock in its original horizontal configuration (Price, 1967b; Treagus, 1973, 1981; Stringer and Treagus, 1980). Price (1967b) has suggested that in a large, multilayered system, the imposition of the maximum principal stress, σ_1, oblique to bedding induces initially asymmetric buckles that amplify and rotate to greater states of asymmetry for as long as the stress is

Table 1

Approximate Attitudes of AC-Planes and Fold Axes through the Strike Belt

Subarea	Locality	Distance (kms)	AC Attitudes	Fold Axis Attitudes
I	R-0	.2	N40W,80SW	N50E
	LV	1.0	N22W,90	N70E
	LS-3	1.1	N32W,76NE	N50E
II	LS-2	1.2	N40W, 90	N50E
I	R-1	1.2	N35W,86SW	N55E
	O-3	1.3	N34W,90	N51E
II	R-3	1.8	N44W,86SW	N48E
	R-4	2.0	N54W,85NE	N40E
	P-1	2.0	N44W,80NE	N46E
	R-7	2.3	N42W,82SE	N50E
	R-8	2.5	N50W,86SE	N40E
	R-9	2.5	N43W,75NE	N47E
III	R11-a	3.3	N12E,72NW	----
			N50W,63NE	N40E
	R11-b	3.3+	N07W,80SW	N80E
	R-12	3.7	N25W,82SW	N65E
	R-13	3.7+	N26W,90	N64E
	LJ-b	3.7	N50W,90	N40E
	LJ-a	3.7+	N25W,90	----
			N43W,80SW	N50E
IV	R-14	6.6	N42W,82SW	N48E
	R-15	7.0	N63W,83SW	N27E

applied. His model was restricted to the buckling of end-loaded beams in two dimensions (Price, 1967b, eq. 1). This is an oversimplified system compared with natural three-dimensional multilayers. But in a theoretical study of asymmetric buckling in three dimensions, Treagus (1981) considered the effects of applying a stress field to a multilayered system in which all of the principal stresses were oblique to the layering. Her results indicated that buckles should nucleate symmetrically, but become progressively asymmetric with continued application of stress. The folded bedding should change simultaneously in strike and dip. The mathematical basis for this behavior is beyond the scope of this report. However, some of the possible physical reasons for it can be discussed qualitatively.

Discussions of dynamic model. It is assumed here that the principal stress directions σ_1, σ_2, and σ_3 remain unchanged in their orientation with respect to a hypothetical, stationary reference frame during stress application. If all the principal stress directions were oblique to bedding, the folds that nucleated in the material would be subjected to turning moments as a result of this asymmetry. This would lead very early to mechanical instabilities that would have to be balanced by two or more simultaneous rotations of the folds' axial surfaces. As long as the stresses were applied,

the folds would become more asymmetric and would continue to change in their trends with respect to the same frame to which the stresses were referenced.

Relationship of modelling to cleavage formation and folding. Borradaile (1978, pp. 482-486) and Stringer and Treagus (1980, p. 327) have applied the results of similar theoreticlal work to real folds in Canada and Scotland. They suggest that in addition to the progressive changes in fold orientation, the imposition of an asymmetric stress field would strongly influence the orientations of fold-related cleavage. First-formed cleavage is expected to closely parallel the σ_2-σ_3 plane of the stress ellipsoid, and the λ_1-λ_2 plane of the bulk strain ellipsoid (Treagus, 1981). In general, however, subsequent cleavage would not be expected to develop in an axial planar relationship to the folds that are induced simultaneously by the same stress field. This relates to the fact that the fold axial surface orientations are constrained by the layers. The layers act as stress guides and respond to the stress field somewhat differently than the cleavage. Cleavage can be refracted between layers of contrasting stiffness, but generally it is not as confined in its orientation by the layering as the fold itself (Borradaile, 1978, pp. 482-486; Stringer and Treagus, 1980, p. 327). By this hypothesis, folds with a transecting and

not an axial planar cleavage should typify deformation in the most general tectonic settings. However, in many naturally occurring multilayered systems, the "two-dimensionally oblique" situation of parallelism and of 0 degrees strike of σ_2 to the bedding is probably closely approximated (Treagus, 1973, 1981). In these systems, cleaved folds will develop with their cleavage-bedding lineations closely parallel to the fold axes, while any syntectonic cleavage should not noticeably transect the developing folds. The progression from initially symmetric to asymmetric buckles should proceed as in the more general case, but without variations in strike of the folded bedding.

Application of model to field area. The study area of this report seems to have been tectonically similar to Treagus' (1973) two-dimensional model up through cleavage formation, as shown both by the axial planar foliation and by the very presence of asymmetric folds. However, the noticeable variation in attitude of folded bedding toward the southeast of the study area (Table 1), not including localities R-11a through R-13, suggests that a more general stress field was responsible for part of the structure after cleavage had developed (also see "Timing of Cleavage with Respect to Folding," Chapter 3). In the study of the two fault populations, previously analyzed for their principal

deformation axes, Y (roughly equivalent to λ_2) was shown to be nearly horizontal, and it approximated the average regional strike of the bedding in its trend. This indicates to a first approximation that the intermediate deformation axis was parallel to an associated intermediate stress axis, σ_2. However, the σ_2 and Y-deformation axes could have departed locally or on a map scale from the trend of the folding bedding during certain stages of the deformation. This could have been caused by local-to-map scale irregularities in strike of the bedding as deformation progressed. For example, when the tectonic wedge to the southeast built up and began moving northwest, an irregular resistance to movement could have been encountered in the foreland. The syntectonic development of the northwesterly adjacent anticline in the thick, stiff Knox Group could have produced such a resistance. Also, the whole Paleozoic sequence has been moved in mass to the northwest along lower-lying decollements (Plate 3). This movement could have altered the strike of the bedding while the primary stress field responsible for the South Holston structures was still acting on them. Additionally, because the primary stress field in the area is believed to be the emplacement of the Holston Mountain thrust sheet, strata to the southeast would have been subjected to deformation for a longer time than strata to the northwest. This would be the principal reason for the

observed marked increase in fold asymmetry to the southeast and a possible additional reason for the observed across-strike variation in bedding trends. The slight but noticeable folding of the two axial planes at localities 0-1 and P-1 (Figures 6, 8c; pp. 27, 30) could also be explained by a continuous, relatively protracted deformation recorded as refolding at these localities. The later folding associated with the closure of the Little Jacob Creek anticline, which begins at about locality R-11a, was clearly noncylindrical in outcrop and in map view (Figures 7v, z, xx, p. 28) (Plate 1). The deformation here overprinted the cylindrical folds formed in an earlier stress field, so that the original structures and bedding attitudes have both been removed in this area. However, the mapped hinge lines of the fold at localities R-12 and R-13 (Plate 1) in the same lithology and at slightly different positions across strike are approximately parallel. This evidence, combined with the observation of near-parallelism in deformation axes at section LJ and locality P-1, suggests that deformation in the Little Jacob Creek anticline was approximately coaxial within the structure itself and with respect to the deformed strata to the northwest that were not influenced by it.

Extension of the theoretical modelling. Some of the recent working hypotheses in dynamic analysis have been

extended to include the development of heterotactic fabrics, such as noncoaxially superposed folds, in one continuous deformation (Borradaile, 1978; Treagus, 1980; Stringer and Treagus, 1980, p. 327). This is theoretically possible in a three-dimensionally asymmetric stress field. The heterotactic fabrics in the study area are similar to those observed by other workers in Valley and Ridge terrains in east Tennessee. They were generally attributed to a polyphase, or noncontinuous deformation occurring over geologically distinct time intervals with different orientations of applied stress (Roeder and Witherspoon, 1978; Roeder et al., 1978). The field evidence from the South Holston region, correlated with theoretical and field work previously discussed, suggest that the movement history of the area was continuous. In some cases, a continuous deformation may be able to explain other heterotactic fabrics diagnosed as indicating noncontinuous, or polyphase deformations. The author mentions this interpretation to explain the heterotactic fabrics observed in the area around South Holston Lake, but cautions that widespread disturbances will occur discontinuously over extended times (Hatcher, 1973, 1978).

CHAPTER 3

FOLDING AND CLEAVAGE RELATIONSHIPS AND FOLD SHAPE MODIFICATION

Overview

If folding mode and shape modification processes can be categorized by characteristic patterns of fold tightness, cleavage fanning and bedding-cleavage angles (see Gray, 1981a), then comparison of real fold patterns with theoretical models of folding may provide a method for inferring the actual folding mechanisms and the relationship of folding with cleavage in the field area. The author examined fold profile photographs of 26 cleaved folds across regional strike in order to determine the angular relationships between cleavage and bedding, to study the relationship of fold interlimb angle (β) as a measure of fold tightness and indirectly of fold flattening with cleavage fan angle (γ), and to compare both with published theoretical fold models. Fold profile geometries and flattening curves were determined, because nearly all the folds in the area have been subjected to substantial shape modification by the imposition of flattening strains. In general, the cleaved folds are of the "buckle" type so that the present discussion is restricted primarily to buckle-type folds.

In most cases where the folds are cleaved, the cleavage fans symmetrically about the folds' axial surfaces. Even where the cleavage fans but little, it parallels the fold axial traces. This suggests a close relationship between cleavage and folding (Hills, 1966; Dietrich, 1969). Field evidence indicates that all the folds studied in this chapter are close to cylindrical forms, so that two-dimensional profile analyses are valid. Regional structural trends can be projected northeast and southwest to the extent of the study area.

Three major lithologies occur in the area, each of which responded more or less distinctly to the deformation. Fine-grained medium-to-thinly interbedded sandstone and siltstone occur throughout most of the area. The fine-grained calcareous mudrock of the lower Sevier occurs in a series of lake shore exposures that start at locality 0-1 and continue in a section toward the northwest up to the base of The Knobs (Plate 1).

Representative folds in the first two lithologies have been treated in the following discussion in some detail. Folds formed in the coarse conglomerate were relatively rare and uncleaved, so that they were not included in the graphical analyses, but they have been discussed qualitatively.

Fold Geometry and Classification

Careful description and classification of fold geometry is important if we are to compare natural folds to those produced in theoretical and experimental models. Ramsay's (1967) classification scheme, which will be used in this discussion, is based upon the (1) orthogonal, or stratigraphic, thickness of folded layers (t), (2) layer thickness parallel to the fold axis surface (T), and (3) inclination of dip isogons (lines connecting points of equal dip in a profile of folded surfaces). The classes in this scheme are presented in Figure 16. In Class 1 folds, dip isogons converge toward the axial plane; Class 2 folds show dip isogons that parallel the axial plane; and in Class 3 folds, dip isogons diverge from the axial plane. According to Ramsay, folds formed by buckling generally fall into Class 1. Folds with a "similar" geometry, thought to be developed by passive slip or flow across the layers in a direction parallel to the fold axial plane form Class 2, though this geometry is not often truly achieved in nature (Ramsay, 1967, p. 431). Generally speaking, folded multilayers do not maintain the same geometry or class from layer to layer. Certain layers may control or exert an influence on other, less "competent" layers in a "zone of contact strain" so that the fold shape varies from layer to layer. As a result, those beds that are

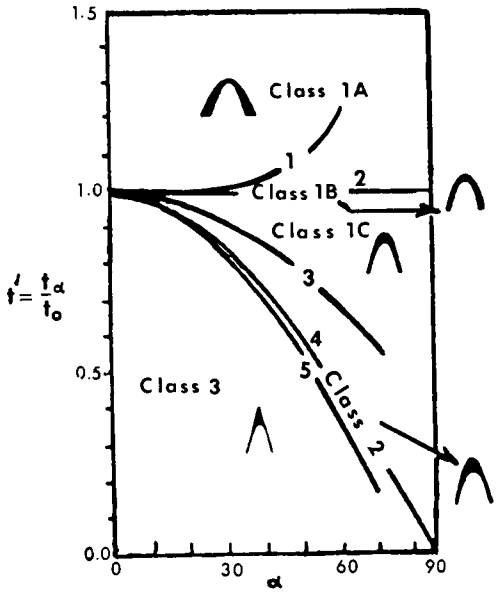

Position of t'_α plots for the various fundamental fold classes.

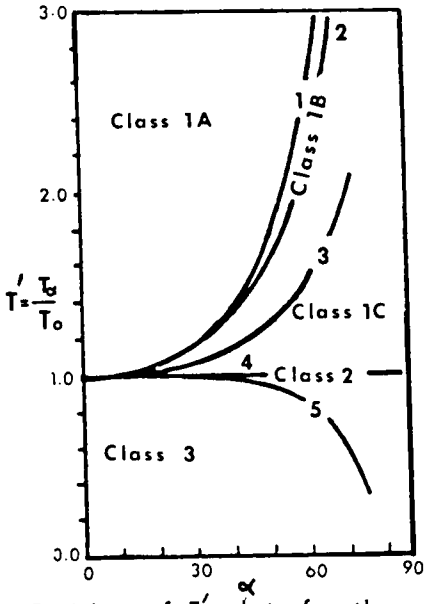

Position of T'_α plots for the various fundamental fold classes.

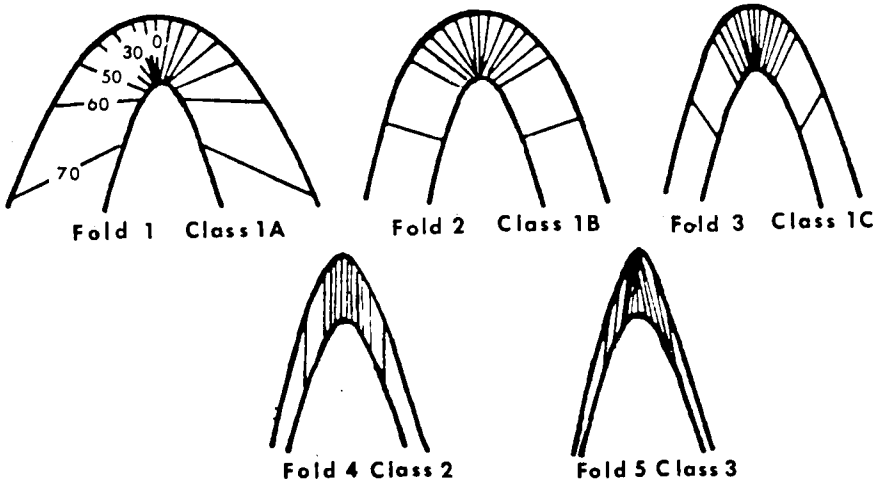

Fundamental types of fold classes. Dip isogons have been drawn at 10° intervals.

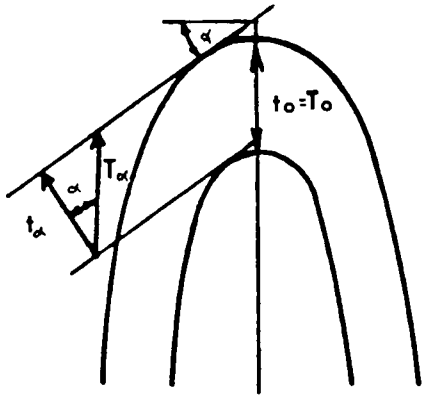

Cross-section of folded layer with geometric parameters.

Figure 16. Classification of fold geometries adopted from Ramsay (1967).

constrained in their geometry by the deformation of the more competent layers generally exhibit a Class 3 geometry.

Another important component of fold geometry is that imposed by flattening strains that accumulate during the folding process. As defined by Ramsay (1967, pp. 411-412), in only two dimensions, fold flattening is superposed on a fold of originally concentric geometry by an homogeneous strain with quadratic extensions λ_1 parallel to the axial surface and λ_2 normal to this surface. This always produces a thickening in the hinge and a thinning in the limbs. This strain, termed Rf in this report, has been evaluated by Ramsay (1967, Fig. 7-79) as $\sqrt{\lambda_2/\lambda_1}$. He has plotted a number of ideal flattening curves expressing the relative thickness ratio of limb to hinge against fold limb dips for comparison with real folds. In more recent work, Gray and Durney (1979, Fig. 14) have modified Ramsay's (1967) flattening curves in order to more accurately reflect the flattening strains imposed on real folds. They show that these strains can be validly determined only up to 60 degrees of limb dip. They have also redefined the limb dips with respect to the orientation of the fold axial surfaces, so that these techniques can also be applied to asymmetric and inclined folds. Gray and Durney (1979) redefine Rf as $\sqrt{\lambda_1/\lambda_2}$, but the definitions of λ_1 and λ_2 are the same as Ramsay's (1967)

definition. The modified version of the fold flattening curves and of Rf will be used in this discussion.

Fold Classification and Fold Flattening Strains in the Study Area

Fold flattening curves have been determined for 26 folded layers at several localities across strike in this study area. Table 2 summarizes the information on fold geometries, flattening strain ratio, and cleavage fan and interlimb angles according to map locality (Plate 1). Rf strains imposed on the folds are seen to vary from unity in the folds that plot in Class 1B to "infinity" for certain folded layers that plot in Class 3 field of Ramsay's (1967, Fig. 7-25) fold classification. Dip isogon patterns show that individual folded layers within single folds consisting of several layers typically alternate between Class 1C (slightly convergent isogons) and Class 3 (strongly divergent isogons). The corresponding Rf values vary also between these two fields, since the two parameters measure the same geometric characteristics (Hobbs et al., 1976, p. 175). Several examples of folds from two localities of calcareous mudstone are representative of the observed geometries and are discussed below.

Locality 0-1 (Lower Sevier)

Figure 17 is a tracing from a portion of the profile from this locality. The folds that were studied are numbered

Table 2

Summary of Interlimb Angle (β), Cleavage Fan Angle (γ), Cleavage-Bedding Geometry ($\alpha/S_0 \wedge S_1$), Flattening Strain Ratio (Rf), and Classification of Folds Investigated in This Study

Locality	Fold No.	β (degrees)	γ (degrees)	Data for $\alpha/S_0 \wedge S_1$ r	m	b	Rf NW	Rf SE	Fold Class NW	Fold Class SE	Lithology
	1	65	23	-0.82	-0.50	71.3	∞->1.8	∞->1.3	3->1C	3->1C	calcareous
	2	114	20	-0.85	-0.50	59.2	-	-	-	-	mudrock
	3	101	5	-0.51	-0.10	17.4	1.0	1.0	1B	1B	
	4A	-	-	-0.81	-0.91	99.4	-	∞->4.0	-	3->1C	
	B	53	42	-0.81	-0.91	99.4	∞	∞	3	3	
0-1	5	57	37	-0.85	-0.79	85.6	2- 10	1.6- 2.5	1C	1C	
	6A	93	37	-0.89	-0.90	84.2	∞	1.6->2.5	3	1C	
	B	90	11	-0.93	-0.86	78.7	∞	∞	3	3	
	7	77	43	-0.92	-1.2	103	1.4->2.5	1.2->∞	1C	1C->3	
	8	103	26	-0.63	-0.40	44.8	-	-	-	-	
	9	90	22	-0.79	-0.70	73.3	-	-	-	-	
	10	106	-	-0.93	-0.81	81	-	3.0	-	1C	
0-2	11	118	18	-0.93	-0.81	81	2.0	1.2	1C	1C	
	12	84	39	-	-	-	-	-	-	-	
(Data	13	-	-	-0.76	-0.90	95	1.6	2.0	1C	1C	
taken	14	-	-	-0.76	-0.90	95	1.7	3.0	1C	1C	
from	15	-	-	-0.93	-0.81	81	1.6	1.2	1C	1C	
selected layers in fold sets 1 and 2, Fig. 19)											
R-1	16	44	-	-	-	-	1.4	1.6	1C	1C	siltstone-
	17	30	17	-0.94	-0.96	93	1.9	1.4	1C	1C	sandstone
R-3	18	40	35	-0.84	-0.99	102	1.3->∞	3.6->∞	1C->3	1C->3	
	19	31	30	(Data for all			-	-	-	-	
	20	34	40	five folds)			-	-	-	-	
R-4	21	31	12	-0.95	-0.99	89	1.1	1.4	1C	1C	
	22	30	4				∞	∞	3	3	
	23	25	-				1.4->∞	10->∞	2	2	
	24	80	25	-0.98	-0.87	80	1.4	1.9	1C	1C	
	25	60	9	-0.95	-.78	76	2.8->∞	-	1C->3	-	
LS-3	26	31	29	-0.95	-0.86	84	∞	1.8	3	1C	
	27	77	17	-0.96	-1.1	101	-	-	-	-	
	28	65	40	-0.91	-1.2	108	-	-	-	-	
Little	29	54	37	-	-	-	3	2.5	1C	1C	
Jacob	30	53	60	-	-	-	2.5	3	1C	1C	
Creek	31	49	18	-	-	-	∞	2.5	3	1C	
(Section LJ)											
P-1	32	78	-	-	-	-	1.6	1.8	1C	1C	

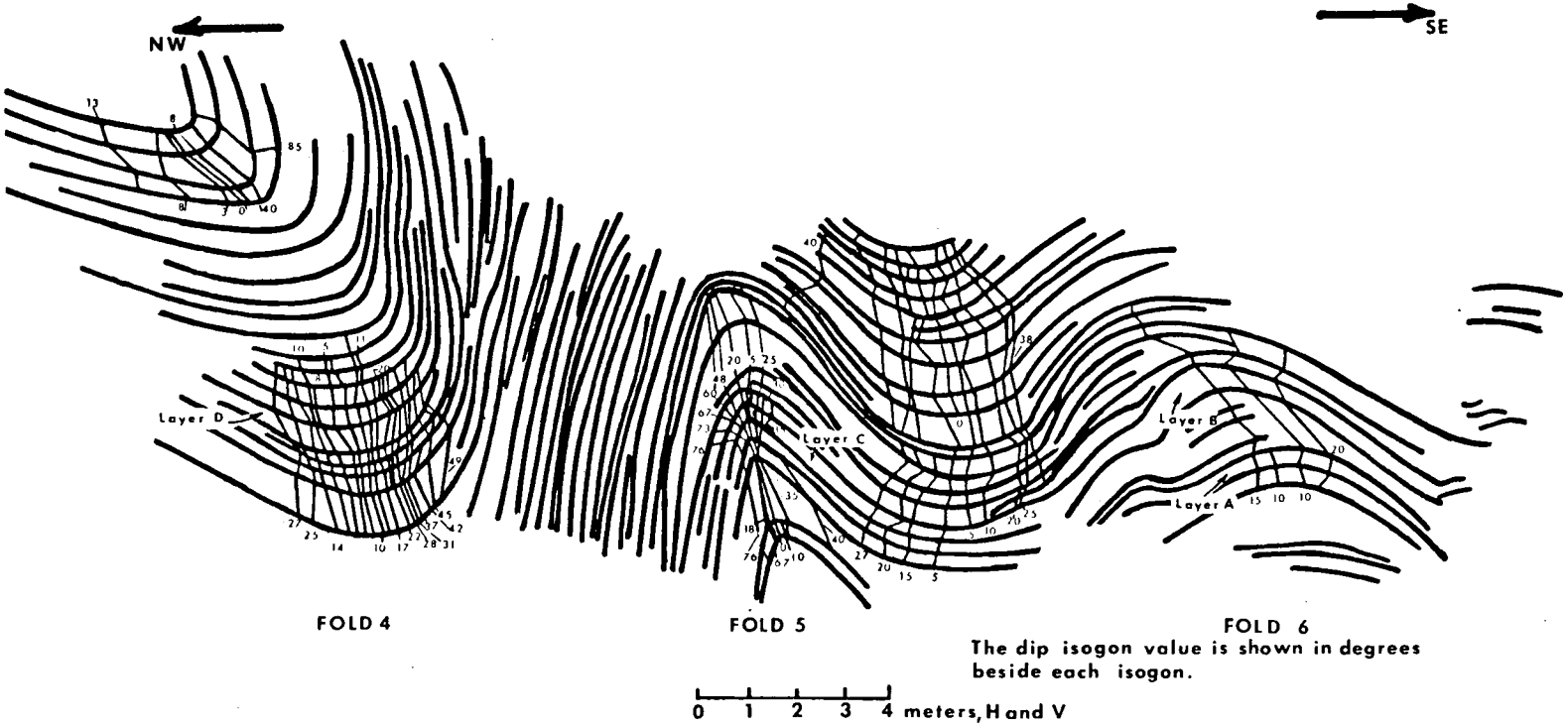

Figure 17. Fold profile from locality 0-1, lower Sevier, with dip isogons included.

4 through 6, and the layers whose flattening curves were plotted are shown by letters A through D. The dip isogons are superposed on the fold profiles, and the corresponding flattening curves are superposed on the ideal flattening curves from Gray and Durney (1979, Fig. 14) in Figure 18. I have included curves showing flattening strains of 1, 1.2, 1.6, 2.5, and infinity (corresponding to a similar fold) on Figure 18. All of the analyzed layers plot within the Class 3 field for at least part of their extent, but particularly so at higher limb dips, so that all of the real flattening curves more or less systematically transgress the idealized curves. Hudleston (1973b, p. 304) demonstrates that such real flattening strains indicate that flattening was imposed on the folds during buckling rather than as homogeneous strains after they had already formed as mature, concentric folds, which is the basis for constructing the ideal curves (Ramsay, 1967, pp. 411-412). The ideal flattening curves also have a regular outline, required by homogeneity, in contrast to the real data (Figure 18). Essentially the same graphical relationships have been seen in the other folds whose flattening values were plotted. The flattening mechanism was therefore more complex than the theory can constrain (Ramsay, 1967; Gray and Durney, 1979). The dip isogon pattern in the anticline labelled 5 (Figure 17) demonstrates a pronounced alternation in fold geometry from

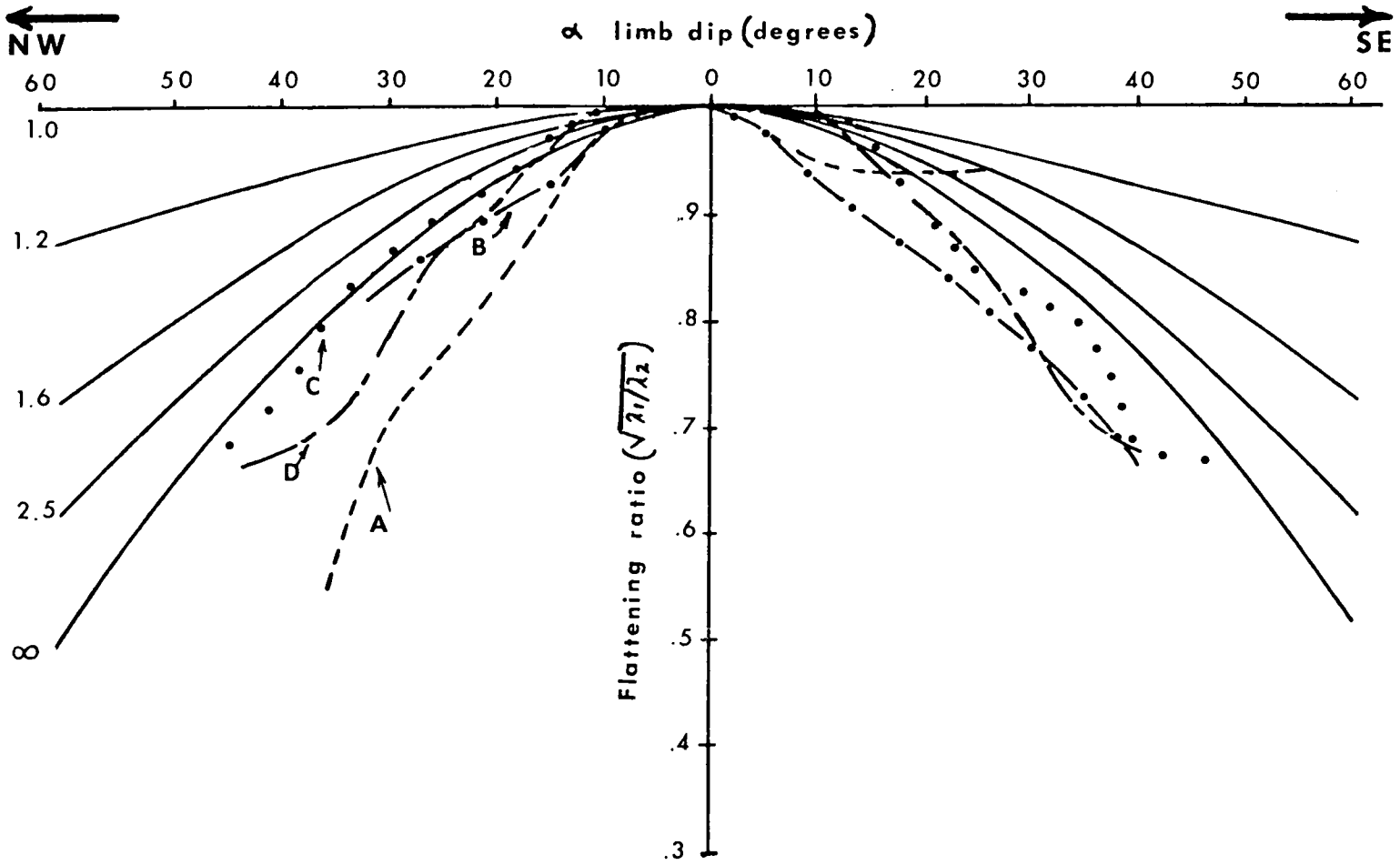

Figure 18. Fold flattening curves for selected layers from profile at locality 0-1, lower Sevier.

Class 3 in the thickened regions to Class 1C in the beds between. The other isogon patterns in neighboring folds resemble that of fold 5. Such alternations in fold geometry are controlled by contrasting ductilities in neighboring beds (Hudleston, 1973a; Currie et al., 1962). An "incompetent" layer will typically plot in the Class 3 field, while the stiff layers usually have a Class 1C geometry. The dip isogon patterns are a direct reflection of the different resistances of the interlayers to deformation in an external compressive stress field, since the "competent" layers tend to retain their original parallel geometry during folding while the "incompetent" layers flatten.

Locality 0-2 (Lower Sevier)

A second example of interlayer variation in fold class occurs at locality 0-2 (Plate 1), reproduced in Figure 19. Here, a slightly coarser-grained lithology than is typical of the Lower Sevier has been deformed into a set of kink-like folds. The author is focusing on layers A, B, and C of fold set 1 in the following discussion. These folds bear features more or less typical of zones of "contact strain" around buckled layers (Ramsay, 1967, p. 416). The most distinctive feature of such folds, characteristic of all such zones of contact strain, is the increase in interlimb angle stratigraphically up and away from the most strongly folded parts of the

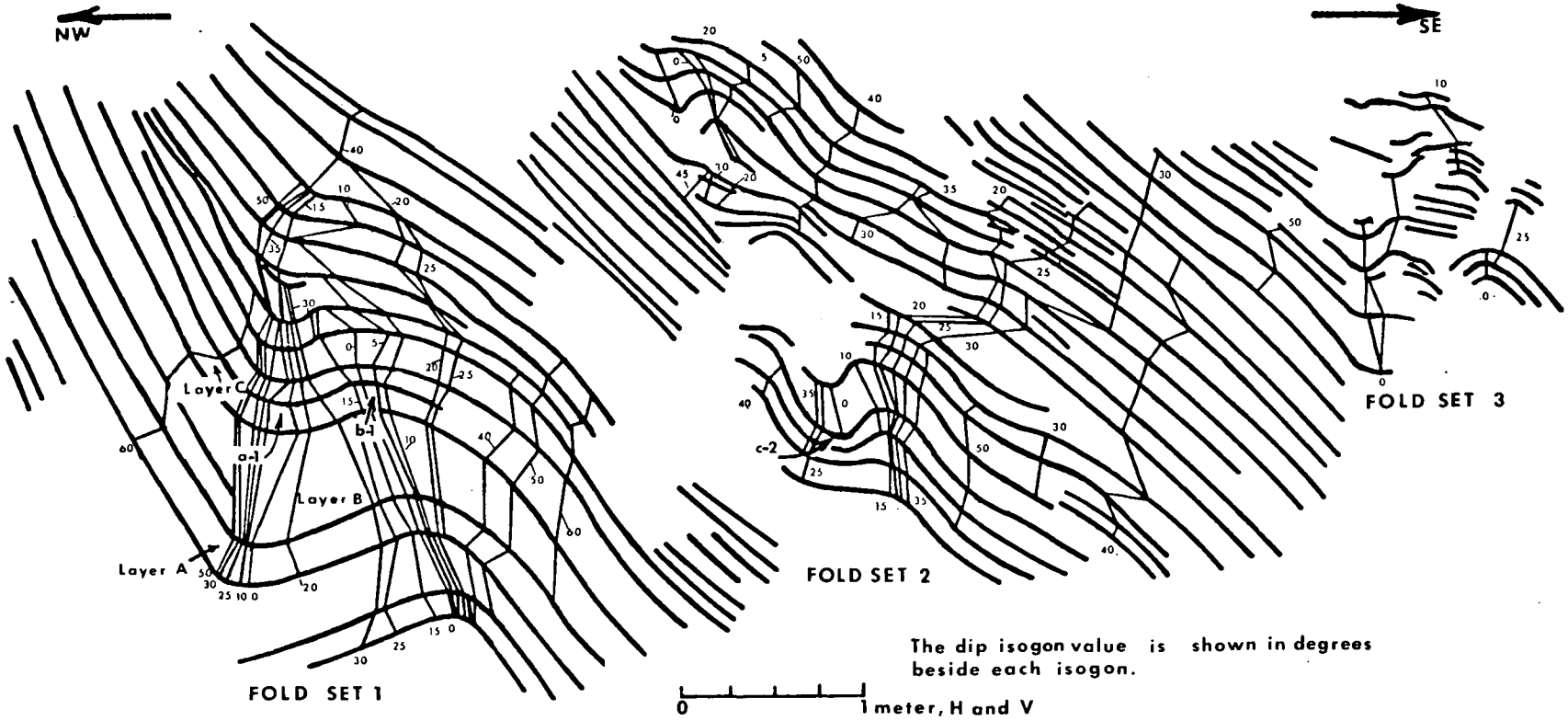

Figure 19. Fold profile from locality 0-2, lower Sevier, with dip isogons included.

folds at their cores. This effect occurs because at some distance away from the actively buckled layers the bedding undergoes homogeneous shortening without folding, but near the buckled layers this bedding is subjected to inhomogeneous strain and assumes a folded form. The profile of the fold set (Figure 19), with its closed isogon pattern and the study of interlimb angle variation (Figure 20) demonstrate this effect. The region bears other features that are more or less identical to those found in other contact strain zones predicted by buckling theory (Ramsay, 1967, Fig. 7-81A) in the shape assumed by adjacent layers. In the idealized example described by Ramsay, the folded incompetent layers within the inner arcs of a stiff buckled layer take up a Class 3 geometry, while in the outer arc they are of a Class 1A. The buckled layer itself of Class 1B throughout, showing that the incompetent beds adjusted themselves to conform to the stiff layer, since its geometry is unchanged. Thus, the stiff layer "controlled" the shape of the fold. In the present study, the large incompetent layer B, which seems to be a composite of several thinner layers, takes up a Class 3 geometry on the inner arcs of buckled layers A and C, which are also composites, while it assumes a less strongly Class 3 geometry on their outer arcs. The stiff layers A and C take up a Class 1C geometry throughout. In the sense of the idealized example (Ramsay, 1967, p. 416), they control

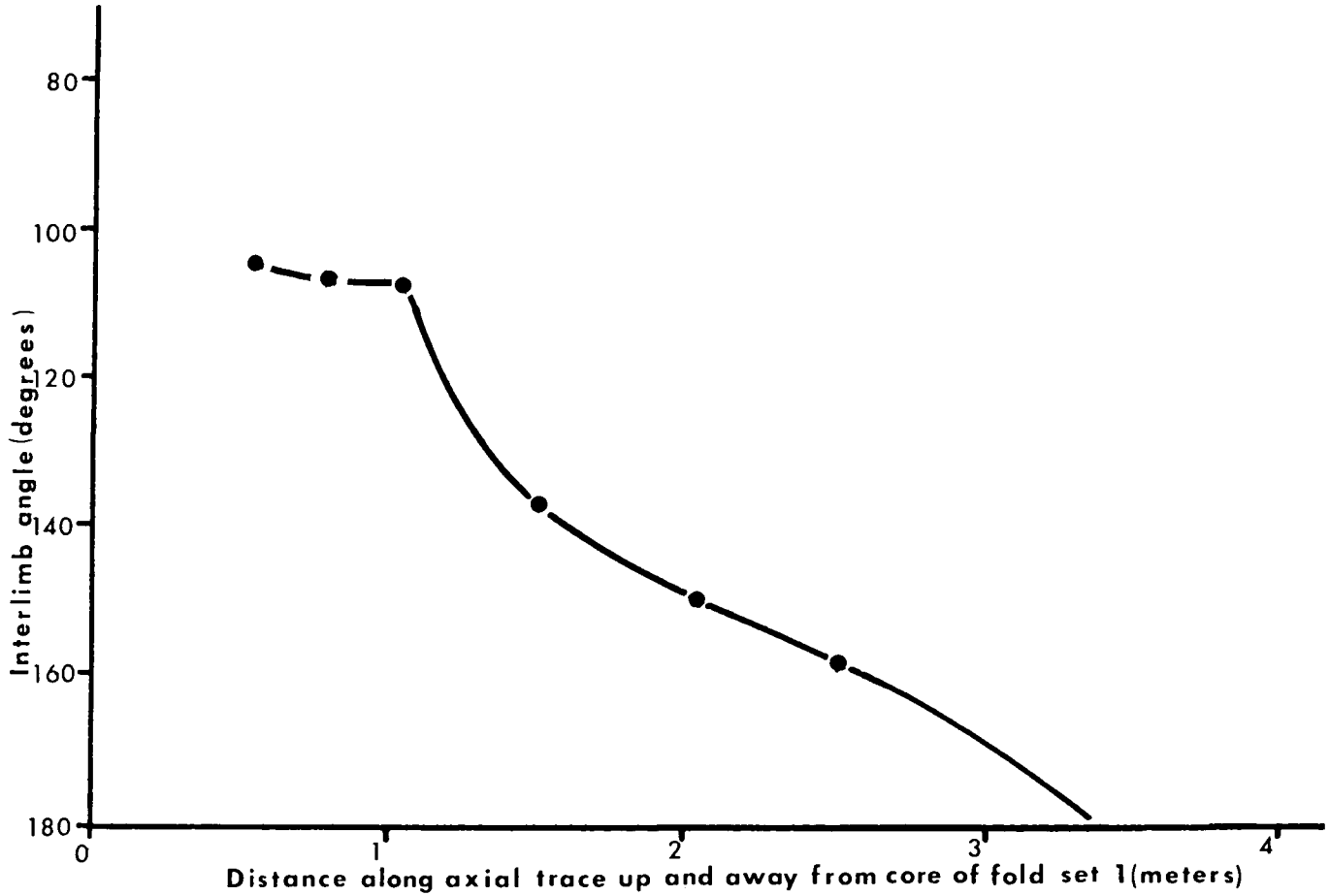

Figure 20. Interlimb angle variation with distance from fold core for fold set 1 at locality 0-2.

the fold geometry. The modified geometries of layers A and C may be produced by uniformly flattening the buckled layers along with their zone of contact strain, while the original fold geometry may have been similar to that described by Ramsay (1967). The actual amounts of flattening sustained by stiff portions a-1 and b-1 in layer C of fold set 1 and by stiff layer c-2 in fold set 2 are shown in Figure 21.

Correspondence of folds at locality 0-2 with theoretical flattening and fold class. The relatively good correspondence of these layers (Figure 21) with theory compared with those of the last example requires explanation. This fold set is suggestive of a recently nucleated fold that has just begun to amplify (see Cobbold et al., 1971, Fig. 10), from its shape and its slight northwesterly vergence. In this case, it would have received proportionately less flattening strain than the other mature folds, which have nearly all sustained more fold flattening (Table 2, p. 71). The alternation from Class 1C to Class 3 geometry, which is repeated twice more in the sequence, suggests that several layers controlled the fold geometry (Hudleston, 1973b). Layers A and C here are analogous to the "lithic units" of Currie et al. (1962). These authors define a lithic unit as a relatively stiff layer in a multilayered system that tends to control the overall geometry of the developing folds. In the case of the

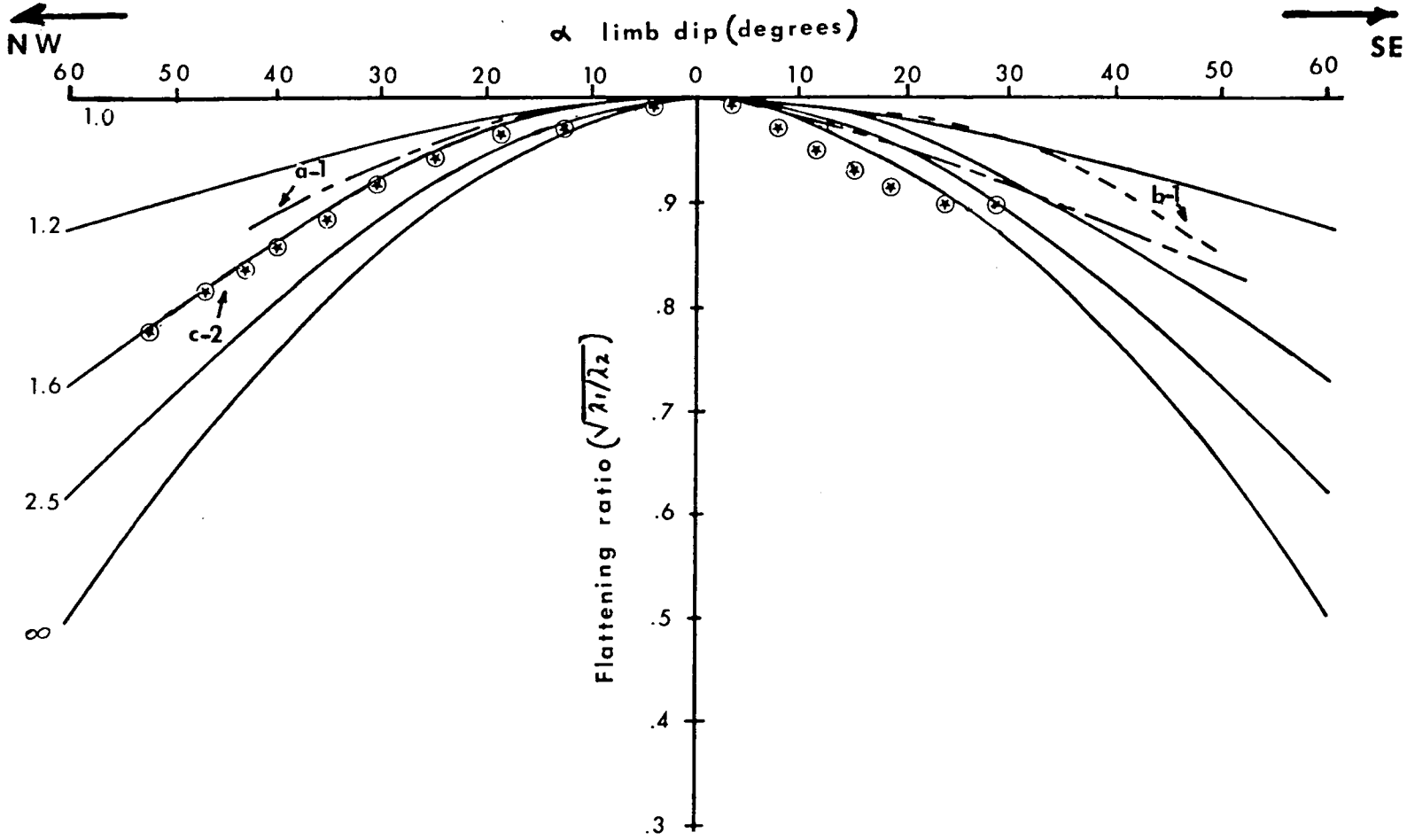

Figure 21. Fold flattening curves for selected layers from profile at locality 0-2, lower Sevier.

folds at 0-2, the presence of the lithic units and their effects in the deformation were not obvious without dip isogon analysis.

Lithic Units and Fold Geometry

Other more obvious examples of lithic units exist in the study area: in particular, the coarse conglomerate beds more than one meter thick that are exposed near locality LS-1 (Plate 1). They are interbedded with much thinner, fine-grained sandstone beds. Where these conglomerate lenses are folded, their forms are nearly parallel and relatively open compared to the folds in the more abundant finer-grained rocks. Figure 22a is an enlarged tracing of the syncline in the middle upper inset of Figure 9 (p. 31) from this locality. This fold has apparently fractured at the hinge. The brittle behavior of the conglomerate has clearly been responsible for the failure of the fold to achieve a tighter interlimb angle before fracturing. Other folds in finer-grained lithologies at this point within the strike belt are normally very tight (see Figure 9). A number of chevron folds that occur in several exposures around South Holston Lake exhibit collapsed hinge structures (Hills, 1963; Cobbold et al., 1971, p. 46; Ramsay, 1974). These were formed when the stiff beds separated from the incompetent layers as the fold tightened beyond the point at which buckling would occur to accommodate

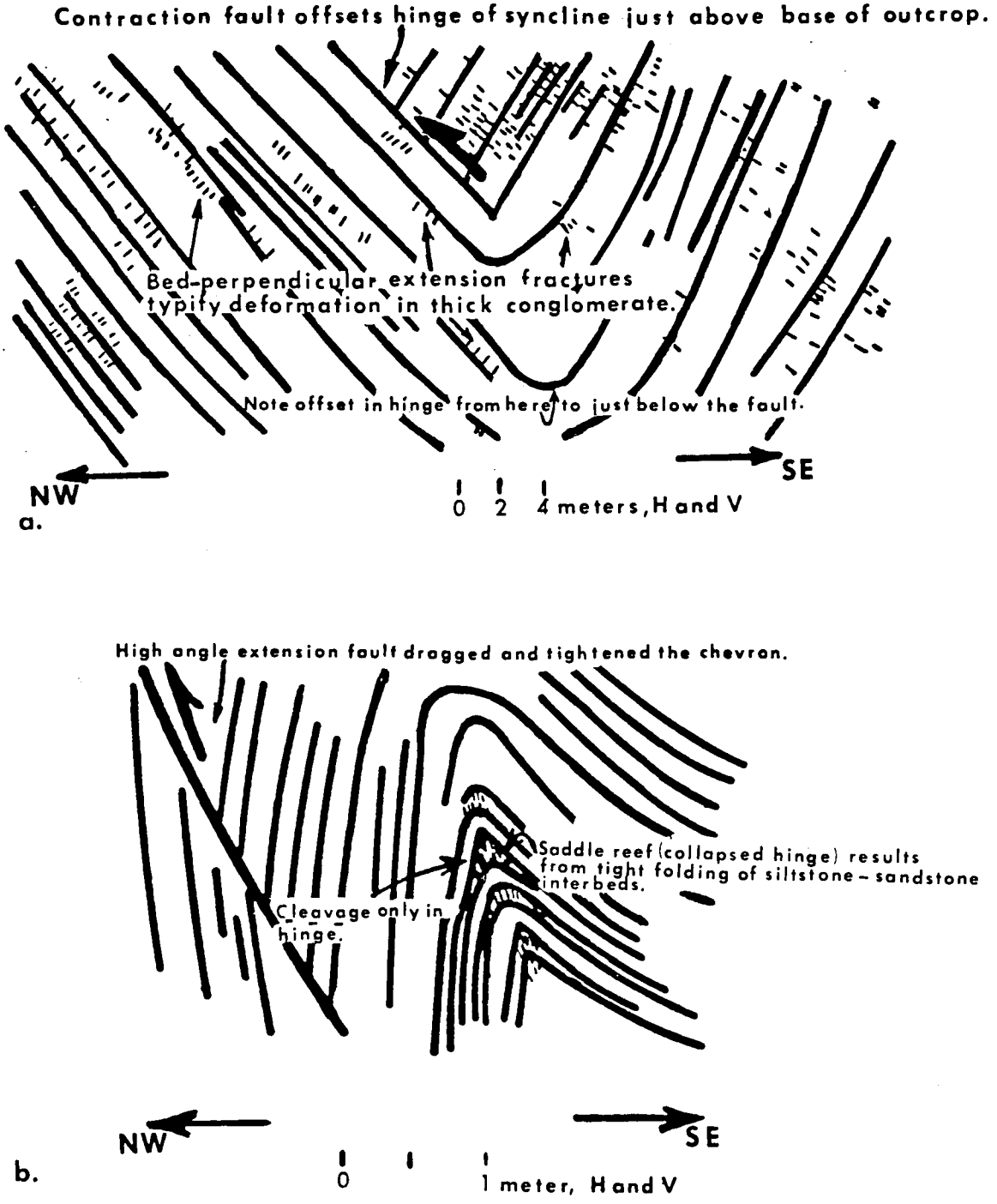

Figure 22. Enlarged profiles from two outcrops showing effects of stiff layers on fold geometries. (a) Relatively open syncline near locality LS-1. (b) Saddle reef structure developed in anticline at locality R-1.

the shortening (Ramsay, 1974, Fig. 8). As the stiffer layers collapsed inward, the finer-grained materials adjusted their shape to conform to that of the stiff layers. Figure 22b is an enlarged tracing of such a structure taken from the upper left inset of Figure 5 (p. 25) at locality R-1 (Plate 1). Medium-bedded, but relatively coarse-grained and stiff sandstone beds have collapsed and produced a "saddle reef" (Ramsay, 1974), apparently in response to a tightening of the fold over a high angle extension fault.

Interlayer Contrasts in Ductility

Hudleston and Stephansson (1973, p. 317) experimentally determined that very low interlayer contrasts in viscosity were required to produce significant fold flattening in multilayers. They found that simultaneous buckling and flattening could proceed only under conditions of similarly low contrast. In this study, I use "ductility" rather than viscosity to describe relative resistances of rock layers to deforming stress. This is because "viscosity" is a specific, measurable parameter and the use of this term implies that one understands the rheology of the rock undergoing deformation (Ramberg, 1964; Biot, 1965). The rheology for any given rock type is rarely known, and it may be unattainable in the field. Nonetheless, the terms "viscosity" and "ductility" are approximately analogous in meaning.

Field evidence indicates that the ductility contrast for the deformed rocks in this study was also relatively "low." In cases where obviously stiffer than normal beds locally exerted dominant control on fold geometries (Figures 22a, b), the higher ductility contrast can be related to the involvement of relatively coarser-grained lithologies in the folding. The author was unable to determine a quantitative value for the contrast that earlier workers could produce from mechanical and digital analogs of folding (Hudleston, 1973a; Hudleston and Stephansson, 1973, p. 317). To do this, a dominant, or most abundant wavelength would need to be determined at each folded locality. This is because interlayer viscosity or ductility contrast is partly dependent on this dominant wavelength (Biot, 1965; Chapple, 1968). Most of the folds in the study area have quite variable wavelengths, and folds of different wavelengths are typically juxtaposed. This is in part the result of the departure of the real rocks from the idealized homogeneous materials assumed in theory. The asymmetry of the real folds also violates one of the bases for application of the dominant wavelength relationship, that which assumes perfectly symmetrical folding (Sherwin and Chapple, 1968; Hudleston, 1973a). Thus, only a qualitative understanding of ductility contrast can be derived from the geometric analyses.

Finite Strain

Finite strain analysis of the deformed Tellico-Sevier was not readily made, partially because there were very few suitable strain markers. Substantial finite shortening must have accompanied the deformation in light of some of the foregoing discussions. In numerical analogs of folding of multilayers at low ductility contrast, shortenings of some tens of percent occurred before the development of significant buckles (Dietrich and Carter, 1969; Hudleston, 1973c). In the present study, as in other deformed regions, buckle shortening, fold flattening and contraction faulting must have added a few more percent to the overall finite strain.

Other field studies. Finite strain studies in thrust sheets are rare in the literature. In one such study, Simon (1981) found that the shortening within a portion of the Narrows thrust sheet in southwest Virginia at the same stratigraphic level as the Tellico-Sevier was quite heterogeneous and locally approached values of about 70 percent. Other workers in Valley and Ridge thrust sheets of southwest Virginia and east Tennessee have shown that finite strains were quite heterogeneous (Wise, 1980; Reks and Gray, 1982), and that the finite shortenings were on the order of at least a few tens of percent. These values can only roughly constrain the shortening in the study area. This is because

the deformed portions in the South Holston region occur between relatively long homoclines, and there has apparently been some complex intraformational thrust faulting with undeterminable displacement. The distribution of finite strains here is probably no less heterogeneous than in these other documented areas.

Cleavage-Fold Geometry and Folding Mechanism

Overview

The close geometric relationship between cleavage and associated folds, and their implicit geometric relationship, suggests that the study of the angular relations between cleavage and folded layers may provide useful information bearing upon fold mechanisms and timing of cleavage development with respect to folding. Gray (1981a) found systematic angular relations between cleavage, bedding, and fold axial planes that could be related to folding mechanisms in deformed calcareous mudrocks in the Narrows thrust sheet in Virginia. Gray's approach, which is employed in this study, is to compare fold limb dips (α) and cleavage-bedding angles $S_0 \wedge S_1$ for each α from real folds with those predicted from several theoretical modes of folding. Comparison of cleavage fan angle (γ) with fold interlimb angle (β) for the two main cleaved lithologies is also made to determine if lithologic controls on cleavage development can be observed. The

various geometric parameters for the analysis are depicted in Figure 23. Four types of theoretical models are used for comparison in this study: (1) Groshong's (1975) pressure-solution modification (Figure 24); (2) Ramsay's (1967) model of tangential-longitudinal strain; (3) Ramsay's (1967) flexural flow model; and (4) Dietrich's (1969) viscous models. Plots of $\alpha/S_0 \wedge S_1$ for models 1 and 3 are presented in Figures 25a and b. The $\alpha/S_0 \wedge S_1$ plots from two versions of model 4 are in Figures 26a and b. Ramsay's model for tangential-longitudinal strain has effectively the same geometry as Groshong's (1975) model A, and so it has not been plotted separately. Ramsay's flexural flow model has also been plotted with fold flattening strains (Rf) equal to 1.5 and 2.0, because many of the studied folds exhibit flattening strains whose average value is roughly the same as these. The calculations for flexural flow were made assuming that cleavage was (1) in existence prior to folding, (2) orthogonal to bedding prior to folding, and (3) rotated as a passive marker surface during folding. Dietrich's (1969) two numerical models are of single layer viscous buckles in which cleavage orientation is controlled by the maximum extension directions of local finite strain ellipsoids within the layer. The maximum extension directions are parallel to the cleavage traces. Cleavage is assumed in Dietrich's (1969) models to have developed synchronously with the folds.

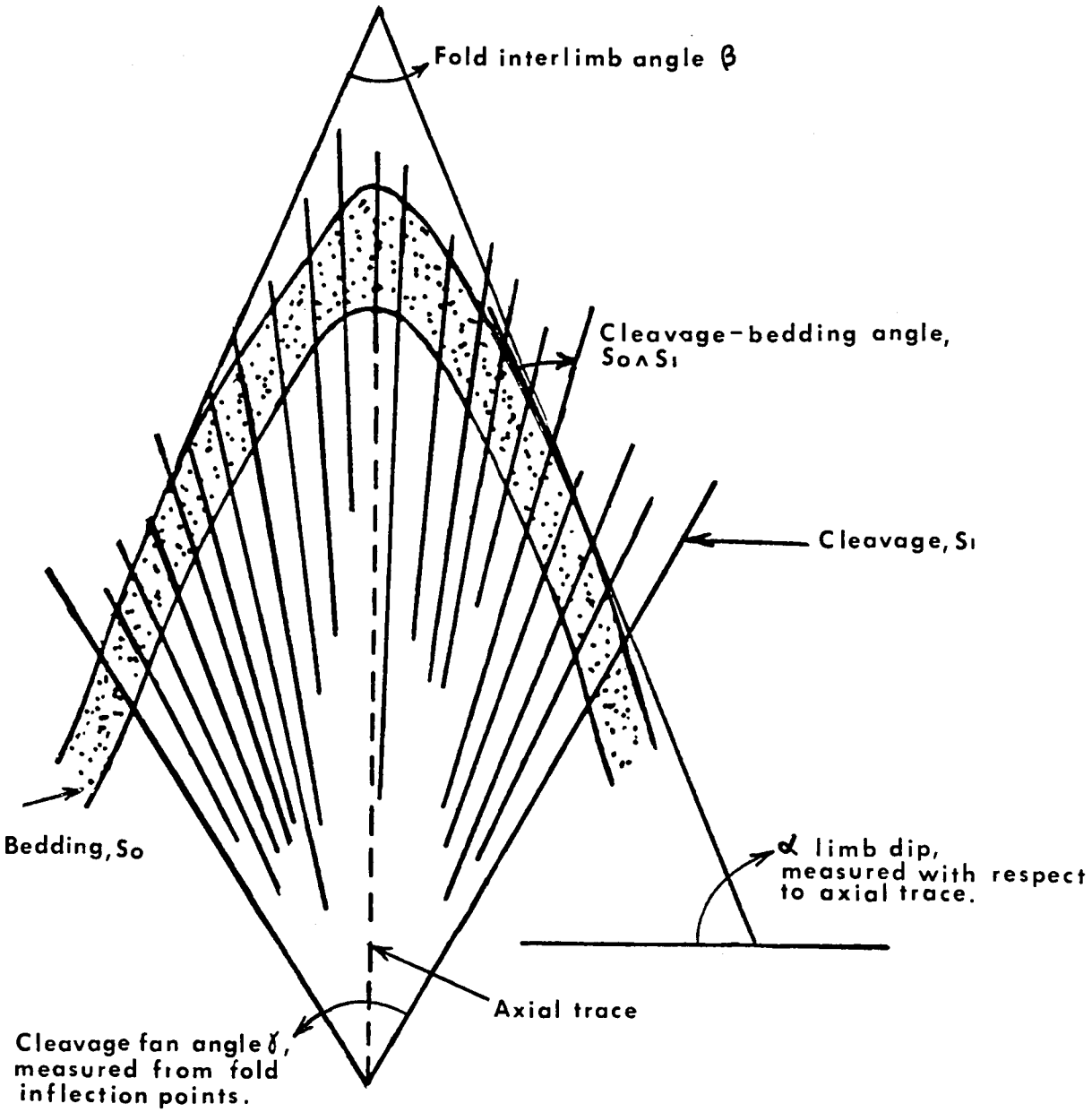

Figure 23. Various parameters required for determination of folding mechanism by cleavage-fold geometry.

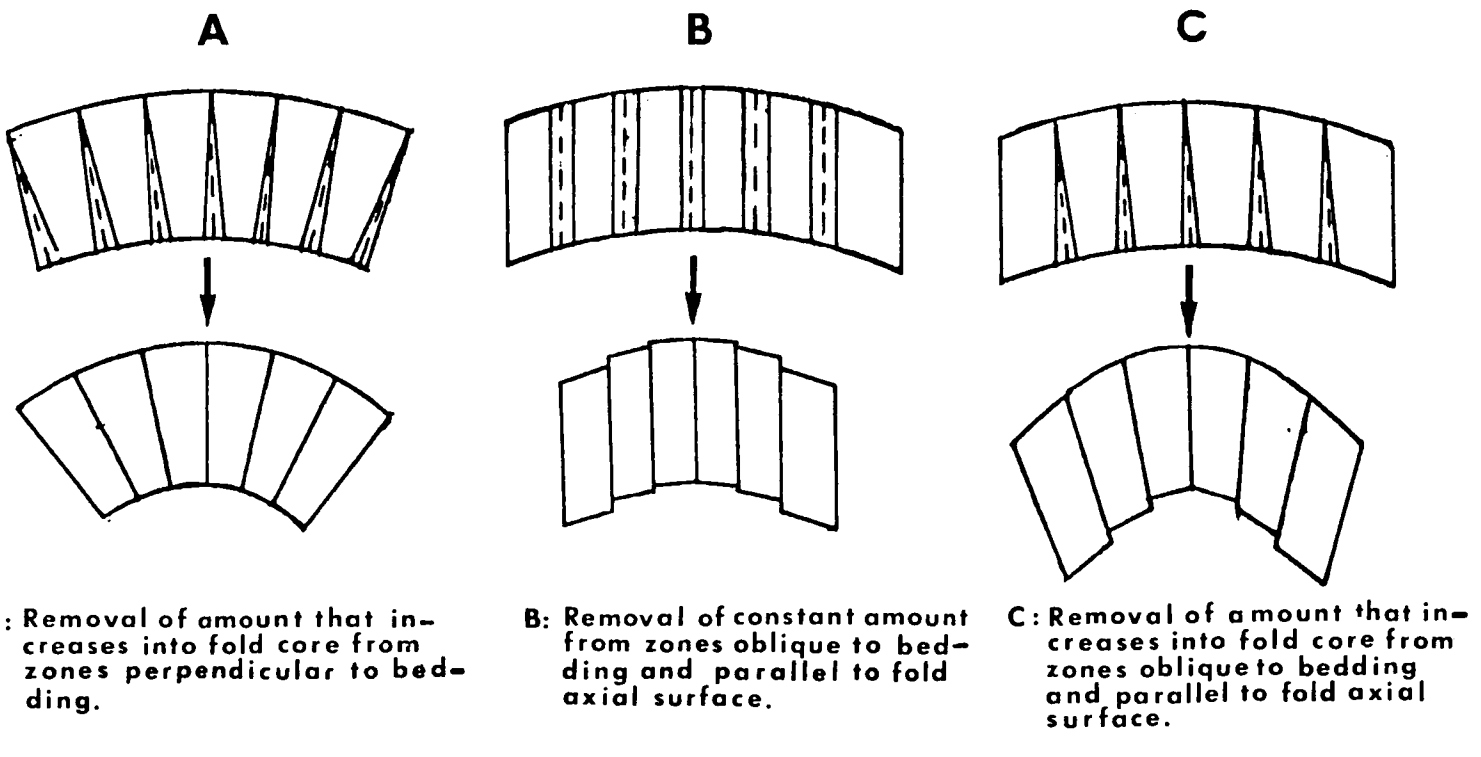

Figure 24. Three models of rigid body deformation by pressure solution shape modification adopted from Groshong (1975).

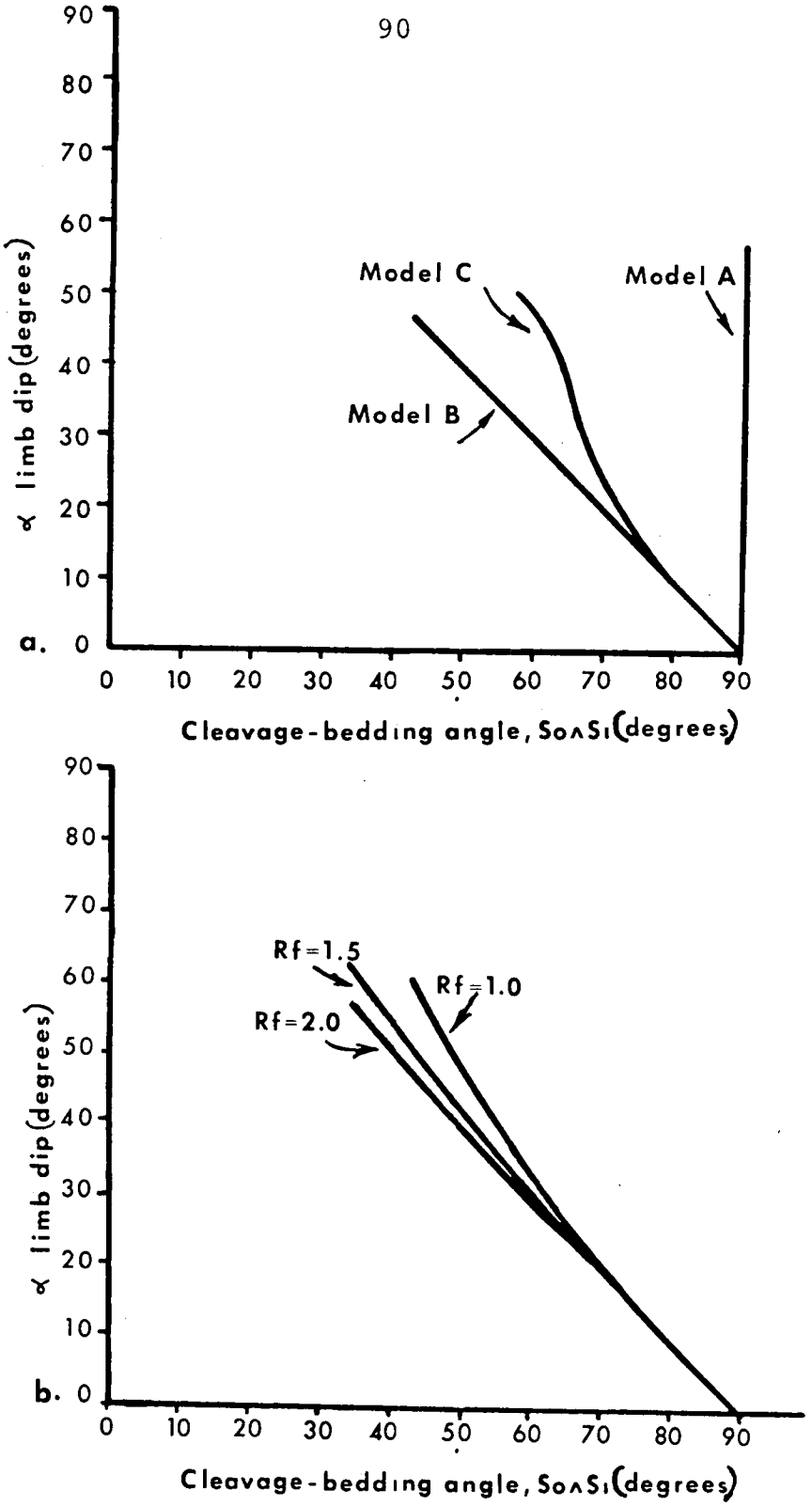

Figure 25. Plots of limb dip (α) against bedding-cleavage angle ($S_0 \wedge S_1$) for two theoretical fold models. (a) Groshong's (1975) pressure solution shape modification. (b) Ramsay's (1967) flexural flow folding.

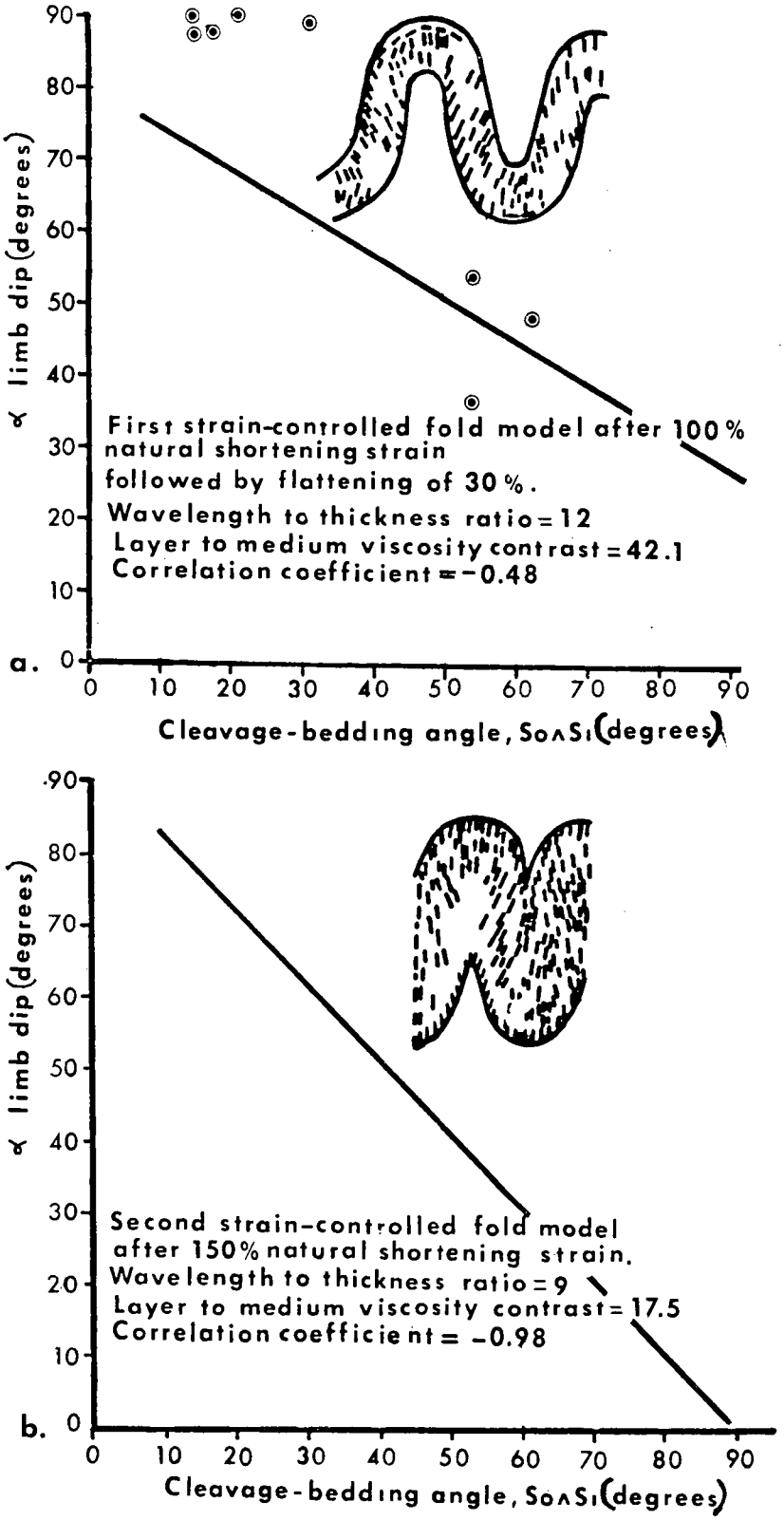

Figure 26. Plots of limb dip (α) against bedding-cleavage angle ($S_0 \wedge S_1$) for two viscous fold models of Dietrich (1969). (a) Model 1. (b) Model 2.

Curves showing the theoretical variation in cleavage fan angle (γ) against interlimb angle (β) for Ramsay's (1967) flexural flow fold mechanisms and for Groshong's (1975) pressure solution appear in Figures 27a and b. In all of the analyses, the data for models 1 and 4 were obtained from idealized fold profiles by direct measurement of the parameters (Figures 24, 26b). For model 3, the theoretical calculations were derived from equations in Ramsay (1967, pp. 391-392, 412).

Discussion of methods of measurement. The angles between cleavage and bedding and the cleavage fan and interlimb angles of folds were determined from photographs of the folds made in the field. In every case, the view was oriented to within about 10 to 15 degrees of structural strike. It can be shown on a Schmidt net that within this angular range the errors due to measuring apparent dips are not more than two degrees less than true dip. I assume in addition one or two degrees of measurement error to either side of the correct angle due to imprecise graphical technique. By these estimates, around each point on the graphs presented in this chapter is a range in angular values of approximately 3 to 4 degrees. Such an error would still be within the normal error bar of plus or minus 5 to 10 degrees anticipated in field measurements made with a Brunton

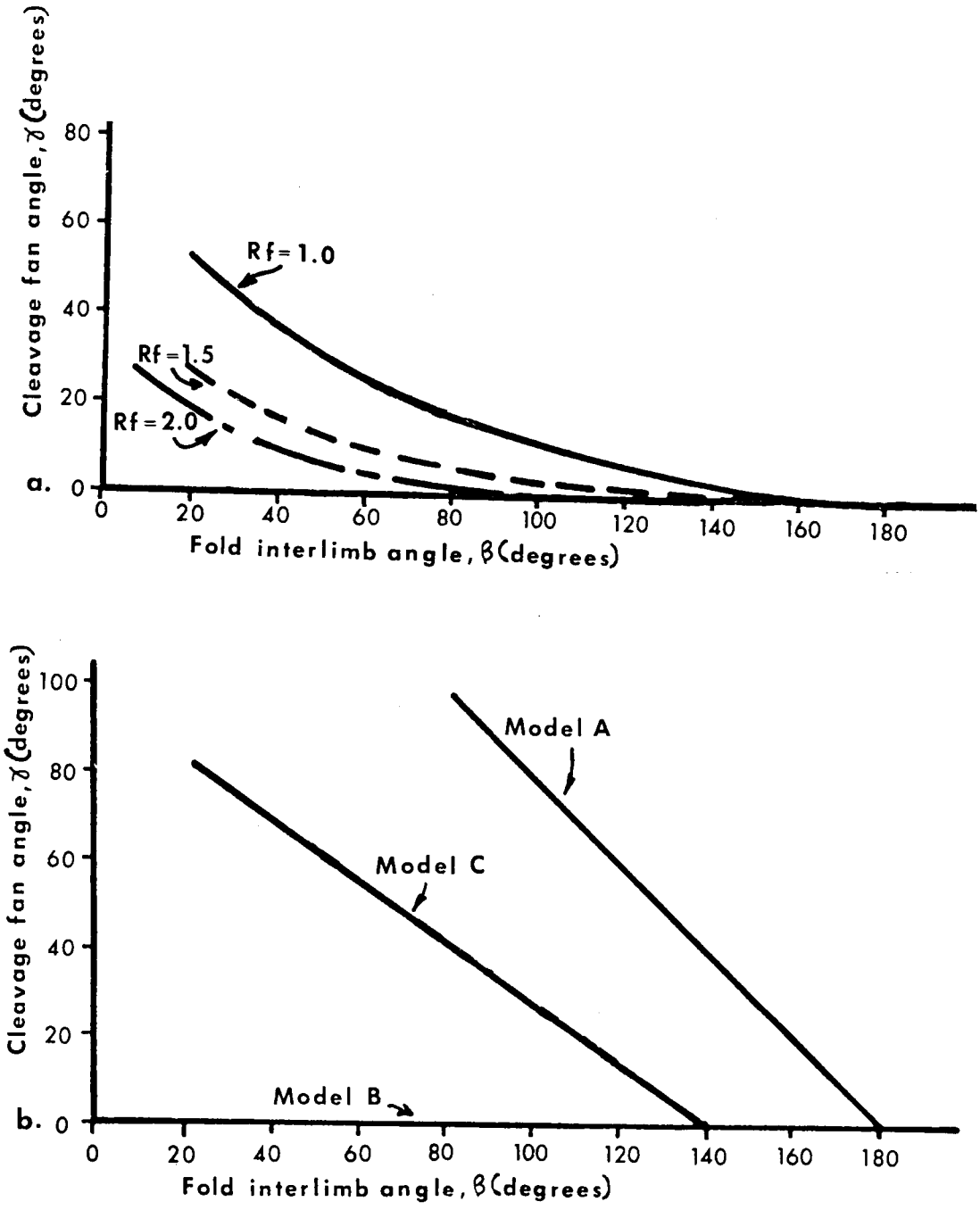

Figure 27. Plots of cleavage fan angle (γ) against interlimb angle (β) for two theoretical fold models. (a) Ramsay's (1967) flexural flow folding. (b) Groshong's (1975) pressure solution shape modification.

compass, so it would lie within that expected in structural field mapping. The measurements also assume that the strikes of the cleavage and of folded bedding coincide, so that true dihedral angles are given by the profile measurements. This assumption is upheld by the axial planar relationship of the cleavage to the folds (Figures 7a-u, p. 28).

Discussion of Theoretical Models

Pressure solution shape modification. Groshong's (1975) models A and B (Figure 24, p. 89) are relatively simple ones for which to plot idealized data. Model A assumes removal of an increasing amount of material toward the core of the fold along cleavage planes that are always orthogonal to bedding throughout the folding. Thus, the plot of γ/β will have a linear slope of -1 (Figure 27b), with the line passing through $\beta = 180°$. The slope of $\alpha/S_0 \wedge S_1$ for A will be infinite, with the line passing through $S_0 \wedge S_1 = 90°$. Model B, which assumes a constant amount of material removed from the fold along cleavage planes parallel to the axial surface, will have zero slope along the β axis in a γ/β plot (Figure 27b). In a graph of $\alpha/S_0 \wedge S_1$, model B will have a linear slope of -1, with the line passing through $S_0 \wedge S_1 = 90°$ (Figure 25a). In pressure solution model C, an increasing amount of material is removed from the fold along cleavage planes that are oblique to the bedding throughout deformation.

This system cannot be uniquely constrained, because many different combinations of bedding-cleavage angle and material removal can occur. Figures 25a and 27b were derived from one possible fold profile (see Figure 24), but some other line representing model C could have been plotted between those for A and B.

Dietrich's viscous models. In Dietrich's (1969) two viscous models, the $\alpha/S_0 \wedge S_1$ data were analyzed by a linear regression. The values of correlation coefficients, slope, and Y-intercept are included on the graphs. The considerable difference in correlation coefficients, r, for the two models relates to their wavelength to thickness ratio, L/h, and to their layer-to-medium viscosity contrast, μ_1/μ_2 (see Figures 26a, b) (Dietrich, 1969, p. 161). The second model has a significantly lower L/h and μ_1/μ_2 than does the first. The cleavage traces are constrained to be oriented orthogonal to the maximum contraction directions of local finite strain ellipsoids. In the first model (Figure 26a), the convex part of the fold hinge has suffered net positive extension strain. In model 2, however, the parameters Dietrich applied to his equation allowed for negative extension strains, only, in all parts of the fold. Hence, the cleavages are all at relatively high angles to bedding, even in the convex part of the hinge. By comparison with Ramsay's (1967, Fig. 7-63) model of

tangential-longitudinal strain, the fold of model 2 has a "neutral surface" which lies above the folded layer, while the neutral surface of model 1 does subdivide the fold into regions of finite extension and contraction. In a later paper, Dietrich (1970) analyzed multilayered folds with the same digital model used in the first paper, which was of a single layer embedded in a more ductile medium. The effect of this modelling were nearly identical to the single layer case.

Flexural flow models. Flexural flow, according to Ramsay's definition (1967, Fig. 7-54), assumes that the folded interlayers do not possess individual thicknesses, so that the folding is unaffected by layer discontinuities. Therefore, the theoretical calculations of cleavage-bedding geometry relevant to this model do not account for the finite thicknesses of the individual layers of real folds, as does his "flexural slip" model (Ramsay, 1967, Fig. 7-55). However, unique relationships in $\alpha/S_0 \wedge S_1$ and in γ/β cannot be derived in flexural slip, because the amount of slip depends on the thickness of each folded layer (Ramsay, 1967, p. 393). In all the studied folds, each layer thickness is quite small in comparison to the size of the fold. Therefore, a predominantly flexural mechanism should closely approximate the "flow" mode (Figure 25b, p. 90).

Comparisons among the idealized plots. Plots of $\alpha/S_0 \wedge S_1$ for Dietrich's model 2 (Figure 26b), for pressure solutions models B and C (Figure 25a) and for the flexural flow models (Figure 25b) are all close to the same shape. Indeed, pressure solution model B and Dietrich's second viscous model coincide. They also nearly coincide with the flattened flexural flow curves. In the case of pressure solution model C and unflattened flexural flow, the difference in the slope of the curves is due only to their slightly differing curvatures. Their predominant slopes, however, are very close to those of the other fold models. The curve of $\alpha/S_0 \wedge S_1$ for pressure solution model A (Figure 25a) is the only one in the group with an obviously different slope. Since it represents a perfectly orthogonal cleavage-bedding relationship for all values of bedding dip (Figure 24), its slope is vertical. Thus, when measurements of α and $\alpha/S_0 \wedge S_1$ are plotted from real fold profiles, the data do not allow for any distinction between Dietrich's second model and pressure solution model B. Neither will the data allow for a fine distinction among the other different mechanisms, unless the measurements can be made precisely enough to demonstrate the slight differences in curvature that some of the theoretical plots display. The previous discussion on measurement methods and accuracy limitations shows that such distinctions generally cannot be seen. Thus, I could establish only

fairly rough constraints on the fold mechanism solely by a comparison of the real $\alpha/S_0 \wedge S_1$ graphs with most of those derived from the published theoretical models of folding presented here. However, the two idealized plots of γ/β (Figures 27a, b) could provide a reasonably good distinction between either predominantly pressure solution shape modification or a purely flexural mechanism. This is because there is enough gross difference in the shapes of these two groups of curves to definitively compare them with the actual data, even with their inherent scatter.

Comparison of Real Folds with Theoretical Plots

Overview. The graphical data from the field examples are summarized in Table 2 (p. 71). For display of representative $\alpha/S_0 \wedge S_1$ plots, data for three representative folds have been presented together, superposed on the corresponding plots for the three folding models considered (Figures 28-30, a-c). Field photographs of the folds are shown in Figures 31a-c. Typically, the real $\alpha/S_0 \wedge S_1$ data have nearly a linear relationship. The three folds whose data have been presented represent both the calcareous mudrock (from localities 0-1 and 0-2), and the interbedded fine-grained sandstone and siltstone (from locality LS-3). There are no obvious lithology-dependent trends in the slopes of their regression lines. In the analysis (Table 2) it was noted that folds

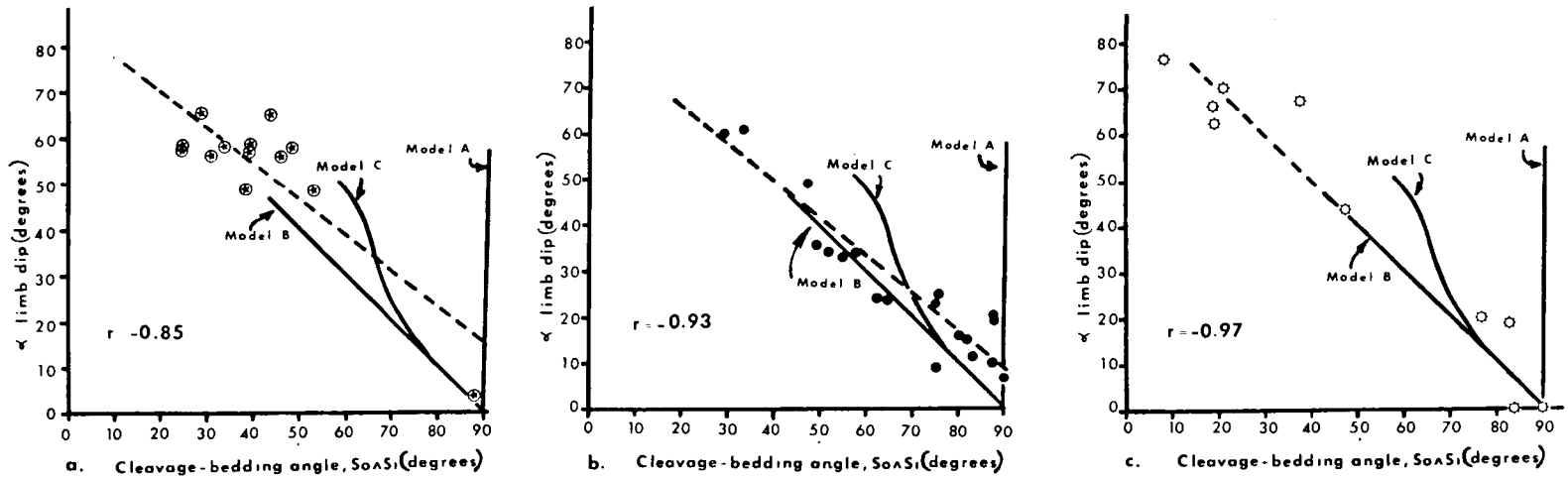

Figure 28. Plots of limb dip (α) against bedding-cleavage angle ($S_0 \Lambda S_1$) for three folds in the study area superimposed on the corresponding graph from Groshong's (1975) pressure solution shape modification fold models. (a) Fold 5, locality 0-1, lower Sevier. (b) Fold sets 1 and 2, locality 0-2, lower Sevier. (c) Fold 26, locality LS-3, upper Sevier.

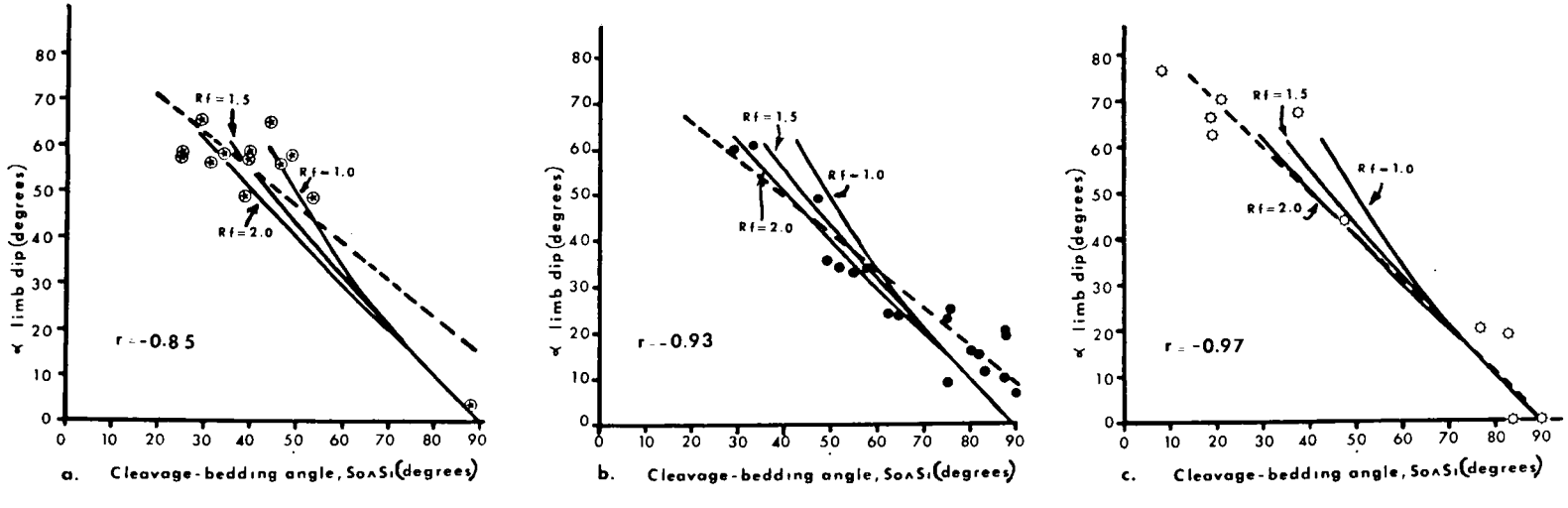

Figure 29. Plots of limb dip (α) against bedding-cleavage angle ($S_0 \wedge S_1$) for three folds in the study area superimposed on the corresponding graph from Ramsay's (1967) flexural flow fold models. (a) Fold 5, locality 0-1, lower Sevier. (b) Fold sets 1 and 2, locality 0-2, lower Sevier. (c) Fold 26, locality LS-3, upper Sevier.

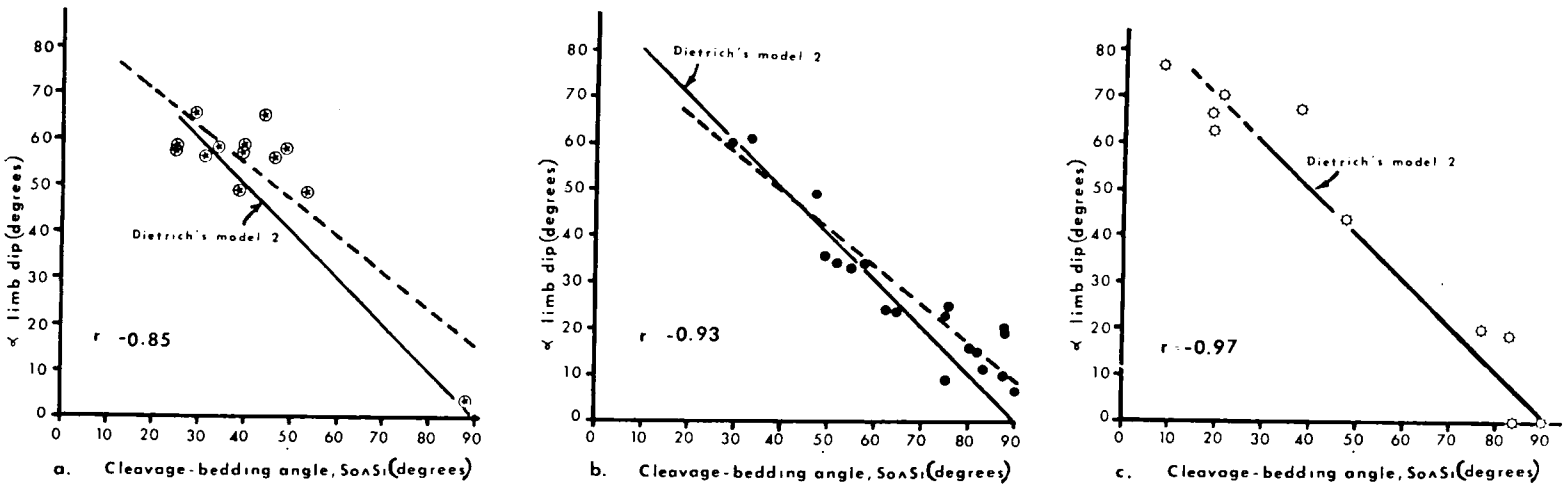

Figure 30. Plots of limb dip (α) against bedding-cleavage angle ($S_0 \Lambda S_1$) for three folds in the study area superimposed on the corresponding graph from Dietrich's (1969) second viscous fold model. (a) Fold 5, locality 0-1, lower Sevier. (b) Fold sets 1 and 2, locality 0-1, lower Sevier. (c) Fold 26, locality LS-3, upper Sevier.

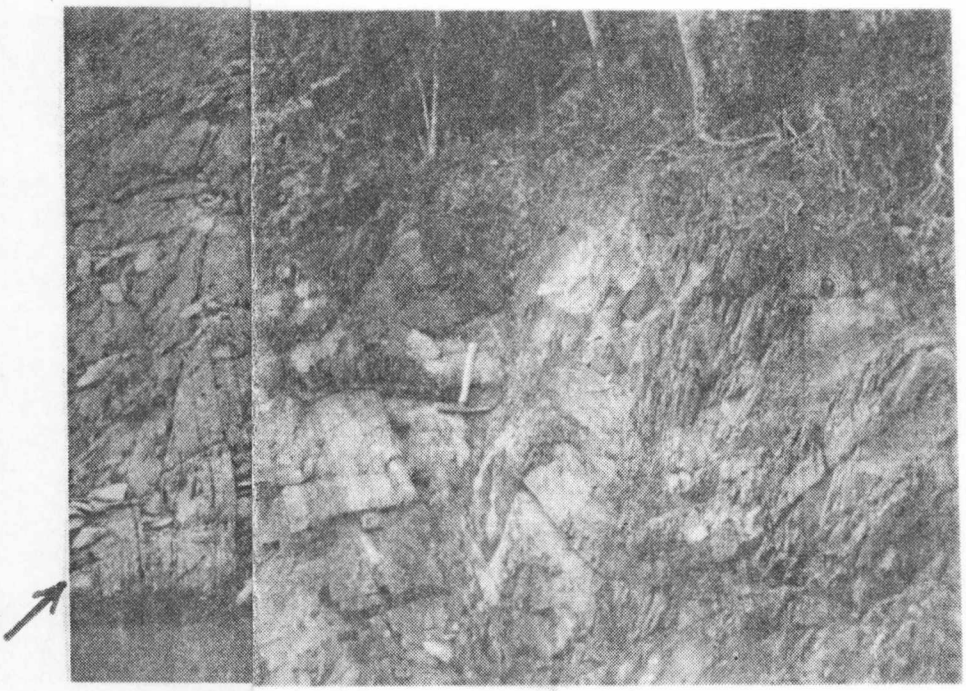

a.

c. 0 1m, H and V

ıted in
Sevier,
ılity 0-2,

even within the same outcrop may have different slopes and intercepts in $\alpha/S_0 \wedge S_1$.

Discussion of real $\alpha/S_0 \wedge S_1$ plots. In Figures 29a-c, the real data resemble more the flattened flexural flow curves than the curve for pure, or unflattened flow, whose Rf value is unity. This is seen in the lower slopes of the real data lines in comparison within the line representing the unflattened mode. Field evidence of slickensides orthogonal to fold axes that are preserved on some of the limbs confirms that these folds were formed at least in part by a flexural mechanism. The lower slopes of the real data in Figures 29a-c would therefore be expected, because all the layers presented here have sustained flattening strains approximately the same as those shown in the model. A comparison of the real data with pressure solution models A, B, and C (Figures 28a-c) clearly rules out model A, because the field data show that the cleavage planes are perpendicular to bedding only in the hinge regions. The slopes and intercepts of the three folds considered are close to model B, but the fanning of the real cleavage also eliminates this model as a mechanism. The coincidence of the points for fold 26 (Figure 28c) to model B seems to be the result of the relative insensitivity of the technique to real geometries. The plot for model C was seen to curve (Figure 25a, p. 90). Curvature cannot be discerned

in the plots of the real data because of their scatter, but the general trend of the line for C roughly resembles those of the actual folds. The cleavage traces in model C also fan (Figure 24, p. 89) so its correspondence with the real folds seems reasonably close within the limits imposed by measurement accuracy. Similarly good correlation exists with Dietrich's (1969) second strain-controlled cleavage model (Figures 30a-c), which was chosen over the first because of the better resemblance of the folds in outcrop to model 2 than to model 1. This correlation suggests that the real cleavage is also (1) orthogonal to the maximum contraction directions of the local finite strain ellipsoids, and suggests (2) that the interlayer contrast in ductility and the L/h ratios of the folds are both low. These two interpretations are the only ones uniquely obtainable from a comparison of my data with Dietrich's (1969) viscous models. The lack of similarity in the slopes of the $\alpha/S_0 \wedge S_1$ plots of the folds noted within the same lithology (Table 2) seems significant. It suggests that the strains due to buckling and to the associated cleavage were imparted heterogeneously. Complex, heterogeneous strains were also expressed by the departure of the real fold flattening curves from those predicted by theory (Figure 18, p. 74).

Discussion of the real γ/β plots. The measured values for the γ/β plots have been superposed on the flexural flow

(Figure 32a), and on the pressure solution models (Figure 32b). The data have been divided according to the two cleaved lithologies in the study area. Several of the points for the calcareous mudrock cluster in the vicinity of pressure solution model C (Figure 32b). They lie well away from either models A or B. The points for the relatively coarser lithologies show much more scatter, but they all plot between the lines for models B and C. In the graph of γ/β for the flexural flow model (Figure 32a), the mudrock points nearly all plot well above the unflattened flexural flow-curve. The points for the sandstone-siltstone interbeds nearly all lie below it, but they show no trend or clustering. These relationships tend to favor pressure solution model C as an important fold mechanism for the finer-grained lithology. The points for the calcareous mudrock also cluster above the unflattened curve for flexural flow (Figure 32a). If a flexural mechanism had been dominant at 0-1, I would expect the points to lie closer to the flattened examples of flexural flow, since most of the folds at 0-1 have been strongly flattened. Points representing the upper Sevier could have resulted from several combinations of a flexural and/or a pressure solution mechanism, but the data will not allow a determination of which was predominant in this case. A slightly different interpretation of the scatter of data in the coarser lithology can be suggested. Reks and Gray (1982,

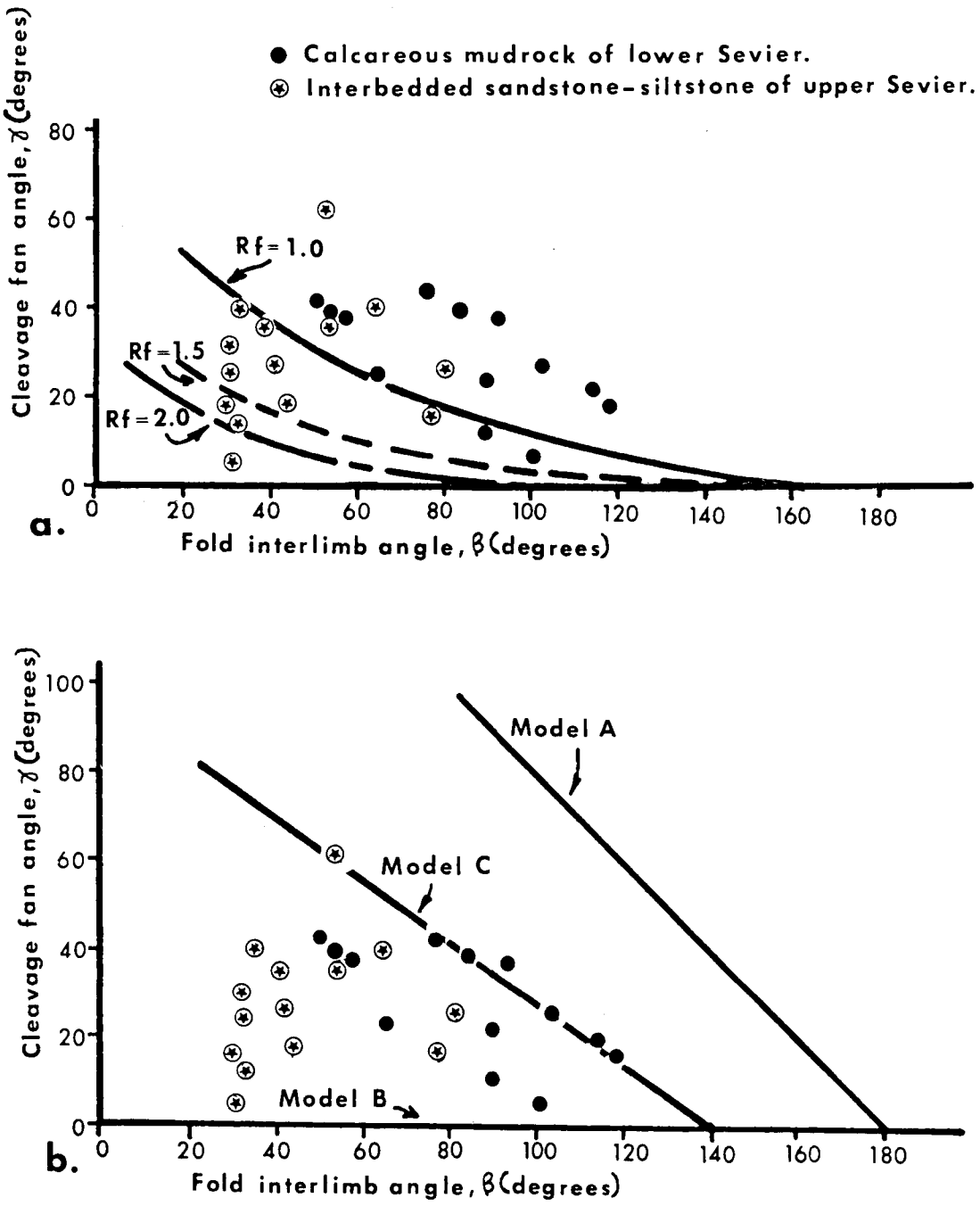

Figure 32. Plots of cleavage fan angle (γ) against interlimb angle (β) for real data superimposed on corresponding plots for two theoretical fold models. (a) Ramsay's (1967) flexural flow folding model. (b) Groshong's (1975) pressure solution shape modification.

ms) have noted that the cleaved folds on the Pulaski thrust sheet in southwest Virginia apparently were affected by cleavage at different stages in the folding process. They determined from considerable finite strain data that the individual folds had reached interlimb angles of from 40° to 110° before cleavage formation. The effect of this in outcrop would be the differing values of cleavage fan observed in folds of the upper Sevier (Hills, 1966) (Figures 32a, b). In either case, pressure solution shape modification processes seem to have strongly influenced the final fold geometries.

Implications for Lithologic Controls on Cleavage

The different behavior of cleavages in folds formed in the calcareous mudrock and in the interbedded sandstone and siltstone is one indication of a lithologic control on its occurrence. The plots (Figures 32a, b) suggest that the behavior of the cleaved mudrocks was slightly more regular in the γ/β plots, because it has less scatter, although its correlation coefficient ($r = -0.6$) is still fairly low. Another possibly better indication of a lithologic control on cleavage geometry is seen in the difference in linear regression coefficients of $\alpha/S_0 \wedge S_1$ graphs between the different folds at locality 0-1 (Plate 1). In the outcrop profile (Figure 33), the large, open anticline labelled 3 and

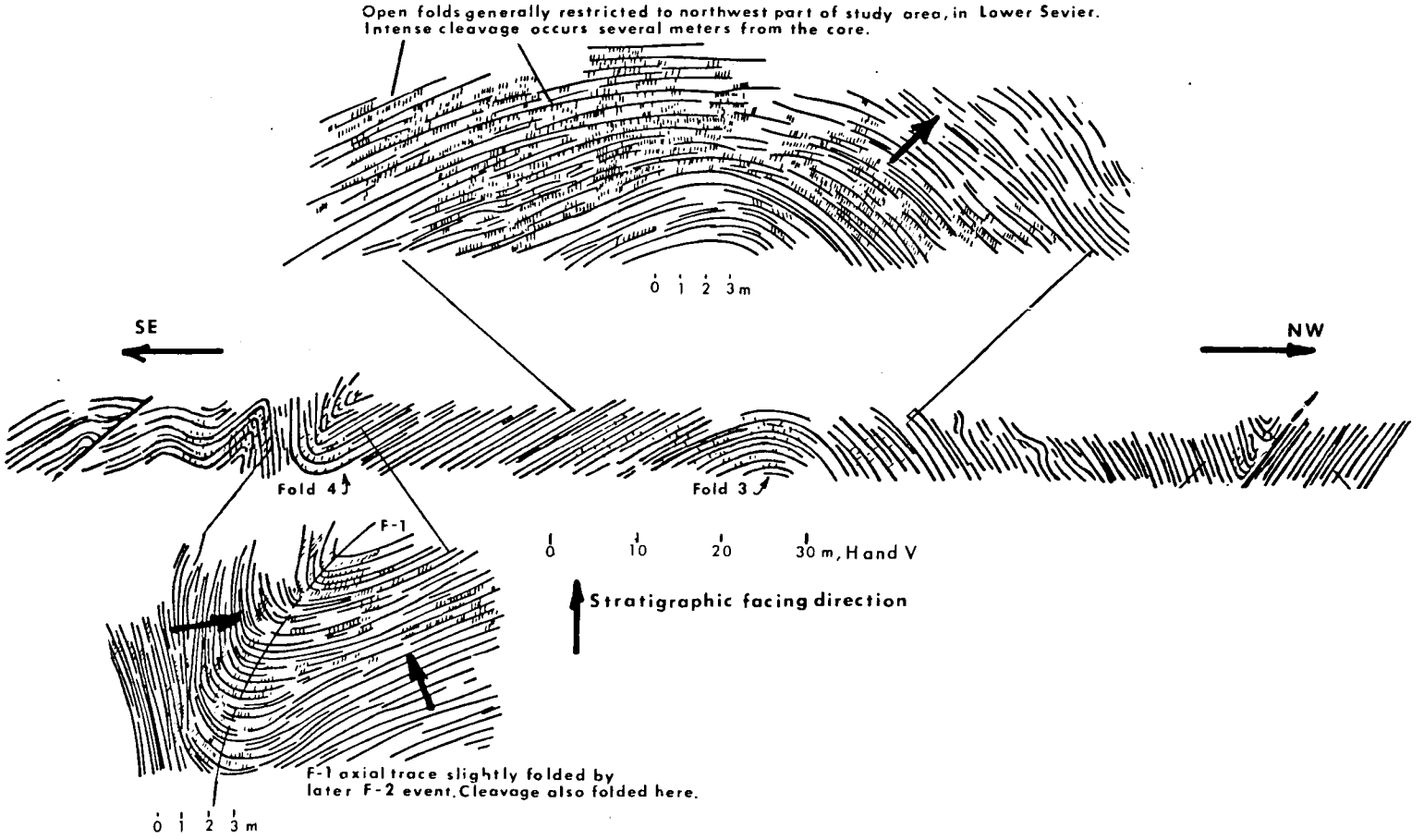

Figure 33. Portion of outcrop at locality 0-1.

referenced in Table 2 has a much lower linear correlation in $\alpha/S_0 \wedge S_1$ than any of the other referenced folds at this location. If no linear correlation is found, it may suggest that the cleavage orientations are not well-controlled by buckling. This is because each point on a straight line in a plot of $\alpha/S_0 \wedge S_1$ denotes a successive stage in the evolution of final fold shape such that for a given limb dip or interlimb angle, there is a specified cleavage-bedding angle (Gray, 1981a). The significant development of bed-parallel contraction which must precede folding in materials with low interlayer ductility contrast such as these (Ghosh, 1966, 1968) may have produced a prefolding cleavage in the folds at locality 0-1. This was controlled in its orientation initially by each of the beds in the outcrop before folding began. This might explain the occurrence of fairly intense cleavage at distances of several meters from the cores of the folds (Figure 33), which contrasts with other folds in upper Sevier lithologies in which cleavage is generally restricted to the hinge areas (see Figures 5, 8a-c; pp. 25, 30). In this case, under the assumption that cleavage in this lithology was affected differently by the folding, as its γ/β graph seems to imply, the less-curved layers would not necessarily show the same relative angular relationships between cleavage and bedding as the more strongly curved beds do. Table 2 shows that all the other folds at locality 0-1

are significantly tighter and flatter than the large anticline, and they also exhibit significantly higher linear correlations in $\alpha/S_0 \wedge S_1$. The two observations (1) that the primary fold mechanism in the lower Sevier lithology was pressure solution model C (Figure 32b) (Groshong, 1975), and (2) the earlier-formed cleavage in the lower Sevier than in the upper Sevier folds suggested by field evidence (Figure 33) tend to support a lithology-dependent relationship of cleavage to folding.

Timing of Cleavage with Respect to Folding

The presence of cleavage fans in nearly all the folds in the study area and the similarity of $\alpha/S_0 \wedge S_1$ plots to the corresponding plot from Dietrich's (1969) second fold model show that cleavage was synchronous, at least, with folding. This is because cleavage which forms while folding is in progress would be expected to rotate with the fold limbs to a degree (Hills, 1966), and because of the assumptions built into Dietrich's fold models. The considerable variation in cleavage fans within folds of the Upper Sevier (Figures 32a, b) may mean that cleavage was imparted to the rock fabric at different stages of development of the fold interlimb angles (Reks and Gray, 1982, ms). However, a cleavage which was quite late in folding would not be expected to fan symmetrically as it does in most of the studied folds, nor to demonstrate roughly predictable relationships in the $\alpha/S_0 \wedge S_1$

graphs from fold to fold (Figures 28-30, pp. 99-101). Therefore, the author suggests that the cleavage in the study area was "early" in the mesoscopic folding. Field evidence additionally suggested a local-to-map-scale noncoaxiality in all three principal directions of applied stress and of induced strain during the protracted deformation that affected these strata (see Chapter 2, "Macroscopic Interpretation"). This probably occurred after cleavage had formed, since some authors suggest that axial planar cleavage is expected to develop only in a bulk stress-strain system that remains coaxial in at least the intermediate principal direction throughout the cleavage-generating deformation (Stringer and Treagus, 1980, p. 327; Treagus, 1981). Specific, localized field evidence to support a relatively early cleavage is seen in the fold labelled 4 at locality 0-1 (Figure 33). The F-2 event that folded the axial surface here also folded the cleavage, but the cleavage remains symmetrical about the axial trace. This shows that the cleavage behavior approximated a preexistent, passive marker during folding of the axial surface.

CHAPTER 4

CONCLUSIONS

Geologic Cross Sections

Regional

The author's regional cross section (Plate 3) and the interpretations of other workers (Rodgers, 1953; Roeder et al., 1978) of the thrust belt through east Tennessee show a region-wide zone of bedding plane detachment in the Cambrian Rome Formation. From the Rome Formation, major faults rise northwesterly through the Paleozoic section of the Valley and Ridge province. The upward-shearing thrusts crumple the Paleozoic strata into a series of regional anticlines and synclines, typically with the development of parasitic outcrop-to-map scale folds along the limbs. The South Holston syncline of the present study is one such regional fold. The Holston Mountain and Pulaski faults, two first-order faults in upper east Tennessee, both have displacements of tens of kilometers and strike extents of hundreds of kilometers. Emplacement of the Holston Mountain thrust sheet predated emplacement of the Pulaski as shown by folding and uplift of the former sheet by the Pulaski at a lower structural level. This same general sequence of events noted at other locations along strike of the present study

area establishes a general east-to-west progression of deformation in the east Tennessee thrust belt.

Local

The interpretive cross section (Plate 2) through the South Holston syncline shows complex intraformational structures believed to have formed above a largely uninvolved upper Knox Group. A small regional fold, the Little Jacob Creek anticline, is interpreted as forming in conjunction with a fold-discordant second-order thrust. This subsurface interpretation is based upon the relatively large across-strike extent of the anticline and on its association with a dense array of mesoscopic faults that cross-cut it. The mesoscopic faults seem related to the much larger thrust fault that has been inferred at depth. The large fault is believed to be coterminous with a second-order, intraplate thrust mapped along strike in southwest Virginia as the Lodi fault (Reks and Gray, 1982).

The considerable overturning of the folds and the thrust faulting thickened the clastic section so that its true stratigraphic thickness is hard to determine. Howze (1983, personal communication) established a maximum thickness of about 5,000 feet for the strata of the South Holston syncline in southwest Virginia. This estimate agrees well with that of King and Ferguson (1960) in the present study area.

Regional Trends and Macroscopic Deformation History

A general progression in deformation is noted through the strike belt toward the southeast from the base of The Knobs (Plate 1). Axial planes of F-1 buckle folds show a progressive rotation toward the northwest with distance into the strike belt. Predominantly recumbent folds and tight kink fold trains that have both been refolded about nearly vertical F-2 axial planes dominate the structure from about three kilometers to the southeast of The Knobs. Cleavage is in all cases axial planar, but it is well-developed only in the upright to moderately inclined buckles in the northwest part of the study area. An overprinting of the normally cylindrical mesoscopic folds by clearly noncylindrical forms near the head of the Lucy Creek embayment (Figure 7v, p. 28; Plate 1) is related to the southwest closure of the Little Jacob Creek anticline.

The general trend in structural style seems related principally to the presence of the Holston Mountain fault, in contact with the Tellico-Sevier in the southeast portion of the strike belt. This would place the timing of the deformation in the study area as earlier than the emplacement of the Pulaski thrust sheet on which the structures were transported. An additional tectonic control was movement in the second-order splay off the Pulaski fault (the Lodi

fault), that terminates by displacement transfer in the Little Jacob Creek anticline (Plate 1).

Relationship of structure to stress and strain. At least three field observations are of importance in inferring the nature of the external stresses responsible for the structure. The first two are the axial planar relationship of the cleavage to the folds and the progression in fold style from nearly symmetric, upright forms to recumbency. The third observation is the noticeable variation in the attitudes of the AC planes and fold axes toward the southeast, exclusive of the obvious noncylindrical overprinting of the structure at localities R-11a and b through R-13 (Table 1, p. 58; Plate 1). Axial planar cleavage and increasing fold asymmetry suggest that the inducing stress was parallel to the strike of the bedding in the intermediate principal direction and oblique in the other two principal directions up until cleavage formation. It also indicates that the cleavage was imparted at a fairly "early" stage in the deformation history. The general westward rotation of the AC plane attitudes through the strike belt is believed to have developed after cleavage formation as the result of a bulk stress-strain configuration that was oblique to layering in all three principal directions. However, the estimated orientations of the

deformation axes associated with two fault populations separated across strike (Figures 15a, b, p. 56) are nearly the same. The across-strike separation of these two groups of faults implies that the absolute orientation of the bulk deformation axes was nearly the same through time. This is because of the general east-to-west propagation of the deformation already established. A bulk stress-strain system which was three-dimensionally oblique to layering late in the deformation could have resulted from local-to-map scale variations in the attitude of the folded bedding caused by an irregular resistance in the adjacent foreland to the movement. Such a resistance could have been caused by the developing anticline just in front of the synclinorium. Alternatively, the lower-lying Pulaski fault could have started moving while the stress field responsible for the structures in the study area was still active. In either case, external stress would be applied to bedding whose strike and dip were changing, and a more or less systematic shift in AC plane attitudes with distance through the strike belt could result. Additionally, the refolding of F-1 folds about F-2 axial planes suggests that stress and strain operated on the layers over a protracted continuum.

Cleavage-Fold Geometry and Fold Mechanisms

Plots of limb dip (α) against cleavage-bedding angle ($S_0 \wedge S_1$) and of cleavage fan angle (γ) against interlimb angle

(β) in the real folds were compared with the same plots derived from published theoretical fold mechanisms. My data provided coarse constraints, only, on the actual mechanism of the folding because of measurement imprecision and natural scatter of the data. But in conjunction with some of the field observations, the data do suggest that the fold mechanism approximated flattened flexural flow (Ramsay, 1967; Gray, 1981), which was influenced by pressure solution shape modification (Groshong, 1975) to varying degrees. The well-cleaved calcareous mudrocks in the lower part of the section exhibit a fold style that tends to favor Groshong's (1975) pressure solution model C (Figure 32b, p. 106). Folds in the coarser-grained upper Sevier seem to have been influenced by either model B or C in variable amounts (Figure 32a). The differing slopes of the straight lines defined by the $\alpha/S_0 \wedge S_1$ plots (Table 2, p. 71) indicate that the cleavage was not imparted to the folds everywhere homogeneously. The scatter of the data points in the graphed γ/β relationships implies that the cleavage may also have been imparted to the rock at different stages in fold development as measured by the fold interlimb angles. The close similarity of the real $\alpha/S_0 \wedge S_1$ graphs to the corre sponding plot from the second viscous fold model of Dietrich (1969) Figures 31a-c, p. 101) establishes that (1) the real cleavage planes are orthogonal to the maximum shortening axes

of local finite strain ellipsoids, (2) that folding and cleavage development were synchronous, and (3) that the folds formed with a generally low interlayer ductility contrast.

Fold flattening. Most of the studied folds have been subjected to variable but significant fold flattening strains. Graphical measurements of fold flattening by the techniques of Ramsay (1967) and of Gray and Durney (1979) showed that mesoscopic folds formed by active buckling in a regional compressive stress field. This is seen in the alternation in fold geometry, or class (Ramsay, 1967) from layer to layer. Typically, the folds alternate from Class 1C (weakly convergent isogons) for the stiff layers to Class 3 (strongly divergent isogons) for the weak layers. The geometry is a reflection of the greater resistance of the stiff layers to buckling. They tend to retain their original parallel shape while the weak layers tend to flatten much more. Thus, the overall fold shapes and buckling strains are controlled by the stiff beds, although their influence can be subtle.

Limitations of the geometric models. The lack of excellent correspondence of the real $\alpha/S_0 \wedge S_1$ curves to the theoretical data is to be expected. For example, the assumption in Ramsay's (1967) flexural flow curves that

cleavage behaves as a passive marker surface is probably incorrect in light of the complexities known to be involved in the formation of pressure solution-type cleavage (Rutter, 1976). In addition, very little is known about the actual means by which cleavage develops in deforming rock because of a lack of experimental data from real rock materials. The departure of the real data from the idealized fold flattening curves of Gray and Durney (1979, Fig. 14) has already been discussed. The observed transgression of actual plotted lines across the family of ideal flattening curves implies that the real fold flattening strains were imposed while the folds were forming. The ideal graphs are constructed from the assumption that the fold flattening is a separate, homogeneous strain component which affects only mature, parallel folds (Ramsay, 1967, pp. 411-412). Because folding and flattening are simultaneous, the resulting flattening strains must be nonhomogeneous, the situation expressed in the shapes of the actual curves (Figure 18, p. 74). A continuous transgression of the theoretical curves by the real data will eventually cause the plotted points to fall below the limit for a similar fold, into the Class 3 field (Figure 16, p. 68). The Rf strains of Class 2 (similar) or Class 3 folds are defined as infinite. But "infinite" strains cannot exist in nature. Thus, those Rf strains which range from a finite number to infinity (Table 2, p. 71), or

vice versa, are a product of the graphical technique, and their "infinite" values are not physically meaningful. In order to accurately define the effects of fold flattening, its nonhomogeneous nature should be properly accounted for.

Suggestions for Future Work

This report is an introductory treatment of the overall complex structure associated with one relatively small part of the Pulaski thrust sheet. Future regional studies on slaty cleavage should properly include a numerical analysis by meso- or microfabric techniques of the finite strains associated with the cleavage and the mesoscopic structure. A finite strain study is the only way to accurately define the cleavage-fold mechanisms. Cleavage itself should be studied under high magnification, because it is a small scale, intergranular feature of the rock fabric. Some recent investigators (Gray, 1981b; Simon, 1981) have subjected cleaved, low grade Valley and Ridge metasediments to analysis by electron microprobe and by scanning electron microscope to obtain ultra-high resolution compositional variations across cleaved zones and to observe the extremely small scale mechanisms by which certain grains have been partially removed. Such techniques were not attempted by the present author, because they would have greatly increased the length and scope of the research. However, the development of

numerical strain data and a narrow definition of the mechanism of pressure-solution cleavage in east Tennessee can only be obtained by such study in the future.

LIST OF REFERENCES

LIST OF REFERENCES

Arthaud, 1969, A graphic method of determination of the shortening, elongation, and intermediate directions from a population of faults: Extraut du Bulletin de la Societe Geologique de France, 7e, Serie t. xt, pp. 720-737.

Bartlett, C. S., Jr., and Biggs, T. H., 1979, Geology of the Abingdon and Shady Valley quadrangles, Virginia: Commonwealth of Virginia Department of Conservation and Economic Development Publication 16, 1:24,000.

Biot, M. A., 1965, Theory of internal buckling of a confined multilayered structure: Geol. Soc. America Bull., v. 75, pp. 563-568.

Borradaile, G. J., 1978, Transected folds: A study illustrated with examples from Canada and Scotland: Geol. Soc. America Bull., v. 75, pp. 481-493.

Bowlin, B. K., Ms, 1979, Description, interpretive, and quantitative study of the coarse clastics of the Middle Ordovician Tellico Formation in the vicinity of South Holston Dam, Tennessee: The Univ. of Tennessee, Knoxville, Dept. of Geol. Sci., Master's Thesis, 256 pp.

_____, and Keller, F. B., 1980, Incised submarine channel fan deposits in the Tellico Formation, South Holston Dam, Tennessee: in Walker, K. R., Broadhead, T. W., and Keller, F. B., Middle Ordovician carbonate shelf to deep water basin deposition in the Southern Appalachians, Field Trip IV: The Univ. of Tennessee, Knoxville, Dept. of Geol. Sci. Studies in Geol., No. 4, pp. 91-109.

Bridge, J., 1956, Disconformity between Lower and Middle Ordovician series at Douglas Lake, Tennessee: Geol. Soc. America Bull., v. 66, pp. 725-730.

Bryant, B., and Reed, J. C., Jr., 1970, Geology of the Grandfather Mountain window and vicinity, North Carolina and Tennessee: U.S. Geol. Survey Prof. Paper 615, 190 pp.

Butts, C., 1940, Geologic map of the Appalachian Valley in Virginia with explanatory text: Va. Geol. Survey Bull., v. 57, 518 pp.

Campbell, M. R., 1899, Description of the Bristol quad: U.S. Geol. Survey Atlas, Folio 5.

Chapple, W. M., 1968, A mathematical theory of finite amplitude folding: Geol. Soc. America Bull., v. 79, pp. 47-68.

Cobbold, P. R., Cosgrove, J. W., and Summers, J. M., 1971, Development of internal structures in deformed anisotropic rocks: Tectonophysics, v. 12, pp. 23-53.

Currie, D. B., Patnode, H. W., and Trump, R. P., 1962, Development of folds in sedimentary strata: Geol. Soc. America Bull., v. 73, pp. 655-724.

Dahlstrom, C. D. A., 1969, Balanced cross sections: Canadian Journal of Earth Sciences, v. 6, pp. 742-757.

Dietrich, J. H., 1969, Origin of cleavage in folded rocks: Am. Journ. Sci., v. 267, pp. 155-165.

_____, 1970, Computer experiments on mechanics of finite amplitude folds: Can. Jour. Earth Sci., v. 7, pp. 467-476.

_____, and Carter, N. L., 1969, Stress-history of folding: Am. Journ. of Sci., vol. 267, pp. 129-154.

Elliott, D., 1976, The energy balance and deformation mechanisms of thrust sheets: Phil. Trans. R. Soc. Lond. A., v. 283, pp. 289-312.

Geiser, P. A., 1975, Slaty cleavage and the dewatering hypothesis--an examination of some critical evidence: Geology, v. 3, pp. 717-720.

Ghosh, S. K., 1966, Experimental tests of buckling folds in relation to the strain ellipsoid in simple shear deformations: Tectonophysics, v. 3, no. 3, pp. 169-185.

_____, 1968, Experiments of buckling of multilayers which permit interlayer gliding: Tectonophysics, v. 6, no. 3, pp. 207-249.

Gray, D. R., 1981a, Cleavage-fold relationships and their implications for transected folds: An example from Southwest Virginia, U.S.A.: Journ. of Struct. Geol., v. 3, No. 3, pp. 265-271.

_____, 1981b, Compound tectonic fabrics from singly folded rocks from southwest Virginia, U.S.A.: Tectonophysics, v. 78, pp. 229-248.

_____, 1979, Investigations of the mechanical significance of crenulation cleavage: Tectonophysics, v. 58, pp. 35-79.

Groshong, R. H., Jr., 1975, "Slip" cleavage caused by pressure solution in a buckle fold: Geology, v. 3, pp. 411-413.

_____, 1976, Strain and pressure solution in the Martinsburg Slate, Delaware Water Gap, New Jersey: Am. Journ. Sci., v. 276, pp. 1131-1146.

Hardeman, W. D., Miller, R. A., and Swingle, G. D., 1966, Geologic map of Tennessee: Tennessee Dept. of Conservation, Div. of Geology, Scale 1:250,000.

Harris, L. D., and Milici, R. C., 1977, Characteristics of thin-skinned style of deformation in the southern Appalachians and potential hydrocarbon traps: U.S. Geol. Survey Prof. Paper 1018, pp. 1-40.

_____, Harris, A. G., DeWitt, W., Jr., and Bayer, K. C., 1981, Evaluation of southern eastern overthrust belt beneath Blue Ridge-Piedmont thrust: Am. Assoc. Pet. Geol. Bull., v. 65, no. 12, pp. 2497-2505.

Hatcher, R. D., Jr., 1972, Developmental model for the southern Appalachians: Geol. Soc. America Bull., v. 83, pp. 2735-2760.

_____, 1978, Tectonics of the western Piedmont and Blue Ridge, southern Appalachians: Review and speculation: Am. Jour. Sci., v. 278, pp. 276-304.

Heim, A., 1921, Geologie der Schweiz, II. Die Schweizer Alpen: Leipzig, Tauchnitz.

Hills, E. S., 1963, Elements of structural geology: John Wiley and Sons, Inc., New York, 483 pp.

_____, 1966, Elements of structural geology: Chapman and Hall, London.

Hobbs, B. E., Means, W. D., and Williams, P. R., 1976, An outline of structural geology: John Wiley and Sons, Inc., New York, 571 pp.

Holeywell, R. E., and Tullis, T. E., 1975, Mineral reorientation and slaty cleavage in the Martinsburg Formation, Lehigh Gap, Pennsylvania: Geol. Soc. America Bull., v. 86, pp. 1296-1304.

House, W. M., and Gray, D. R., 1982, Displacement transfer at thrust terminations in southern Appalachians--Saltville thrust as example: A.A.P.G. Bull., vol. 66, no. 7, pp. 830-842.

Hudleston, P. J., 1973a, Fold morphology and some geometric implications of theories of fold development: Tectonophysics, v. 16, pp. 1-46.

_____, 1973b, The analysis and interpretation of minor folds developed in the Moine Rocks of Monar, Scotland: Tectonophysics, v. 16, pp. 1-40.

_____, 1973c, An analysis of "single-layer" folds developed experimentally in viscous media: Tectonophysics, v. 16, pp. 184-214.

_____, and Stephansson, O., 1973, Layer shortening and fold shape development in the buckling of single layers: Tectonophysics, v. 17, pp. 299-321.

Kellberg, J. M., and Grant, L. F., 1956, Coarse conglomerates of the Middle Ordovician in the southern Appalachian Valley: Geol. Soc. America Bull., v. 67, pp. 697-716.

Keller, F. B., and Walker, K. R., 1980, Introduction to the southeastern phase of the Sevier foreland basin, in Walker, K. R., Broadhead, T. W., and Keller, F. B., Middle Ordovician carbonate shelf to deep water basin deposition in the southern Appalachians, field trip 10: The Univ. of Tenn., Dept. of Geol. Sci. Studies in Geol., no. 4, pp. 67-69.

King, P. B., and Ferguson, H. W., 1960, Geology of northeasternmost Tennessee: U.S. Geol. Survey Prof. Paper 311, 136 pp.

Newman, R. B., 1955, Middle Ordovician rocks of the Tellico-Sevier belt, eastern Tennessee: U.S. Geol. Survey Prof. Paper 274F, pp. 114-178.

Price, R. A., 1967a, The tectonic significance of mesoscopic subfabrics in the southern Rocky Mountains of Alberta and British Columbia: Can. Journ. Earth Sciences, v. 4, pp. 39-70.

Price, N. J., 1967b, The initiation and development of asymmetric buckle folds in non-metamorphosed competent sediments: Tectonophysics, v. 4, no. 2, pp. 173-201.

Ramberg, H., 1964, Selective buckling of composite layers with contrasted rheological properties, a theory for simultaneous formation of several orders of folds: Tectonophysics, v. 1, no. 4, pp. 307-341.

Ramsay, J. G., 1967, Folding and fracturing of rock: McGraw-Hill, Inc., New York, 568 pp.

_____, 1974, Development of chevron folds: Geol. Soc. America Bull., v. 85, pp. 1741-1754.

Read, J. F., 1980, Carbonate ramp to basin transitions and foreland basin evolution, Middle Ordovician, Virginia, Kentucky, and Tennessee: Am. Assoc. Pet. Geol. Bull., v. 64, no. 10, pp. 1575-1612.

Reks, I. J., and Gray, D. R., 1982, Pencil structure in weakly deformed mudstone and siltstone: J. Struct. Geol., v. 4, no. 3.

Rich, J. L., 1934, Mechanics of low-angle overthrust faulting as illustrated by Cumberland thrust block, Virginia, Kentucky, and Tennessee: Am. Assoc. Pet. Geol. Bull., v. 13, pp. 1584-1596.

Rodgers, J., 1953, Geological map of east Tennessee with explanatory text: Tennessee Dept. of Conservation, Div. of Geology Bull. 58, pt. 2, 186 pp.

Roeder, D., Gilbert, O. E., and Witherspoon, W. D., 1978, Evolution and macroscopic structure of Valley and Ridge thrust belt, Tennessee and Virginia: The Univ. of Tennessee, Knoxville, Dept. Geol. Sci. Studies in Geol. 2, 25 pp.

Rutter, E. H., 1976, The kinetics of rock deformation by pressure solution: Phil. Trans. R. Soc. Lond. A., v. 283, pp. 203-219.

Sander, B., 1948, An Introduction to the Study of Fabrics of Geological Bodies, Part I, trans. Phillips, F. C., and Windsor, G. (1970): Pergamon Press, London, 215 pp.

Sherwin, J., and Chapple, W. M., 1968, Wavelengths of single layer folds: A comparison between theory and observation: Am. Journ. of Sci., no. 266, pp. 167-179.

Simon, R. I., 1981, Implications of strain and mesoscopic structure in part of the Narrows thrust sheet of the southern Appalachian foreland zone, southwestern Virginia: Virginia Poly. Inst. and State Univ. M.S. thesis.

Stringer, P., and Treagus, J. E., 1980, Non-axial planar cleavage in the Hawick rocks of the Galloway area, Southern Uplands, Scotland: Journ. of Struct. Geol., vol. 2, no. 3, pp. 317-331.

Treagus, S. H., 1973, Buckling stability of a viscous single layer system, oblique to the principal compression: Tectonophysics, v. 19, pp. 271-289.

_____, 1981, A theory of stress and strain variations in viscous layers, and its geological implications: Tectonophysics, v. 72, pp. 75-103.

Turner, F. J., and Weiss, L. E., 1963, Structural analysis of metamorphic tectonites: McGraw-Hill, Inc., New York, 545 pp.

U.S. Geological Survey, 1980, CDP data in the Appalachian overthrust--set no. 1: open file from National Geophysical and Polar-Terrestrial Data Center: National Oceanographic and Atmospheric Administration, Boulder, Colorado.

Walker, K. R., 1980, Introduction to the stratigraphy and paleoenvironment of the Middle Ordovidian of Tennessee (Southern Appalachians, U.S.A.) in Walker, K. R., Broadhead, T. W., and Keller, F. B., Middle Ordovician carbonate shelf to deepwater basin deposition in the southern Appalachians, field trip 10: The Univ. of Tenn. Dept. of Geol. Sci., Studies in Geol., no. 4, pp. 4-12.

Wise, T., Ms, 1980, Significance of solution cleavage in the Chapman Ridge Anticline, east Tennessee: The Univ. of Tennessee, Knoxville, Dept. of Geol. Sciences Master's thesis, 106 pp.

Witherspoon, W. D., Ms, 1981, Structure of the Blue Ridge thrust front, Tennessee, Southern Appalachians: The Univ. of Tennessee, Knoxville, Dept. of Geol. Sci. Ph.D. dissertation, 165 pp.

Yust, W. W., Ms, 1976, A mesoscopic fabric analysis of a portion of the Tellico-Sevier belt of east Tennessee: The Univ. of Tennessee, Knoxville, Dept. o Geol. Sci. Master's thesis, 106 pp.

VITA

Charles D. Conway was born in Birmingham, Alabama, on September 6, 1944. He was educated in public schools in northern and central Virginia. He graduated from the University of Virginia in 1972 with a Bachelor of Arts degree in environmental sciences. He entered graduate school at The University of Tennessee, Knoxville, in September 1979 and completed requirements for a Master of Science degree with a major in geology in June 1983.



DETAILED SKETCH MAP OF STUDY AREA
PLATE 1

LEGEND

- Fault, showing dips
- Fault, location uncertain
- Plunging anticline
- Plunging syncline
- Anticline, location uncertain

3° MN
TN



DETAILED SKETCH MAP OF STUDY AREA
PLATE 1

LEGEND

- Fault, showing dips
- Fault, location uncertain
- Plunging anticline
- Plunging syncline
- Anticline, location uncertain
- Syncline, location uncertain
- Overturned anticline
- Overturned syncline
- Axial trend and profile of small folds
- Strike and dip of bedding
- Strike and dip of overturned bedding
- Strike and dip of vertical bedding
- Horizontal bedding
- Strike and dip of crumpled beds
- Strike and dip of bedding uncertain
- Strike and dip of foliation
- Studied outcrop area
- Subarea boundary

3° MN TN

0 24 48 72 96 120 (meters x 10)

0 1 2 3 4 (ft x 10^3)

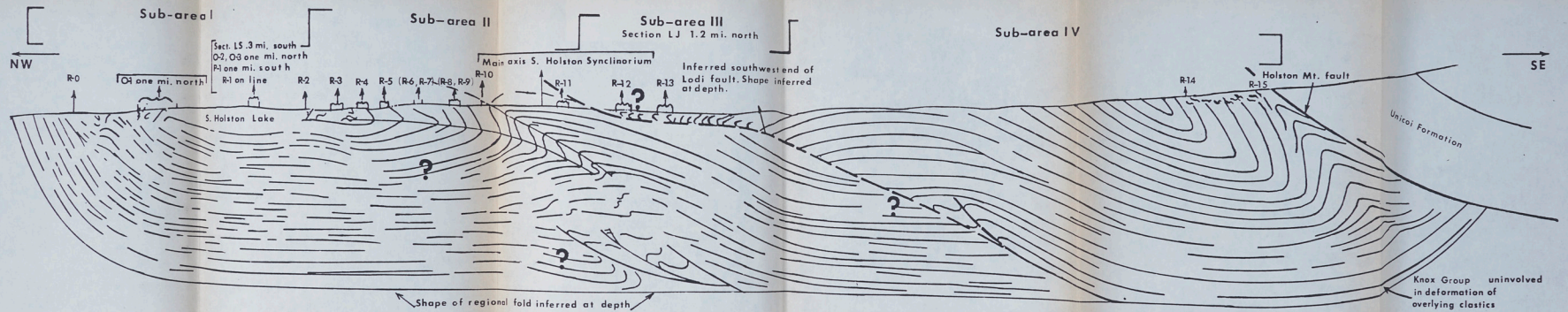

INTERPRETIVE CROSS-SECTION THROUGH STUDY AREA

Plate 2

H&V

0	305	610	915 meters
0	1000	2000	3000 feet

INTERPRETIVE REGIONAL CROSS-SECTION A-A'

Plate 3

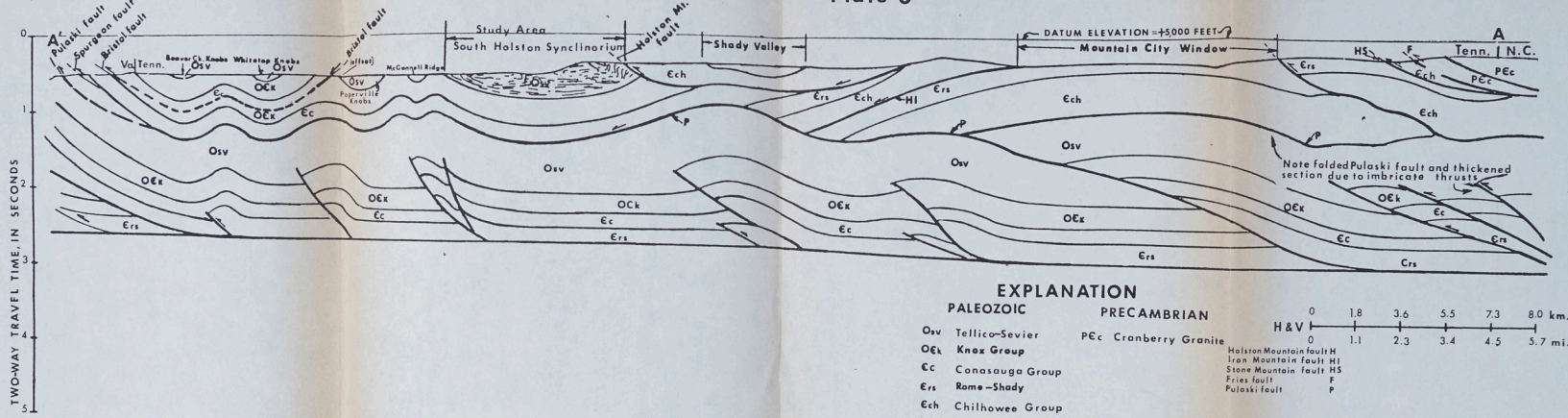

EXPLANATION

PALEOZOIC

- Osv Tellico–Sevier
- OЄk Knox Group
- Ec Conasauga Group
- Ers Rome–Shady
- Ech Chilhowee Group

PRECAMBRIAN

- PEc Cranberry Granite

H&V

	0	1.8	3.6	5.5	7.3	8.0 km.
	0	1.1	2.3	3.4	4.5	5.7 mi.

Holston Mountain fault H
Iron Mountain fault HI
Stone Mountain fault HS
Fries fault F
Pulaski fault P